*minerals*

MDPI

*Article*

# Marker Minerals in Volcanics and Xenoliths—An Approach to Categorize the Inferred Magmatic Rocks Underneath the Present-Day Volcanic Landscape of Tenerife, Spain (NW African Rare Mineral Province)

**Harald Gerold Dill [1,*] and Kurt Anton Rüsenberg [2,†]**

[1] Department of Mineralogy, Gottfried Wilhelm Leibniz University, Welfengarten 1, D-30167 Hannover, Germany
[2] Sudetenstraße 85, D-86609 Donauwörth, Germany; ruesenberg88@hotmail.com
* Correspondence: haralddill@web.de
† Retired.

**Abstract:** A mineralogical mapping (terrain analysis) based on micro-mounts has been performed in the Archipelago of the Canary Islands, Spain. The rare elements Be, F, Li, Nb, Ta, Zr, Hf, and rare earth elements (REE) were investigated on the largest island of the Canary Islands Archipelago, Tenerife, Spain. This study forms a contribution to the metallogenetic evolution of the offshore area of the NW African Rare Mineral Province. The finds made at Tenerife were correlated by means of minero-stratigraphy with the adjacent islands La Gomera, Gran Canaria and Fuerteventura, where typical critical element host rocks, e.g., carbonatites, are exposed. At Tenerife, these hidden rock types are only indicated by a wealth of 128 compositional first-order marker minerals hosting Be, F, Zr, Nb, Ta, Zr, Hf, Li, Cs, Sn, W, Ti and REE plus Y and another 106 structural second-order marker minerals describing the geodynamic and morpho-structural evolution of Tenerife (Mn, Fe, Pb, U, Th, As, Sb, V, S, B, Cu, Zn, Mo, Au). Based upon the quantitative micro-mineralogical mapping of lithoclasts and mineralogical xenoliths (foid-bearing monzodiorite/gabbro, (nepheline) syenite, phonolite trachyte) in volcanic and volcaniclastic rocks, hidden intrusive/subvolcanic bodies can be delineated that are associated with contact-metasomatic, zeolitic and argillic alteration zones, as well as potential ore zones. Two potential types of deposits are determined. These are pegmatite-syenites with minor carbonatites bound to a series of agpaitic intrusive rocks that are genetically interlocked with rift zones and associated with a hotspot along a passive continental margin. Towards the east, the carbonatite/alkali magmatite ratio reverses at Fuerteventura in favor of carbonatites, while at Gran Canaria and La Gomera, shallow hypogene/supergene mineral associations interpreted as a marginal facies to Tenerife occur and a new REE discovery in APS minerals has been made. There are seven mineralizing processes different from each other and representative of a peculiar metallogenic process (given in brackets): Protostage 1 (rifting), stages 2a to 2d (differentiation of syenite–pegmatite), stages 3 to 4b (contact-metasomatic/hydrothermal mineralization), stages 5a to 5b (hydrothermal remobilization and zeolitization), stage 6 (shallow hypogene-supergene transition and kaolinization), and stage 7 (auto-hydrothermal-topomineralic mineralization). The prerequisites to successfully take this holistic approach in economic geology are a low maturity of the landscapes in the target area, a Cenozoic age of endogenous and exogenous processes amenable to sedimentological, geomorphological, volcano-tectonic and quantitative mineralogical investigations. The volcanic island's mineralogical mapping is not primarily designed as a proper pre-well-site study on the Isle of Tenerife, but considered a reference study area for minero-stratigraphic inter-island correlation (land–land) and land–sea when investigating the seabed and seamounts around volcanic archipelagos along the passive margin, as exemplified by the NW African Craton and its metallogenic province. This unconventional exploration technique should also be tested for hotspot- and rift-related volcanic islands elsewhere on the globe for mineral commodities different from the ones under study.



**Citation:** Dill, H.G.; Rüsenberg, K.A. Marker Minerals in Volcanics and Xenoliths—An Approach to Categorize the Inferred Magmatic Rocks Underneath the Present-Day Volcanic Landscape of Tenerife, Spain (NW African Rare Mineral Province). *Minerals* **2023**, *13*, 1410. https://doi.org/10.3390/min13111410

Academic Editor: Alexandre V. Andronikov

Received: 22 September 2023
Revised: 26 October 2023
Accepted: 30 October 2023
Published: 3 November 2023

**Keywords:** mineralogy (micro-mounts); exploration; critical elements; hidden ore deposits; Tenerife, Spain

## 1. Introduction

At the NW part of the African continent, a Rare Mineral Province evolved from the Precambrian period to recent times, which, so far, has attracted little attention among economic geologists. It is a series of REE-, Nb-, and Fe-bearing deposits in carbonatites and pegmatites (Figure 1). They have been investigated in on-shore Morocco and Mauretania as well as off-shore in some islands of the Canary Islands Archipelago, Spain [1–7]. Deposits of the elements REE, Nb, Ta, Be, Li, F, and Zr are grouped among the so-called critical elements, which become more and more important for final products for energy supply and storage of electricity, making use of different platforms such as photovoltaic systems, solar thermal systems, hydroelectric power plants, geothermal heat and power plants, lithium-ion battery storage systems, bio-fuel production and as well as in the defense industry where the dissipative consumption plays an enormous part and thus needs ever-increasing amounts of critical elements with little or no chance of being recycled or substituted without a loss in quality of the weapons. Therefore, these elements and their mineral constituents of the Earth's crust gain special attention for their economic value and concentration in various mineral deposits [8,9]. They are subjected to a tripartite subdivision: (1) ore minerals and metallic resources, (2) industrial minerals and rocks, and (3) gemstones and ornamental stones. They can also be subjected to a binary subdivision into non-metallic and metallic resources so as to create a convenient way for a cross-border use that might also be applicable for social sciences, economics and technical sciences [9]. And, last but not least, they also justify the application of unconventional methods of exploration.

What is the scope of the current research article?

1. It is to emphasize that the plethora of rare minerals, which are often mocked as a playground for rockhounds and mineral hunters, warrant more attention in applied economic geology, particularly those parts devoted to those commodities classified as critical ones.
2. It is to discuss a type of mineral exploration joining mineralogy, lithology and applied sedimentology, geomorphology and to encourage applied geoscientists to leave the beaten tracks of routine exploration of mineral deposits.

The current study dealing with the deeper levels of Tenerife, Spain, is the mineralogical part of a binary study which is linked with a geomorphological terrain analysis focusing on the evolution of the landscape and landforms of those volcanic islands of the Canary Islands hosting these critical elements [10] (Tables 1 and 2).

This case history deals with an area that one rarely finds in one of the mining journals at a prominent place or will miss in textbooks on the economic geology of mineral deposits: the Isle of Tenerife, Spain. The region under study is more devoted to "turismo" rather than "minas de explotación a cielo abierto". It is known as a "hot" destination among holyday-makers flocking in from across the globe by airplane or cruise ship. Regarding geosciences, it is an oceanic magmatic hotspot worth being investigated by geophysics, structural geologists, and petrologists, mainly those paying attention to modern volcanic activities [11–13].

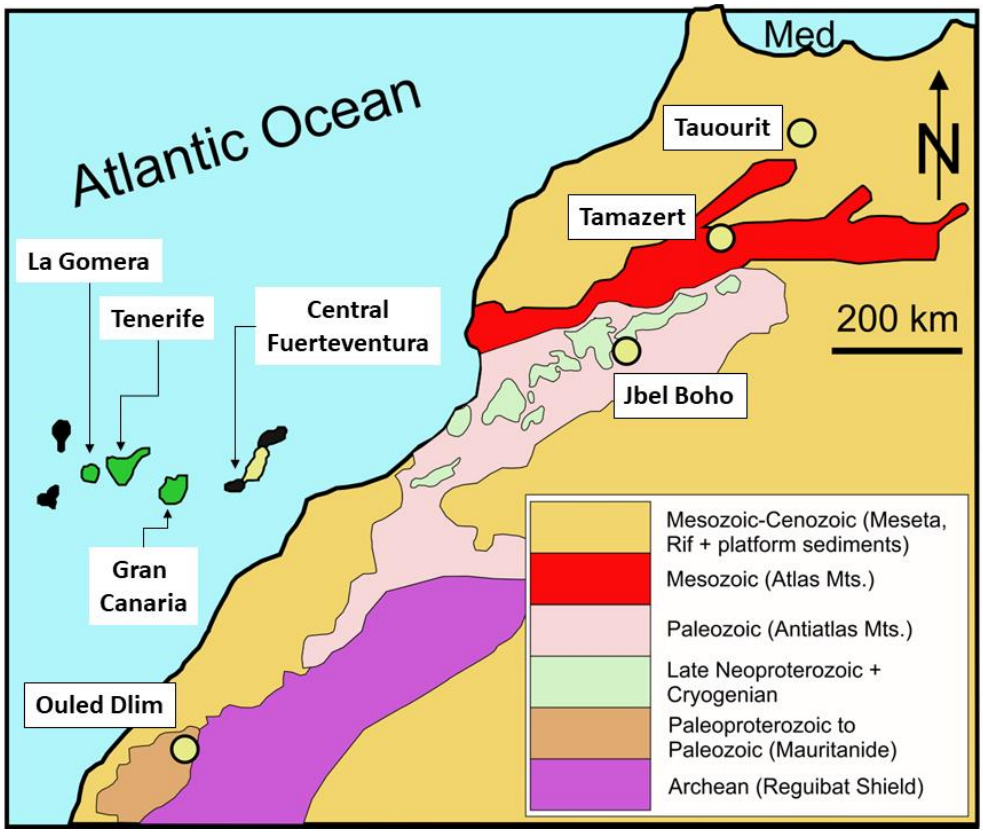


**Figure 1.** The NW African Rare Mineral Province with the most prominent rare mineral-bearing carbonatites (yellow), rare mineral-bearing alkaline magmatic complexes of the Canary Island Archipelago (green), and barren islands La Palma, El Hierro, Lanzarote, and SW Fuerteventura (black) indicated. Med: Mediterranean Sea. See also Figure 2 and text for sources [1–7,10].

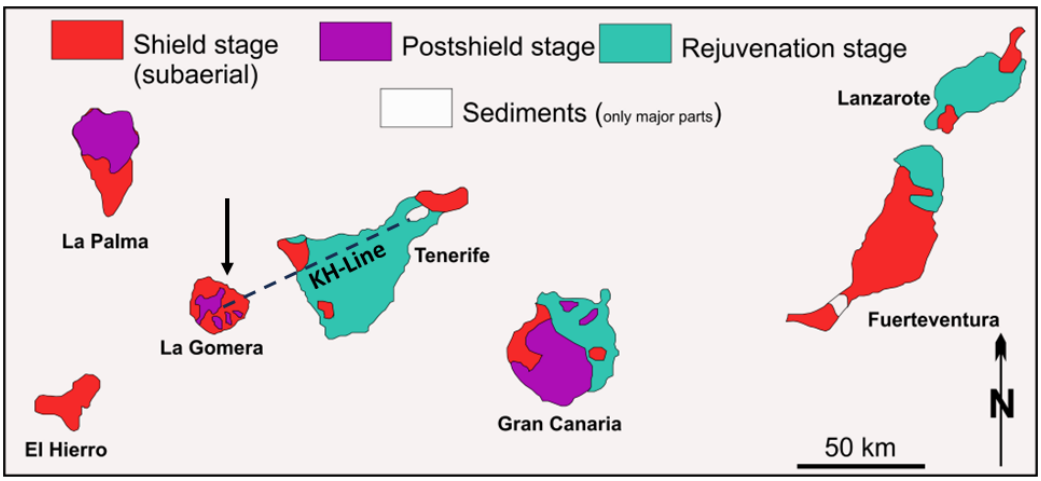


**Figure 2.** The Canary Islands Archipelago, Spain, on display on a volcano-geodynamic map with the three main stages of magmatic evolution (shield, post-shield, rejuvenation stages). Modified from [12]. KH Line = kaolinite-halloysite line. The REE occurrence discovered in the course of this project via micro-mount mapping is indicated by the arrowhead.

**Table 1.** Structural landforms and their landform series relevant for rare mineral exploration (see [10]).

| Structural landform | 1st | Volcanic edifice | | |
|---|---|---|---|---|
| | 2nd | Cinder/scoria cones | Scoria/lava domes, cryptodomes | Necks, palisade mesas and crater lakes |
| | Landform series of structural landforms | 1. Country and wall rocks landform series | 1. Country- and wall rock landform series | 1. Country- and wall rock landform series |
| | | 2. Cone-shaped landform series | 2. Domal landform series | 2. Crater landform series |
| | | 3. Pediment landform series | 3. Moat landform series | 3. Neck landform series |
| | | 4. Gutter landform series | 4. Coastal landform series | 4. Palisade mesa series |
| | | 5. Coastal landform series | | |

Impact on REE mineralization: red: negative, yellow: neutral, green: positive.

**Table 2.** Sculptural landforms and their land-forming processes, landforms and their parameters for distinction relevant for rare mineral exploration (see [10]). +++ = abundant, --- = missing.

| | **Metallogenic Province** | **Fuerteventura-Lanzarote** | **Gran Canaria** | **La Gomera-Tenerife** |
|---|---|---|---|---|
| **Land-Forming Processes** | **Landforms Parameters** | **Poly-Volcanic Island (Continental Shelf Edge)** | **Mono-Volcanic Island (Transitional Oceanic)** | **Mono-Volcanic Island (Oceanic)** |
| Mass wasting landform processes | Rock avalanche | +++ | +++ | +++ |
| | Rotational slide | +++ | +++ | +++ |
| | Translational slide | +++ | +++ | +++ |
| | Flow | +++ | +++ | +++ |
| | Creep | +++ | +++ | +++ |
| | Fall | +++ | +++ | +++ |
| | Fluvial mass wasting transitional landforms | +++ | --- | |
| Fluvial landform processes | Channel pattern | +++ | +++ | +++ |
| | Channel sinuosity (sinuosity rate) | +++ | +++ | +++ |
| | Channel density | +++ | +++ | +++ |
| | Channel orientation | | +++ | +++ |
| | Slope angle (angle in brackets) and altitude | +++ | +++ | +++ |
| Coastal marine landform processes | Coastline landforms (*sensu lato*) | +++ | +++ | +++ |
| | Transitional coastal landforms | +++ | +++ | +++ |
| | Foreshore | +++ | +++ | +++ |
| Aeolian landform processes | Unimpeded coastal dunes | +++ | +++ | --- |
| | Impeded coastal dunes | +++ | --- | |
| | Hinterland eolian landforms | +++ | | |
| Lacustrine landform processes | Volcano-sedimentary lakes | --- | | +++ |

## 2. Mineral Deposits of Critical Elements with Special Reference to Carbonatites, Pegmatites and Alkaline Magmatic Host Rocks as Potential Host Environments

The classification of mineral deposits follows the quadripartite scheme proposed by [9]: (1) magmatic mineral deposits, (2) structure-related mineral deposits, (3) sedimentary mineral deposits, and (4) metamorphic mineral deposits (Table 3).

**Table 3.** Classification of mineral deposits following the classification schemes of mineral deposits proposed by [9,14]. (a) Beryllium mineral deposits. (b) Zirconium-hafnium mineral deposits. (c) Fluorine mineral deposits. (d) Lithium mineral deposits. (e) Niobium-tantalum deposits. (f) Rare Earth element deposits. Only those deposits which are bound to carbonatites, pegmatites, and alkaline intrusive rocks and which might be expected underneath the landscape of Tenerife and its neighboring islands are listed.

| (**a**) |
|---|
| (1) Magmatic beryllium deposits |
| (1) Beryl-emerald-euclase-hambergite-bearing granite pegmatites |
| (2) Be silicate and Be phosphate-bearing greisen deposits |
| (3) Be-bearing alkaline intrusive rocks (nepheline syenite) |
| (4) Be-bearing alkaline-ultrabasic magmatic massifs with carbonatites |
| (5) Chrysoberyl within rare element pegmatites |
| (6) Beryl-bearing pegmatoids |
| (2) Metamorphic beryllium deposits |
| (1) Schist-related emerald deposits with or without pegmatitic mobilisates (gemstone) |
| (2) Metamorphosed Be pegmatite (Metapegmatites) |
| (3) Chrysoberyl in pegmatitic mobilisates in the contact zone |
| (1) Meta ultrabasic rocks |
| (2) Metapelites |
| (**b**) |
| Magmatic zirconium deposits |
| (1) Zircon-sapphire-bearing alkali basalt |
| (2) Zr- REE-P-Nb-Ta-F-(Be-Th) carbonatite-alkaline igneous complex |
| (3) (Li-Zn-Th-F-Nb-Ta)-Be-REE-Zr-bearing pegmatites |
| (**c**) |
| Magmatic fluorine deposits |
| (1) Fluorite deposits related to U-REE carbonatites and alkaline intrusive rocks |
| (2) Pegmatite-hosted F-(Sc) deposits |
| (3) Multielement cryolite pegmatite deposit related to metasomatic A-type granites |
| (**d**) |
| Magmatic lithium and cesium deposits |
| (1) Pegmatitic Li (including gem spodumene) and Cs deposits |
| (2) Tainiolite in carbonatites |
| (**e**) |
| (1) Magmatic niobium-tantalum-(scandium) depositsSn-Ta-Nb-Sc concentrations in calc-alkaline and alkaline |
| (1) Granites |
| (2) Pegmatites |
| (2) Nb- enriched deposits related to alkaline igneous complexes and carbonatites |
| (1) Pyrochlore-dominated concentric shell-type intrusions and carbonatites |
| (2) Nb-perovskite-dominated laccolites |
| (**f**) |
| Magmatic rare earth element deposits |
| (1) REE-P-Nb-Ta-Y-F-(Be-Zr-Th) deposits related to carbonatites |
| (2) REE-P-Ti deposits related to alkaline igneous complexes |
| (3) REE-U-Nb-bearing pegmatites (in places, transitional into intragranitic deposits with Mo-W-U-Be) |
| (4) Polygenetic carbonate-hosted REE-Nb-P-F-bearing hydrothermal iron deposits with carbonatitic impact |
| (5) Be- and Y-bearing alkaline intrusive rocks (nepheline syenite) |

### *2.1. Beryllium—Mineral Deposits and Their Origin*

Beryllium is a minor constituent of the Earth's crust with an average grade of 3 ppm Be. Due to their similarities in the ionic radii, Be can replace Si during igneous processes

and, hence, it is more widely dispersed than accumulated in the main stage of magma differentiation. It is concentrated during the magmatic and metamorphic part of lithogenesis mainly in pegmatites, pegmatoids and meta-pegmatites and to a lesser extend in carbonatites (part a of Table 3) [15–19]. Beryllium minerals are very variegated with a marked predominance of Be silicates, over Be phosphates/arsenates, Be oxides/hydroxides, Be borates and Be antimonate arranged in order of decreasing abundance [20]. There is a dominance of beryllium-bearing gemstones within the older cratons, which have been disrupted by modern plate tectonics, such as the opening of the Atlantic Ocean conspicuously demonstrated by the Brazilian and Nigerian gemstone provinces on both sides of the Atlantic Ocean and the fragmentation of the eastern edge of Africa where Madagascar, Sri Lanka and India are top scorers of gemmy Be minerals. These deposits are lined up along deep-seated fault zones and of pegmatitic origin [21]. The largest beryllium accumulation of economic interest is located in the Spor Mountain District, USA [22,23]. The bertrandite and beryl mineralization is associated with Mn, F, U, Li, and REE concentrated in pipes and veins of a series of Eocene to Miocene volcanic and volcaniclastic rocks which are genetically associated with 21 Ma old, high-silica, topaz rhyolite. It is interpreted as an epithermal, stratiform, replacement deposit in porous basal pyroclastic sediments.

### *2.2. Zirconium and Hafnium—Mineral Deposits and Their Origin*

Zircon, tourmaline and rutile rank first among heavy minerals regarding their resistance to meteoric and intrastratal solutions. Hence, they may survive even diagenesis upon deepest burial as well as long distance transport in stream sediments, leading them to often end up in coastal placer deposits [24]. This is also valid for metamorphic rocks where zircon appears up to the highest metamorphic grade and is eventually passed over into granitoid and pegmatoid mobilisates. The crystal morphology of zircon, the most widespread host of zirconium, shows such an extreme variability and good correlation between crystal habit and the temperature of formation that some petrologists felt encouraged to use this mineral as a mineralogical–crystallographic geothermometer [25,26]. Apart from this ubiquitous silicate zircon, there are also Zr oxides and very complex Zr silicates, some of which can be used as pathfinder minerals to obtain a better insight into the regional geology of the exploration area, as shown later in this study (part a of Table 4) [27].

**Table 4.** Marker minerals in xenoliths, pyroclastic, volcaniclastic and volcanic rocks of Tenerife, Spain. The minerals are subdivided into and denominated as first-order mineral (part a) and second-order mineral assemblages (part b) (see also Figure 4), and zeolite minerals (part c).

| (a) | | | | | | | | | | | | | | | | | | | |
|---|---|---|---|---|---|---|---|---|---|---|---|---|---|---|---|---|---|---|---|
| **Name** | **Chemical Composition** | **Adjacent Islands** | **Puerto de Santiago** | **Alcala** | **San Juan** | **P. d. Paraiaso** | **Los Humilladeros** | **P.d. Enramada** | **Los Abrigos** | **Centinela** | **La Mareta** | **Mt. Pelada** | **Tajao** | **B. Hondo** | **Mt. Reventada** | **Los Blanquitos** | **Poris de Abona** | **Santa Cruz** |
| **Adamsite-(Y)** | $NaY(CO_3)_2 \cdot 6H_2O$ | | | | | | | | | | | | | | | 1 | | |
| **Aeschinite-(Y)** | $(Y,La,Ca,Th)(Ti,Nb)_2(O,OH)_6$ | | | | 1 | | | | | | | 1 | | | | | | |
| **Alflarsenite** | $NaCa_2Be_3Si_4O_{13}(OH) \cdot 2H_2O$ | | | | | | | | | | | | | | 1 | | | |
| **Allanite** | $(Ce,Ca,Y)_2(Al,Fe)_3(SiO_4)_3(OH)$ | FUE | 1 | 1 | | | | | | | | | 1 | | | | 1 | |
| **Almarudite** | $K(\square,Na)_2(Mn,Fe,Mg)_2[(Be,Al)_3Si_{12}]O_{30}$ | | | | 1 | | | | | | | | | | | | | |
| **Ankylite-(Ce)** | $SrCe(CO_3)_2(OH) \cdot H_2O$ | | | 1 | | | | | | | | | | | | | | |
| **Ankylite-(La)** | $Sr(La,Ce)[OH \mid (CO_3)_2] \cdot H_2O$ | | | | | | | | | | | | | | | | 1 | |
| **Apatite** | $Ca_5(PO_4)_3$ (OH,F,Cl) REE-bearing | FUE GC | 1 | 1 | | | 1 | 1 | 1 | | 1 | 1 | 1 | 1 | 1 | 1 | 1 | 1 |
| **Astrophyllite** | $K_2NaFe^{2+}{}_7Ti_2Si_8O_{26}(OH)_4F$ | | | 1 | 1 | | 1 | | | | | 1 | | | | | | |
| **Baddeleyite** | $ZrO_2$ | | 1 | | | | | | 1 | | 1 | | 1 | 1 | | | | |
| **Barylite** | $Be_2Ba(Si_2O_7)$ | | | 1 | | | | 1 | | | | | | | | | 1 | |
| **Bastnaesite** | $Ce(CO_3)F$ | FUE GC | | 1 | 1 | | 1 | | | | 1 | | 1 | | | 1 | | |
| **Bavenite** | $Ca_4Be_2Al_2Si_9O_{26}(OH)_2$ | | | 1 | 1 | | | | | | | 1 | 1 | 1 | | | | |
| **Behoite** | $Be(OH)_2$ | | | 1 | | | | | | | | 1 | | | | | | |
| **Berborite 2H** | $Be_2(BO_3)(OH,F) \cdot H_2O$ | | | | | | | | | | | 1 | | | | | 1 | |
| **Berezanskite** | $KTi_2Li_3Si_{12}O_{30}$ | | | | | | | | | | 1 | | | | | | | |
| **Bertrandite** | $Be_4(Si_2O_7)(OH)_2$ | | 1 | | | | | 1 | | | 1 | | | | | 1 | 1 | |

**Table 4.** *Cont.*

| | | | | | | | | | | | | | | | | | | |
|---|---|---|---|---|---|---|---|---|---|---|---|---|---|---|---|---|---|---|
| **Bikitaite** | $LiAlSi_2O_6\ H_2O$ | | | | | | | | | | 1 | | 1 | | | | | |
| **Britholite-(Ce)** | $(Ce,Ca,Th,La,Nd)_5(SiO_4,PO4)_3(OH,F)$ | FUE | | 1 | | | | | | | | | | | | | | |
| **Burbankite** | $(Na,Ca)_3(Sr,Ba,Ce)_3(CO_3)_5$ | | 1 | 1 | 1 | | | | | | 1 | | 1 | | 1 | 1 | 1 | |
| **Burpalite** | $Na_2CaZrSi_2O_7F_2$ | | | | | | | | | 1 | | | | | | | | |
| **Byrudite** | $(Be,\square)(V^{3+},Ti,Cr)_3O_6$ | | | | | | | 1 | | | | | | | | | | |
| **Calcio-Catapleite** | $CaZr(Si_3O_9)\ 2H_2O$ | | | 1 | | | | | | | | | | | | | | |
| **Cassiterite** | $SnO_2$ | | | | | | | | | | | | 1 | | | | | |
| **Cerianite** | $CeO_2$ | GC | | | | | | | | | | | | | | | | |
| **Cerite** | $(Ce,La,Ca)_9(Mg,Fe^{3+})(SiO_4)_3(SiO_3OH)_4(OH)_3$ | | | | | | | | | | | 1 | | | | | | |
| **Clinozoisite/epidote** | $Ca_2(Al,Fe)_3[O \mid OH \mid SiO_4 \mid Si_2O_7]$ | FUE | 1 | | | 1 | | | 1 | 1 | | | | | | | | |
| **Chevkinite-(Ce)** | $(Ce,La,Ca,Na,Th)_4(Fe^{2+},Mg)_2(Ti,Fe^{3+})_3Si_4O_{22}$ | | | 1 | | | 1 | 1 | 1 | 1 | | | 1 | | | 1 | | |
| **Chiavennite** | $CaMnBe_2Si_5O_{13}(OH)_2{\cdot}2H_2O$ | | 1 | | 1 | | | | | | | | 1 | | | 1 | | |
| **Chkalovite** | $Na_2BeSi_2O_6$ | | | 1 | | | | | | | | | | | | | | |
| **Churchite-(Y)** | $(Y,Er,La)[PO_4]{\cdot}2H_2O$ | | | | 1 | | | | | | | | | | | | | |
| **Colquiriite** | $CaLi[AlF_6]$ | | | | | | | | | | | | | | | 1 | | |
| **Cookeite** | $(LiAl_4\square)[AlSi_3O_{10}](OH)_8$ | | | 1 | | | | 1 | | | 1 | | | 1 | | | | |
| **Cordylite-(Ce)** | $NaBaCe_2[F \mid (CO_3)_4]$ | | | | | | | | | | | | 1 | | | | | |
| **Cryolite** | $Na_2NaAlF_6$ | | | 1 | | 1 | | | | | | | | 1 | 1 | 1 | 1 | |
| **Cuspidine** | $Ca_4Si_2O_7(F,OH)_2$ | FUE | | | | | | | | 1 | | | | 1 | | | | |
| **Dalyite** | $K_2ZrSi_6O_{15}$ | | | 1 | | | | | | 1 | | | | | | | 1 | |
| **Davanite** | $K_2TiSi_6O_{15}$ | | 1 | 1 | 1 | | | | | | | | | | | | | |
| **Dissakisite-(Ce)/ferri-dissakisite-(REE)** | $CaCe(Al_2Mg)[Si_2O_7][SiO_4]O(OH)$ | FUE | | | | | | | | | | | | | | | | |
| **Elbaite** | $Na(Li_{1.5}Al_{1.5})Al_6(Si_6O_{18})(BO_3)_3(OH)_3(OH)$ | | | | | | | 1 | | | | | 1 | | | | | |
| **Eliseevite** | $LiNa_{1.5}Ti_2(H_{1.5}Si_4O_{12})O_2\ 2H_2O$ | | | | | | | | | | | | | 1 | | | | |
| **Elpidite** | $Na_2ZrSi_6O_{15}\ 3H_2O$ | | | | | | | | | 1 | | | | | | | | |
| **Emmerichite** | $Ba_2Na(Na,Fe^{2+})_2(Fe^{3+},Mg)Ti_2(Si_2O_7)_2O_2F_2$ | | | | 1 | | | | | | | | 1 | | | | | |
| **Epididymite** | $Na_2Be_2Si_6O_{15}\ H_2O$ | | 1 | 1 | 1 | | | | | | 1 | | | | | | 1 | |
| **Epistolite** | $Na_2(Nb,Ti)_2(Si_2O_7)O_2\ nH_2O$ | | 1 | 1 | | | | 1 | | | | | | | | | 1 | |
| **Eudidymite** | $Na_2Be_2Si_6O_{15}\ H_2O$ | | | 1 | | | | | | | 1 | | 1 | | | 1 | 1 | |
| **Eudyalite** | $Na_{15}Ca_6Fe_3Zr_3Si(Si_{25}O_{73})(O,OH,H_2O)_3(Cl,OH)_2$ | | | 1 | | | | | | | 1 | | | | | 1 | | 1 |
| **Eudyalite-(Mn)** | $Na_{14}Ca_6Mn_3Zr_3[Si_{26}O_{72}(OH)_2](H_2O,Cl,O,OH)_6$ | | | | | | | 1 | | 1 | 1 | | | 1 | | | | |
| **Fergusonite-(Y)** | $YNbO_4$ | | | | | | | 1 | | | | 1 | | | | | | |
| **Ferrocolumbite** | $Fe^{2+}Nb_2O_6$ | | | | | | | | | | | | | 1 | | | | |
| **Ferrokentbrooksite** | $Na_{15}Ca_6(Fe,Mn)_3Zr_3NbSi_{25}O_{73}(O,OH,H_2O)_3Cl_2$ | | | | | | 1 | | | 1 | | | | | | | | |
| **Fersmanite** | $Ca_4(Na,Ca)_4(Ti,Nb)_4(Si_2O_7)_2O_8F_3$ | | | | | | | | | | | 1 | | | | | | |
| **Fersmite** | $Ca(Nb,Ta)_2O_6$ | FUE | | 1 | | | | | | | | | | | | | | |
| **Florencite-(Ce)** | $CeAl_3(PO_4)_2(OH)_6$ | GO | | | | | | | | | | | | | | | | |
| **Fluorite** | $CaF_2$ | | | 1 | | | | | 1 | | | | | 1 | 1 | 1 | | |
| **Garmite** | $CsLiMg_2(Si_4O_{10})F_2$ | | | | | | | | | | 1 | | | | | | | |
| **Gittinsite** | $CaZrSi_2O_7$ | FUE | | | | | | | | | | | | | | | | |
| **Goetzenite** | $Ca_4NaCa_2Ti(Si_2O_7)_2(OF)F_2$ | | 1 | 1 | 1 | | | | | | | 1 | | | | | | |
| **Griceite** | $LiF$ | | | | | | | | | | 1 | | | 1 | 1 | 1 | | |
| **Grossularite** | $Ca_3Al_2(SiO_4)_3$ | FUE | | | | | 1 | | | | | | | | | | | |
| **Gugiaite** | $Ca_2Be[Si_2O_7]$ | | | | | | | | | | 1 | 1 | 1 | 1 | | 1 | 1 | |
| **Hainite-(Y)** | $Na_{1.75}Ca_{4.25}REE_{0.1}Ti_{0.75}Zr_{0.4}Mn_{0.25}Fe_{0.125}Si_{3.9}O_{13.75}F_{4.15}$ | | | | | | | | | | | | | | | 1 | | |
| **Hambergite** | $Be_2(BO_3)(OH)$ | | 1 | 1 | 1 | | | 1 | | | 1 | 1 | | | | 1 | 1 | |
| **Helvine** | $Be_3Mn^{2+}{}_4(SiO_4)_3S$ | | | | | | | 1 | | | 1 | | | | | | | |
| **Holmquisite** | $Li_2(Mg,Fe^{2+})_3Al_2Si_8O_{22}(OH)_2$ | | | | | | | | | | 1 | | | 1 | 1 | | | |
| **Isolueshite** | $(Na,La)NbO_3$ | | | | | | | | | | | | | 1 | | | 1 | |
| **Janhaugite** | $(Na,Ca)_3(Mn^{2+},Fe^{2+})_3(Ti^{4+},Zr,Nb)_2(Si_2O_7)_2O_2(OH,F)_2$ | | | | 1 | | 1 | 1 | | | | | | | | | | |
| **Kentbrooksite** | $Na_{15}(Ca,Ce,La)_6(Mn^{2+},Fe^{2+})_3Zr_3Nb[O \mid (F,Cl,OH) \mid Si_3O_9 \mid Si_9O_{27}]_2{\cdot}2H_2O$ | | | | | | 1 | | | 1 | | | 1 | | | | | 1 |
| **Khomyakovite** | $Na_{12}Sr_3Ca_6(Fe,Mn)_3Zr_3W[Si_{25}O_{73}](O,OH,H_2O)_3(OH,Cl)$ | 2 | | | | | | | | | | | | 1 | | | | |
| **Cryolite** | $Na_3AlF_6$ | | | | | | | | | | 1 | | | | | | | |
| **Kukharenkoite-(Ce)** | $Ba_2Ce(CO_3)_3F$ | | | | | | | | | | | | | | | 1 | | |
| **Labuntsovite-(Mg)** | $Na_4K_4(Ba,K)_2MgTi_8(Si_4O_{12})_4(O,OH)_8\ 10H_2O$ | | | | | | | 1 | | | | | | | | | | |
| **Lamprophyllite** | $(SrNa)Ti_2Na_3Ti(Si_2O_7)_2O_2(OH)_2$ | | 1 | | | | | | | | | 1 | | | | | | |
| **Latrappite** | $(Ca,Na)(Nb,Ti,Fe)O_3$ | | | 1 | | | | 1 | | | | | 1 | | | | | |
| **Låvenite** | $(Na,Ca)_2(Mn,Fe^{2+})(Zr,Ti)Si_2O_7(O,OH,F)$ | | | 1 | | | | | | 1 | | | | | | | 1 | |
| **Lepidolite** | $KLi_2Al(Si_4O_{10})(F,OH)_2$ to $K(Li_{1.5}Al_{1.5})(AlSi_3O_{10})(F,OH)_2$ | | | | | | | | | | | | | 1 | | | | |
| **Lintisite** | $LiNa_3Ti_2(Si_2O_6)_2O_2\ 2H_2O$ | | | | | | | | | | 1 | | 1 | 1 | | | | |
| **Lithiotantite** | $Li(Ta,Nb)_3O_8$ | | | | | | | | | | 1 | | | | | | | |
| **Lorenzite** | $Na_2Ti_2Si_2O_9$ | | | 1 | | | | | | 1 | 1 | | | 1 | | | | |
| **Loparite-(Ce)** | $(Na,Ce,Sr)(Ce,Th)(Ti,Nb)_2O_6$ | FUE | 1 | 1 | 1 | 1 | 1 | 1 | | | 1 | | 1 | 1 | 1 | 1 | 1 | 1 |
| **Lovdarite** | $K_2Na_6Be_4Si_{14}O_{36}\ 9H_2O$ | | | | | | | | | | | | | | 1 | | | |
| **Lucasite-(Ce)** | $(Ce,La)Ti_2(O,OH)_6$ | | | 1 | 1 | | | 1 | | | | | | | | | | |
| **Lueshite** | $NaNbO_3$ | | | 1 | | | | 1 | | | | | | 1 | | | | |
| **Magnesio-Columbite** | $Mg(Nb,Ta)_2O_6$ | | | | | | | | | | | | | 1 | | | | |
| **Mangano-Neptunite** | $Na_2KLiMn^{2+}{}_2Ti_2Si_8O_{24}$ | | | | | | | | | | | | | 1 | | | | |
| **Monazite-(Ce)** | $(Ce,La,Nd,Sm)\ PO_4$ | FUE GC | | 1 | | | | | 1 | | 1 | | | 1 | | | | |
| **Montebrasite** | $LiAl(PO_4)(OH)$ | | | | | | | | | | 1 | | 1 | | | | | |
| **Monticellite** | $CaMgSiO_4$ | FUE | | | | | | | | | | | | 1 | | | | |
| **Mosandrite-(Ce)** | $Ti(\square,Ca,Na)_3(Ca,REE)_4(Si_2O_7)_2[H_2O,OH,F]_4{\cdot}H_2O$ | | | 1 | | | | | 1 | | 1 | | 1 | | | | | |
| **Nabesite** | $Na_2BeSi_4O_{10}\ 4H_2O$ | | 1 | | 1 | | | 1 | | | | | | | 1 | | 1 | |
| **Nenadkevichite** | $Na_{6\text{-}8}(Nb,Ti)_4[(OH,O)_2 \mid Si_4O_{12}]_2{\cdot}8H_2O$ | | | 1 | | | | 1 | | | | | | | | | | |

**Table 4.** *Cont.*

| | | | | | | | | | | | | | | | | | | |
|---|---|---|---|---|---|---|---|---|---|---|---|---|---|---|---|---|---|---|
| **Neptunite** | $KNa_2Li(Fe^{2+},Mn)_2Ti_2Si_8O_{24}$ | | 1 | | | | | 1 | | | 1 | | | | | | | |
| **Niocalite** | $Ca_7Nb(Si_2O_7)_2O_3F$ | FUE | 1 | | | | | 1 | 1 | | 1 | | | | 1 | | | |
| **Niveolanite** | $NaBe(CO_3)(OH)\ 2H_2O$ | | | | | | | | | | | | | 1 | | | | |
| **Nordite-(Ce)** | $(Ce,La)(Sr,Ca)Na_2(Na,Mn)(Zn,Mg)Si_6O_{17}$ | | | | | | | | | | 1 | | | | | | | |
| **Normandite** | $NaCa(Mn,Fe)(Ti,Nb,Zr)(Si_2O_7)OF$ | | 1 | | | | 1 | | | | | | | | | | | 1 |
| **Peatite-(Y)** | $Li_4Na_{12}Y_{12}(PO_4)_{12}(CO_3)_4(F,OH)_8$ | | | | | | | | | | | | | 1 | | | | |
| **Perovskite** | $CaTiO_3$ | FUE | | | | | | | | | | | | | | | | |
| **Perrierite-(La)** | $(La,Ce,Ca)_4(Fe^{2+},Mn)(Ti,Fe^{3+},Al)_4[(Si_2O_7)O_4]_2$ | | 1 | | | | | 1 | | | | | | | | | | |
| **Perrierite-(Ce)** | $(La,Ce,Ca)_4(Fe^{2+},Mn)(Ti,Fe^{3+},Al)_4[(Si_2O_7)O_4]_2$ | | | | | | | | | 1 | | | | | | | | |
| **Petalite** | $LiAl(Si_4O_{10})$ | | | | | | | 1 | | | | | | | | | | |
| **Peterandresenite** | $Mn_4Nb_6O_{19}\ 14H_2O$ | | | | | | | | | 1 | | | | | | | | |
| **Phenakite** | $Be_2SiO_4$ | | | | | | | | | | 1 | | 1 | | | | | |
| **Pollucite** | $(Cs_{0.75}Na_{0.25})(Si_2Al)O_6{\cdot}nH_2O$ | | | | | | | 1 | | 1 | 1 | | 1 | | | | | |
| **Polylithionite** | $KLi_2AlSi_4O_{10}(F,OH)_2$ | | 1 | | | | | 1 | | 1 | | | | | | | | |
| **Priderite** | $K(Ti^{4+}{}_7Fe^{3+})O_{16}$ | | | 1 | | | 1 | | | | | | | | | | | |
| **Pyrochlore** | $(Na,Ca)_2Nb_2O_6(OH,F)$ | FUE | 1 | | | 1 | 1 | | 1 | | 1 | 1 | | | 1 | | | |
| **Rhabdophane-(Ce)** | $Ce(PO_4){\cdot}H_2O$ | GC | 1 | | | | | | | | | | | | | | | |
| **Rinkite-(Ce)** | $(Ca_3\ Ce)\ Na(NaCa)(TiNb)(Si_2O_7)_2(OF)F_2$ | | 1 | 1 | | | | | | | | | 1 | | | | | |
| **Sabinaite** | $Na_4Zr_2TiO_4(CO_3)_4$ | | | | | | | | | | | | | | 1 | | | |
| **Sazhinite-(Ce)** | $Na_2CeSi_6O_{14}(OH){\cdot}nH_2O$ | | 1 | | | 1 | | | | | | | | | | | | |
| **Scheelite** | $CaWO_4$ | | | | | | | | | 1 | | | | | | | | |
| **Schüllerite** | $Na_2Ba_2Mg_2Ti_2(Si_2O_7)_2O_2F_2$ | | | | | | 1 | 1 | | | | | | | | | | |
| **Sellaite** | $MgF_2$ | | 1 | 1 | | 1 | | 1 | 1 | 1 | | 1 | | 1 | | | | |
| **Shcherbakovite** | $(K,Na,Ba)_3(Ti,Nb)_2Si_4O_{14}$ | 1 | | 1 | | | | | | | | | | | | | | |
| **Sørensenite** | $Na_4SnBe_2Si_6O_{16}(OH)_4$ | | 1 | | | | | | | | | | | | | | | |
| **Spodumene** | $LiAlSi_2O_6$ | | | | | 1 | | 1 | | | 1 | | | | | | | |
| **Steenstrupine-(Ce)** | $Na_{14}Mn^{2+}{}_2(Fe^{3+},Mn^{3+})_2Ce_6(Zr,Th)(Si_6O_{18})_2(PO_4)_6(HPO_4)(OH)_2\cdot 2H_2O$ | | 1 | | | | | | | | | | | | | | | |
| **Stronalsite** | $SrNa_2Al_4Si_4O_{16}$ | | | | | | | | | | | | | | | | | |
| **Tainiolite** | $KLiMg_2Si_4O_{10}F_2$ | | | | | | | 1 | | 1 | | | | | | | | |
| **Tapiolite-(Fe)** | $(Fe^{2+},Mn^{2+})(Ta,Nb)_2O_6$ | | 1 | | | | | | | | 1 | | | | | | | |
| **Titanite** | $CaTiSiO_5$ | FUE GC | | 1 | | 1 | 1 | | 1 | 1 | 1 | 1 | | | 1 | | | |
| **Tsepinite-(Ca/K)** | $(Ca,K,Na)_2(Ti,Nb)_2(Si_4O_{12})(OH,O)_2{\cdot}4H_2O$ | | 1 | 1 | 1 | | | | | | | | | | | | | |
| **Tvedalite** | $(Ca,Mn)_4Be_3Si_6O_{17}(OH)_4\ 3H_2O$ | | | | | | | | 1 | 1 | | | | | | | | |
| **Vesuvianite-(Mn)** | $Ca_{19}(Mg,Mn^{2+})_2(Al,Mn^{3+},Fe^{3+})_{10}Mn^{3+}[O\mid(OH)_9\mid(SiO_4)_{10}\mid(Si_2O_7)_4]$ | FUE | | | | | 1 | | | | 1 | | | | | | | |
| **Villieaumite** | $NaF$ | | 1 | | 1 | | | | | | 1 | | | | | | | |
| **Vinogradovite** | $(Na,Ca,K)_5(Ti,Nb)_4(Si_6BeAl)O_{26}{\cdot}3H_2O$ | | 1 | | | | | | | | | | | | | | | |
| **Vuonnemite** | $Na_{11}Nb_2Ti^{3+}Si_4O_{12}(PO_4)_2O_5F_2$ | | 1 | 1 | 1 | | | | | | | | | | | | | |
| **Wadeite** | $K_2ZrSi_3O_9$ | | | | | | | | 1 | | | | | | | | | |
| **Watatsumiite** | $Na_2KLi(Mn^{2+},Fe^{2+})_2V^{4+}{}_2[Si_8O_{24}]$ | | | | | | | | | | 1 | | | | | | | |
| **Woehlerite** | $Na_2Ca_4ZrNb(Si_2O_7)_2O_3F$ | | 1 | 1 | | 1 | | | | 1 | | | | | 1 | | | |
| **Wollastonite** | $CaSiO_3$ | FUE | | | | 1 | | 1 | | 1 | | 1 | | | | | | |
| **Xenotime-(Y)** | $YPO_4$ | FUE | 1 | 1 | | 1 | | 1 | 1 | | | 1 | | | 1 | | | |
| **Zinnwaldite** | $KLiFe^{2+}Al(AlSi_3)O_{10}(F,OH)_2$ | | | | | | | | | | | 1 | | | | | | |
| **Zircon** | $ZrSiO_4$ | FUE | 1 | | 1 | 1 | 1 | 1 | 1 | 1 | 1 | 1 | | 1 | 1 | | | |
| **Zirconolite** | $CaZrTi_2O_7$ | | 1 | | | 1 | | 1 | | 1 | 1 | | | 1 | | | | |

**(b)**

| **Name** | **MnS** | **Puerto de Santiago** | **Alcala** | **San Juan** | **P. d. Paraiso** | **Los Humilladeros** | **P.d. Enramada** | **Los Abrigos** | **Centinela** | **La Mareta** | **Mt. Pelada** | **Tajao** | **B. Hondo** | **Mt. Reventada** | **Los Blanquitos** | **Poris de Abona** |
|---|---|---|---|---|---|---|---|---|---|---|---|---|---|---|---|---|
| **Alabandite** | $MnS$ | | | | | | | | | | | | | | 1 | 1 |
| **Alleghanyite** | $Mn_5(SiO_4)_2(OH)_2$ | | 1 | | | | | | 1 | | | | | | | |
| **Anglesite** | $PbSO_4$ | | | | | 1 | 1 | | | | | | 1 | | | |
| **Ankerite** | $Ca(Fe^{2+},Mg,Mn)(CO_3)_2$ | | 1 | | 1 | | | | | 1 | | | | | 1 | |
| **Ansermetite** | $MnV_2O_6\ 4H_2O$ | | | | | | | | | 1 | | | 1 | | | |
| **Name** | $Cu_3(CO_3)_2(OH)_2$ | | 1 | | | | 1 | | | | | | | | | |
| **Bixbyite** | $(Mn^{3+},Fe^{3+})_2O_3$ | 1 | 1 | | | | 1 | 1 | 1 | 1 | | 1 | | | 1 | |
| **Babingtonite** | $Ca_2(Fe^{2+},Mn)Fe^{3+}Si_5O_{14}(OH)$ | | | 1 | | | | 1 | | | | | | | | |
| **Braunite** | $Mn^{2+}Mn_6{}^{3+}O_8SiO_4$ | 1 | | 1 | | | | | | | | | | | | |
| **Bustamite** | $CaMn^{2+}Si_2O_6$ | | | | | | | | 1 | | | | | | | |
| **Caryopilite** | $Mn^{2+}{}_3Si_2O_5(OH)_4$ | | | | 1 | | 1 | | | | | 1 | | | | |
| **Cassagnaite** | $(Ca_{0.75}Mn_{0.25})_4(Fe_{0.6}Mn_{0.3}Al_{0.1})_4(OH)_4(V_{0.6}Mg_{0.3}Al_{0.1})_2(O_{0.75}(OH)_{0.25})_4(Si_3O_{10})(SiO_4)_2$ | | | | | 1 | | | | | | | | | | |
| **Cerussite** | $PbCO_3$ | | | | | | | | | | | | | | | 1 |
| **Coffinite** | $U(SiO_4)_{1-x}(OH)_{4x}$ | | | | | | | | | | | | | | 1 | |
| **Copper** | $Cu$ | | 1 | | | | | | | | | | | | | |
| **Cotunnite** | $PbCl_2$ | | | | | | 1 | | | | | | 1 | | | 1 |
| **Coulsonite** | $Fe^{2+}V_2{}^{3+}O_4$ | | | | | | 1 | | | | | | 1 | | | |
| **Cuprite** | $Cu_2O$ | | 1 | | | | | | | | | | | | | |

**Table 4.** *Cont.*

| | | | | | | | | | | | | | | |
|---|---|---|---|---|---|---|---|---|---|---|---|---|---|---|
| **Descloizite** | $PbZn(VO_4)(OH)$ | | | | 1 | 1 | | | | 1 | | | | |
| **Fairfieldite** | $Ca_2(Mn,Fe^{2+})(PO_4)_2 \cdot 2H_2O$ | | | | | | | 1 | | | | | | |
| **Fernandinite** | $(Ca_{0.6}Na_{0.3}K_{0.1})_{0.9}(V_{0.55}V_{0.3}Fe_{0.1}Ti_{0.05})_8O_{20} \cdot 4H_2O$ | | | | | 1 | | | | 1 | | | | |
| **Fervanite** | $Fe^{3+}{}_4V^{5+}{}_4O_{16} \cdot 5H_2O$ | | | | 1 | | | | | | | | | |
| **Fiedlerite** | $Pb_3Cl_4F(OH)_2$ | | | | | | | | | 1 | | | | |
| **Franciscanite** | $Mn^{2+}{}_6V^{5+}(SiO_4)_2(O,OH)_6$ | | | | 1 | | | | | | | | 1 | |
| **Galaxite** | $(Mn,Fe^{2+},Mg)(Al,Fe^{3+})_2O_4$ | | | | | | | 1 | | | | | 1 | |
| **Galenite** | $PbS$ | | | | 1 | 1 | | | | 1 | | | | 1 |
| **Gatehouseite** | $Mn_5{}^{2+}[(OH)_2 \mid PO_4]_2$ | | | | | | 1 | | | | | | | |
| **Gold** | $Au$ | | | | | | | | | 1 | | | | 1 |
| **Gravegliaite** | $Mn^{2+}(S^{4+}O_3) \cdot 3H_2O$ | | | | | | | | 1 | | | | 1 | |
| **Groutite** | $Mn^{3+}O(OH)$ | | | | | | | | | | | | 1 | |
| **Hausmannite** | $Mn^{2+}Mn_2{}^{3+}O_4$ | | | | | 1 | | | | | | | | |
| **Hewettite** | $CaV_6{}^{5+}O_{16} \cdot 9H_2O$ | | | | | | | 1 | | | | | | |
| **Hollandite** | $Ba(Mn^{4+}{}_6Mn^{3+}{}_2)O_{16}$ | 1 | | 1 | | | 1 | 1 | | | | | | |
| **Jacobsite** | $(Mn^{2+},Fe^{2+},Mg)(Fe^{3+},Mn^{3+})_2O_4$ | | | | 1 | | | | | | | | | 1 |
| **Johannsenite** | $CaMnSi_2O_6$ | | | | | | | | | 1 | | | | |
| **Karpholite** | $MnAl_2Si_2O_6(OH)_4$ | | | | | | | | | | | | 1 | |
| **Kombatite** | $Pb_{14}(VO_4)_2O_9Cl_4$ | | | | 1 | | | | | 1 | | | | |
| **Kutnohorite** | $CaMn^{2+}(CO_3)_2$ | 1 | 1 | | | 1 | | 1 | 1 | 1 | | | | |
| **Lanarkite** | $Pb_2(SO_4)O$ | | | | | | | | | 1 | | | | |
| **Laurionite** | $PbCl(OH)$ | | | | | | | | | 1 | | | | 1 |
| **Leucophoenicite** | $Mn_7(SiO_4)_3(OH)_2$ | | | 1 | | 1 | | | | | | | | |
| **Litharge** | $PbO$ | | | | | | | | | 1 | | | | |
| **Macedonite** | $PbTiO_3$ | | | | | | | | | 1 | | | | 1 |
| **Marokite** | $CaMn_2{}^{3+}O_4$ | | | | | | | | | | | | 1 | |
| **Marsturite** | $NaCaMn_3Si_5O_{14}(OH)$ | | | 1 | | | | | | | | | | |
| **Massicot** | $PbO$ | | | | | | | | | 1 | | | | |
| **Matlockite** | $PbFCl$ | | | | | | | | | 1 | | | | |
| **Magnesiocoulsonite** | $MgV_2{}^{3+}O_4$ | | | | 1 | 1 | | | | 1 | | | | |
| **Malachite** | $Cu_2(CO_3)(OH)_2$ | | 1 | | | | | | | | | | | |
| **Manganbabingtonite** | $Ca_2(Mn,Fe^{2+})Fe^{3+}Si_5O_{14}(OH)$ | | | 1 | | | | | | | | | | |
| **Manganite** | $Mn^{3+}O(OH)$ | | | | | | | 1 | | | | | | |
| **Manganogrunerite** | $\square Mn_2(Fe,Mg)_5Si_8O_{22}(OH)_2$ | | | | | | 1 | | | | | | | |
| **Medaite** | $(Mn_{0.75}Ca_{0.25})_6(V_{0.75}As_{0.25})Si_5O_{18}(OH)$ | | | | 1 | | | | | 1 | | | | |
| **Melanovanadite** | $Ca(V_2{}^{5+}V_2{}^{4+})O_{10} \cdot 5H_2O$ | | | | | | | | | 1 | | | | |
| **Mendigite** | $Mn^{2+}{}_2(Mn^{2+}{}_{1.33}Ca_{0.67})_{\Sigma 2}(Mn^{2+}{}_{0.5}Mn^{3+}{}_{0.28}Fe^{3+}{}_{0.15}Mg_{0.07})(Ca_{0.8}Mn^{2+}{}_{0.2})(Si_{5.57}Fe^{3+}{}_{0.27}Al_{0.16}O_{18})$ | | | 1 | 1 | | 1 | | 1 | | 1 | | 1 | |
| **Minasragrite** | $V^{4+}[O \mid SO_4] \cdot 5H_2O$ | | | | | | | 1 | | 1 | | | 1 | |
| **Minium** | $Pb^{2+}{}_2Pb^{4+}O_4$ | | | | | | | | | 1 | | | | |
| **Molybdenite** | $MoS_2$ | | | | | | | 1 | | | | | | |
| **Mozartite** | $CaMn^{3+}[OH \mid SiO_4]$ | | | | | | 1 | | | | | | | |
| **Namansilite** | $NaMn^{3+}[Si_2O_6]$ | 1 | 1 | | 1 | | | | 1 | | | | | |
| **Nealite** | $Pb_4Fe^{2+}(As^{5+}O_3)_2Cl_4 \cdot 2H_2O$ | | | | | | | | | 1 | | | | |
| **Olmiite** | $CaMn[SiO_3(OH)](OH)$ | | | | | | | | 1 | | | | | |
| **Paralaurionite** | $PbCl(OH)$ | | | | | | | | | | | | | 1 |
| **Pascoite** | $Ca_3V^{5+}{}_{10}O_{28} \cdot 17H_2O$ | | | | 1 | | | | | 1 | | | | |
| **Patronite** | $VS_4$ | | | | | 1 | | 1 | | 1 | | | 1 | |
| **Penfieldite** | $Pb_2Cl_3(OH)$ | | | | | | | | | 1 | | | | |
| **Phosgenite** | $Pb_2(CO_3)Cl_2$ | | | | | | | | | | | | | 1 |
| **Piemontite** | $Ca_2(Al,Mn,Fe)_3[O \mid OH \mid SiO_4 \mid Si_2O_7]$ | | | | | | | 1 | | | | | | |
| **Plattnerite** | $PbO_2$ | | | | | 1 | | | | 1 | | | | 1 |
| **Poldervaartite** | $Ca(Ca_{0.75}Mn_{0.25})(SiO_3OH)(OH)$ | | | | | | 1 | | | | | | | |
| **Pyrobelonite** | $PbMn^{2+}VO_4(OH)$ | | | | | | | | | 1 | | | | |
| **Pyrolusite** | $MnO_2$ | 1 | | 1 | 1 | | | | | | | | 1 | |
| **Pyromorphite** | $Pb_5(PO_4)_3Cl$ | | | | 1 | 1 | | | | | | | | |
| **Pyrophanite** | $MnTiO_3$ | | 1 | 1 | 1 | 1 | | 1 | | 1 | | | 1 | |
| **Pyroxferroite** | $(Fe^{2+},Mn,Ca)SiO_3$ | | | | | | 1 | | | | | | 1 | |
| **Pyroxmangite** | $Mn^{2+}SiO_3$ | | | | | 1 | 1 | | | 1 | | | | |
| **Ramsdellite** | $MnO_2$ | | 1 | | | | | | | | | | | |
| **Rancieite** | $(Ca,Mn^{2+})_{0.2}(Mn^{4+},Mn^{3+})O_2 \cdot 0.6H_2O$ | | | | | | 1 | | | | | | 1 | |
| **Reppaite** | $Mn^{2+}{}_5(VO_4)_2(OH)_4$ | | | | 1 | | | | | | | | 1 | |
| **Rhodochrosite** | $Mn(CO_3)$ | | | | | | | | | | | | 1 | |
| **Rhodonite** | $CaMn_3Mn[Si_5O_{15}]$ | | | | | 1 | 1 | 1 | | | | | | |
| **Ribbeite** | $(Mn^{2+},Mg)_5(SiO_4)_2(OH)_2$ | | | | | | 1 | 1 | | | | | | |
| **Ronneburgite** | $K_2Mn^{2+}[V_4O_{12}]$ | | | | 1 | | | | | | | | | |
| **Saneroite** | $Na_2(Mn_{0.75}Mn_{0.25})_{10}Si_{11}VO_{34}(OH)_4$ | | | | 1 | | | | | | | | | 1 |
| **Schäferite** | $\{Ca_2Na\}[Mg_2](V^{5+}{}_3)O_{12}$ | | | | 1 | | | | | 1 | | | | |
| **Schubnelite** | $Fe_{2-x}{}^{3+}(V^{5+},V^{4+})_2O_4(OH)_4$ | | | | 1 | | | | | | | | | |
| **Serandite** | $NaMn^{2+}{}_2Si_3O_8(OH)$ | 1 | 1 | 1 | 1 | | 1 | 1 | 1 | 1 | | | | |
| **Shigaite** | $NaMn_6{}^{2+}Al_3[(OH)_{18} \mid (SO_4)_2] \cdot 12H_2O$ | | | | | | 1 | | | | | | | |
| **Sincosite** | $Ca(VO)_2(PO_4)_2 \cdot 4H_2O$ | | | | 1 | 1 | | | | | | | | |
| **Sonolite** | $Mn_9(SiO_4)_4(OH,F)_2$ | | | | | | 1 | | | | | | | |
| **Stanleyite** | $V^{4+}[O \mid SO_4] \cdot 6H_2O$ | | | | | | | | | 1 | | | | |

**Table 4.** *Cont.*

| Name | Composition | Teide | Vilaflor | Riokar | Puerto de Santiago | Alcala | Playa San Juan | Playa de Enramada | Centinela | Los Blanquitos | Mt Pelada | Tajao | Bar. Hondo | Palm Mar | San Juan de la RamblaRambla |
|---|---|---|---|---|---|---|---|---|---|---|---|---|---|---|---|
| Stolzite | $PbWO_4$ | | | | | | | | | | | 1 | | | |
| Sursassite | $Mn_2^{2+}Al_3(SiO_4)(Si_2O_7)(OH)_3$ | | | | | 1 | | | | | | | | | |
| Tephroite | $Mn_2SiO_4$ | | | | | | | 1 | | | 1 | | | | |
| Thorianite | $ThO_2$ | | | | | | | | | | | | | 1 | |
| Thorikosite | $Pb_3(Sb^{3+},As^{3+})O_3(OH)Cl_2$ | | | | 1 | | | | | | | 1 | | | |
| Thorite | $ThSiO_4$ | | | | | | | | | | 1 | | | 1 | |
| Thorogummite | $Th(SiO_4)_{1-x}(OH)_{4x}$ | | | | | | | | | | | | | 1 | |
| Tinzenite | $Ca_2Mn^{2+}{}_4Al_4[B_2Si_8O_{30}](OH)_2$ | | 1 | | | 1 | | 1 | | | | | | | |
| Tiragalloite | $Mn_4^{2+}As^{5+}Si_3O_{12}(OH)$ | | | | | | | | | | | | | 1 | 1 |
| Tweddilldilldildite | $CaSr(Mn^{3+},Fe^{3+})_2Al[O \mid OH \mid SiO_4 \mid Si_2O_7]$ | 1 | | | | | | | | | | 1 | | 1 | |
| Ungarettiite | $(Na,K)Na_2(Mn^{2+},Mg)_2Mn_3{}^{3+}[O \mid Si_4O_{11}]_2$ | | | | | | | 1 | | | | | | | |
| Vanadinite | $Pb_5(VO_4)_3Cl$ | | | | 1 | | | | | | | | | | |
| Vanalite | $NaAl_8V^{5+}{}_{10}O_{38}\cdot 30(H_2O)$ | | | | | | | | | | | 1 | | | 1 |
| Vuorelainenite | $(Mn^{2+},Fe^{2+})(V^{3+},Cr^{3+})_2O_4$ | | | | | | | | | | | 1 | | | |
| Yofortierite | $Mn^{2+}{}_5Si_8O_{20}(OH)_2\cdot 7H_2O$ | | | 1 | | | | | | | | | | | |

(c)

| Name | Composition | Teide | Vilaflor | Riokar | Puerto de Santiago | Alcala | Playa San Juan | Playa de Enramada | Centinela | Los Blanquitos | Mt Pelada | Tajao | Bar. Hondo | Palm Mar | San Juan de la RamblaRambla |
|---|---|---|---|---|---|---|---|---|---|---|---|---|---|---|---|
| Analcime | $Na(Si_2Al)O_6\cdot H_2O$ | 1 | 1 | 1 | 1 | 1 | | | | 1 | 1 | | 1 | | |
| Chabazite-(Ca) | $Ca(Si_4Al_2)O_{12}\cdot 6H_2O$ | | | | 1 | | 1 | | | | 1 | 1 | | | |
| Chabazite-(Na) | $(Na,K,Ca)_2(Si,Al)_6O_{12}\cdot 6H_2O$ | | | | 1 | | 1 | 1 | | | | | | | |
| Clinoptilolite-(Ca) | $Ca_3(Si_{30}Al_6)O_{72}\cdot 20H_2O$ | | | | | | | | | | 1 | | | | |
| Clinoptilolite-(Na) | $Na_6(Si_{30}Al_6)O_{72}\cdot 20H_2O$ | | | | 1 | | | | | | 1 | | | | |
| Gonnardite | $(Na_{0.75}Ca_{0.25})_2(Si_{0.75}Al_{0.25})_5O_{10}\cdot 3H_2O$ | 1 | | | | | | | | | | | | 1 | 1 |
| Heulandite-(Na) | $(Na,Ca)_6(Si,Al)_{36}O_{72}\cdot 24H_2O$ | | | | 1 | | | 1 | | | | | | | |
| Laumontite | $Ca(Si_4Al_2)O_{12}\cdot 4H_2O$ | | | 1 | | | | | 1 | | | | | | |
| Natrolite | $Na_2(Si_3Al_2)O_{10}\cdot 2H_2O$ | 1 | | | 1 | 1 | 1 | | 1 | | | | | | 1 |
| Offretite | $KCaMg(Si_{13}Al_5)O_{36}\cdot 15H_2O$ | | | | | 1 | | | | | | | | | |
| Phillipsite-(Ca) | $Ca_3(Si_{10}Al_6)O_{32}\cdot 12H_2O$ | | | | 1 | | | | | | 1 | 1 | | | |
| Phillipsite-(Na) | $Na_6(Si_{10}Al_6)O_{32}\cdot 12H_2O$ | | | | 1 | | | | 1 | | | 1 | | | |
| Stilbite-(Ca) | $(Ca_{0.5},Na,K)_9(Si,Al)_{36}O_{72}\cdot 28H_2O$ | | | | 1 | | | | | | | | | | |
| Stilbite-(Na) | $Na_9(Si_{27}Al_9)O_{72}\cdot 28H_2O$ | | | | 1 | | | | | | | | | | |
| Thomsonite-(Ca) | $NaCa_2(Al_5Si_5)O_{20}\cdot 6H_2O$ | | | | 1 | | 1 | | | | | | | | |

GO = La Gomera, GC = Gran Canaria, FUE = Fuerteventura, 1 marks presence at sampling site.

The major proportion of zirconium and hafnium has been derived from the exploitation of marine zircon placer deposits, which resulted from the erosion of metamorphic and magmatic rocks and the reworking of older sediments rife with zircon (part b of Table 3). Gem-quality zircon hyacinth originated from deeply weathered alkali basalts and is exploited in SE Asia [28]. It is found in terrains where primary Zr deposits are situated ((Li-Zn-Th-F-Nb-Ta)-Be-REE-Zr-bearing pegmatites and Zr-REE-P-Nb-Ta-F-(Be-Th) carbonatite-alkaline igneous complexes) (part b of Table 3). The most well-known deposit of that kind is the Strange Lake pegmatite, Canada, a (Li-Zn-Th-F-Nb-Ta)-Be-REE-Zr pegmatite-aplite in alkaline magmatic rocks [29–31] published a hydrothermal mobilization model of this peralkaline magmatic system, which led to the concentration of F and Zr at temperatures around 250 °C, whereas the REE were mobilized by saline HCl-bearing fluids at higher temperatures, around 400 °C. In peralkaline miaskitic rocks, Zr and Hf are incorporated in minerals like zircon, sphene and ilmenite, whereas in agpaitic varieties, these elements form complex Na-(Zr, Ti)-silicates. In the Chuktukon alkaline carbonatite complex, Russia, aillikite–damtjernite and carbonatite give way to Zr, Nb and REE mineralization [32]. These carbonatites may reap the benefit from the presence of zircon being the principal target mineral for the common U/Pb dating [33]. Zirconium-bearing minerals hosted either by carbonatites or pegmatites manifest an ensimatic origin as is common in rift systems like the present one.

### *2.3. Fluorine—Mineral Deposits and Their Origin*

Fluorine deposits occur in two magmatic environments, in fluorite deposits related to U-REE carbonatites and alkaline intrusive rocks, as well as in pegmatite-hosted F-(Sc) deposits (part c of Table 3). The experimental results of [34] showed that 8 wt.% fluorine lowers the minimum melting and liquidus temperatures to a similar extent to that of very large amounts of water and can thereby account for the intrusion and the ascent of carbonatites and a wealth of F-bearing minerals and deposits in these special magmatic rocks. Carbonatite magma rising adiabatically will solidify at depth in association with alkalic rocks and intensive fenitization [9]. Fluorite deposits genetically related to carbonatites are mined at Amba–Dongar in Gujarat State, India, at Okurusu, Namibia, Speewah, Australia, Snowbird, Montana, USA, and Rock Canyon Creek, Canada [35,36].

Fluorine deposits in pegmatites are not very common. The pegmatite at Crystal Mountain in Montana, USA, is an example of it and of the enrichment in Be (euclase) and in thortveitite (Sc), as is the case for Sn-bearing leucogranites at East Kempville, Canada [37]. A F-bearing pegmatite warrants particular attention. It is the F-REE-Li vein-type granite pegmatite which is associated with rare HREE minerals such as xenotime-(Y) and gagarinite-(Y) (part c of Table 3). It forms part of the Madeira world-class Sn-Nb-Ta-cryolite deposit at the Pitinga mine [38].

### *2.4. Lithium—Mineral Deposits and Their Origin*

Lithium, one of the most looked-for mineral commodities in energy storage, is found in two principal types of deposits, "soft-rock Li deposits" and "hard-rock Li deposits". Soft-rock Li, also known as low-grade–large-tonnage deposits are synonymous with the sediment-hosted monometallic Li concentrations in playa lakes, e.g., Salar de Atacama, Salar de Maricunga, Chile, and Salar de Hombre Muerto, Bolivia, as well as geothermal and oil-field formation waters (part d of Table 3). Hard-rock Li concentrations are encountered in polymetallic high-grade–low-tonnage pegmatitic and granitic rocks such as Bessemer City, USA, Greenbushes, Australia, and Bikita, Zimbabwe. Normally, these pegmatitic deposits are exploited for Nb and Ta and the light metals Li, Rb and Cs are only found as a byproduct (Bernic Lake, Canada, Manono-Kitotolo, DR Congo). The Li-Cs-(Rb) pegmatite, Bikita, Zimbabwe, is, besides Bernic Lake (Lac-du-Bonnet), Canada, the only site where another alkaline element rubidium was accumulated at such a high level so as to make its recovery from ore feasible [39]. Late Paleozoic, lithium-bearing pegmatites extend from Germany into the Czech Republic and Poland with lepidolite, amblygonite and triphylite pegmatites around Pleystein-Hagendorf, Germany, Rožná and Dobrá Voda, Czech Republic, and are also found across the Atlantic Ocean in their contemporaneous geodynamic sites [21,40].

There is little known about Li in carbonatites and only one mineral, tainiolite, has been described from soviet-containing xenoliths of ijolite, syenite and fenitized granite from the Dicker Willem, Namibia, and in carbonatites of the Haast River Area, New Zealand, a lamprophyre-dominated dyke swarm, introduced into country rock schists around 25 to 21 Ma [41] (part a of Table 4).

### *2.5. Niobium-Tantalum—Mineral Deposits and Their Origin*

Calc-alkaline and alkaline pegmatites both give way to Sn–Ta–Nb–Sc mineralization. The zoned Tanco pegmatite at Bernic Lake, Canada, is one of the main producers of Ta in the world. The occurrence resembles that of lithium, mentioned in Section 4.4, such as the Sn–Ta-Nb deposits of Manono-Kitotolo, DR Congo, the Be–Li–Ta–Nb–REE–U pegmatites of the Alto Ligonha province, Mozambique, or smaller similar deposits in the Variscan Fold Belt [42–44]. The pegmatite-related Nb-Ta deposits are also known by the term COLTAN that refers to the common Nb-Ta s.s.s. columbite–tantalite in the pegmatite ore [21]. In contrast to the pegmatite-related Nb-Ta concentration, equivalent ones related to alkaline magmatic complexes and carbonatites show pyrochlore-dominated concentric shell-type intrusions. Pyrochlore-dominated deposits developed geodynamically in a stable craton and platform setting. Their venting processes along deep-seated lineamentary fault zones,

in rift structures and grabens are characterized by mineral assemblages with phosphate, vermiculite, fluorite, barite, and zircon, and ore minerals accommodating Th, U, REE, Nb, Ta and Ti in their crystal lattice [21]: St. Honore, Canada; Lovozero Complex, Russia; Araxa, Brazil; Chilwa-Province, Malawi; and Lueshe and Bingo; DR Congo. The lithology of their host rocks ranges from calciocarbonatite (sovite) to ferro-carbonatites. Another type of Nb deposit bound to alkaline magmatic rocks stands out by its niobian-perovskite laccolites.

The world's largest laccolitic alkaline magmatic complex at Lovozero, Russia, resulting from a multistage process, contains Nb ore in seams of varying thickness and made up of pyrochlore, loparite (Nb-Ta-REE perovskite), murmanite, lomonosovite, eudialyte, lorenzenite and pyrochlore [45,46].

### *2.6. Rare Earth Elements (REE)—Mineral Deposits and Their Origin*

The REE-P-Nb-Ta-F-(Be-Zr-Th) deposits which are related to effusive, intrusive, and carbonatitic magmatic rocks are the most common host rocks for these rare elements [47] (part f of Table 3). Their host rocks are very different in their lithological aspects, including Calcitic (sovite), dolomitic (beforsite), ankeritic carbonatites (ferro-carbonatite). Some of these carbonatite-hosted deposits prevalently exploited for REE are located at Sarfartôq and Qaqarssuk, Greenland, Mount Weld and Nolans Bore, Australia, and Hoidas Lake, Canada. The Elisenvaara REE-P-Ti deposit in Karelia, Russia, is hosted by alkaline and peralkaline syenites and pertains to the REE-P-Ti deposits typical of alkaline igneous complexes. The REE-U-Nb-bearing pegmatites pass into intragranitic deposits with Mo-W-U-Be. The Radium Hill REE-U deposit, South Australia, is a reference example of one of the few felsic REE deposits with uranium, leading to the refractory Ti-Fe-U-REE mineral davidite.

The term rare earth elements is not only a misnomer in terms of the metals' crustal abundance but also in terms of minerals accommodating REE into their crystal lattice. [48] listed about 200 rare earth minerals attributed to a great variety of categories in terms of crystal classes as well as anions (part a of Table 4). This is also true as far as the associated elements of economic interest with which they share the same mineralization or mineral deposit are concerned (part a–f of Table 3). This is all found in the world's largest source of REE, the giant but still enigmatic REE-Nb-P-F-bearing hydrothermal iron deposit at Bayan Obo (Baotou), China. It is also the largest fluorite deposit of one of its "byproducts" due to high quantities of Fe, P, and Nb while missing significant U and base metal contents. Its genetic attribution to the frequently used Fe-oxide Cu–Au type is fraught with difficulties [49–54]. In addition to the metals mentioned above, there are complex hydrothermal and metasomatic processes accumulating gold and iron that are associated with slates, carbonatitic, skarnoid, and dolomitic marble host rocks. The age dating of the ore bodies, which are of stratiform, vein, and dissemination type, yielded a wide range concluded from bastnäsite and riebeckite, and REE-F carbonates and aeschynite covering the time span from 1350 Ma to 450 Ma [55–57].

The common denominator of all these REE mineralizations is their close spatial relationship to rifting marked by large-scale, intra-plate fractures, and grabens in the continental lithosphere and less frequently in oceanic environments. This geodynamic features form the tie line to the Canary Island Archipelago, Spain, with the Isle of Tenerife forming the largest volcanic island of this archipelago.

## 3. The Geological Setting of the Isle of Tenerife, Spain

The Isle of Tenerife is the largest island and the "heart" of the Canary Islands Archipelago, as can be deduced from the volcano-geodynamic map depicting the various stages of the evolution of the volcanic islands with the age of formation decreasing from East to West (Figure 2) [12]. The largest island of the Archipelago is made up of three basement areas (shield stage), Roque del Conde (11.0 to 3.5 Ma), Teno (6.7 to 4.5 Ma), and Anaga Massifs (>6.5 to 3.3 Ma), with the younger Teide Volcano in the center of the rift triple junction (Figure 2) [58–62]). The Canary Island Archipelago is a marine hotspot area in front of the African continent [11,13,63,64]. The most recent study heralding the complex and

polygenetic evolution of the hotspot island under consideration has been published by [65] (Figures 2 and 3).

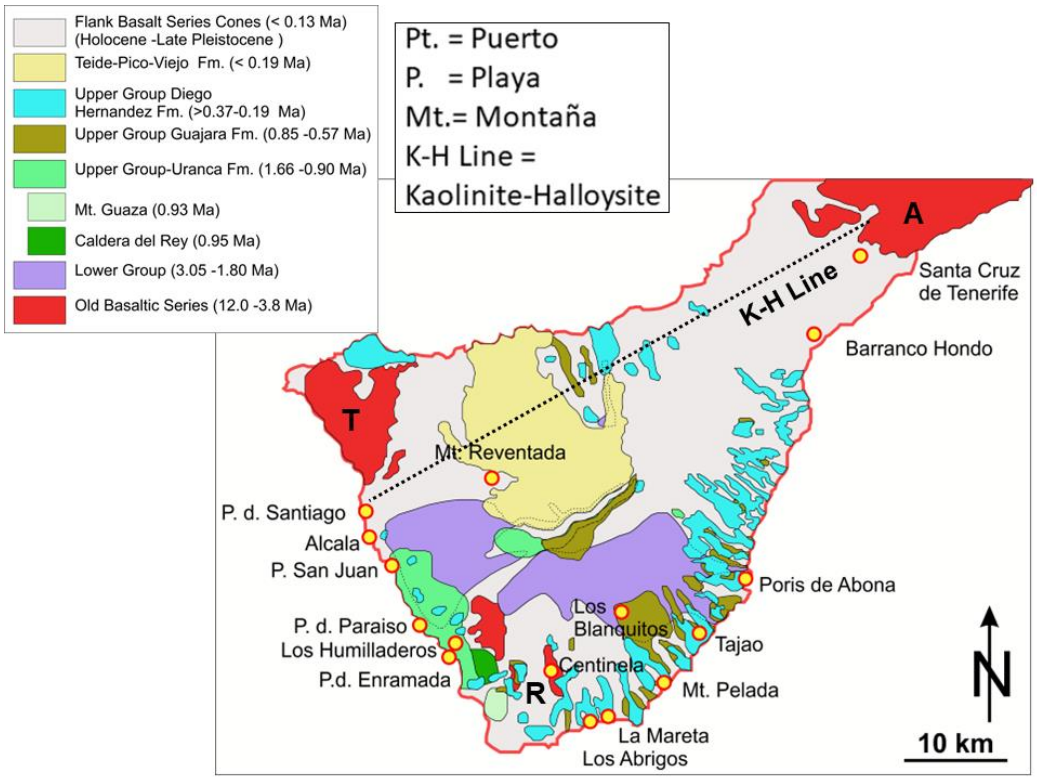


**Figure 3.** The polygenetic evolution of Tenerife, Spain, (modified from [65]); the sampling sites of critical elements are given by the yellow dots framed in red.

## 4. Geomorphology and Lithology of Rare Mineral Host Rocks as an Exploration Tool

### *4.1. From the Common to the Unconventional Exploration*

It is common practice in geochemical exploration to subdivide this method into two different subsections according to the type of anomalies targeted. In lithochemical exploration, geochemical anomalies are caused by primary processes when an ore deposit is emplaced under high T and P conditions in different types of country rocks, and surrounded by reaction zones between ore and country rock. In the first-mentioned type drill cores, drill cuttings and rock chips are shipped to the laboratory for chemical analysis.

Geochemical anomalies may also be due to secondary processes when an ore deposit is exposed to weathering and erosion and the constituent minerals and trace elements are dispersed and transported downstream into lakes or the sea by rivers, mass wasting and aeolian processes. In the second case, weathering and erosion of the hard rocks and transport of the unconsolidated rocks lead to different sample types: (1) clastic sediments (e.g., stream sediments, placers, heavy minerals concentrates); (2) soil samples; (3) water samples; (4) soil gas (headspace gas exploration), e.g., Rn, He; and (5) floral remains. The geochemical exploration method implies a systematic sampling and analyses of inorganic and organic natural material to detect anomalous concentrations of elements derived from mineral deposits. The concentrations of elements are plotted on maps and contoured at different intervals showing the element contents to distinguish anomalous areas from barren grounds as shown by many publications in geochemistry, with a few of these papers being cited here for reference [66–68]. Excluding the heavy mineral analysis, no or only little information be deduced from the data about the origin of the targeted mineral deposits [69–76].

This unconventional exploration method presented for the first time is more complex, indeed. As a prerequisite, it needs skillful "samplers" endowed with a wide variety of

knowledge and experience in geomorphology, sedimentology and, last but not least, economic geology and mineralogy. But the user of this technique reaps the benefit of obtaining an overview of what is going on at depth under high P-T conditions concomitantly under near-ambient physical–chemical conditions. Every mineral can tell a story about how it might have formed and, based upon its chemical composition, a (semi) quantitative approach can also be taken to delineate anomalous areas and account for their origin (Figures 3 and 4, Table 4). In the succeeding subsection, sampling is consequently followed up from the small scale (landscape) to the large scale (mineral and its chemical composition) (Figure 4a–c, part a,b of Table 4).

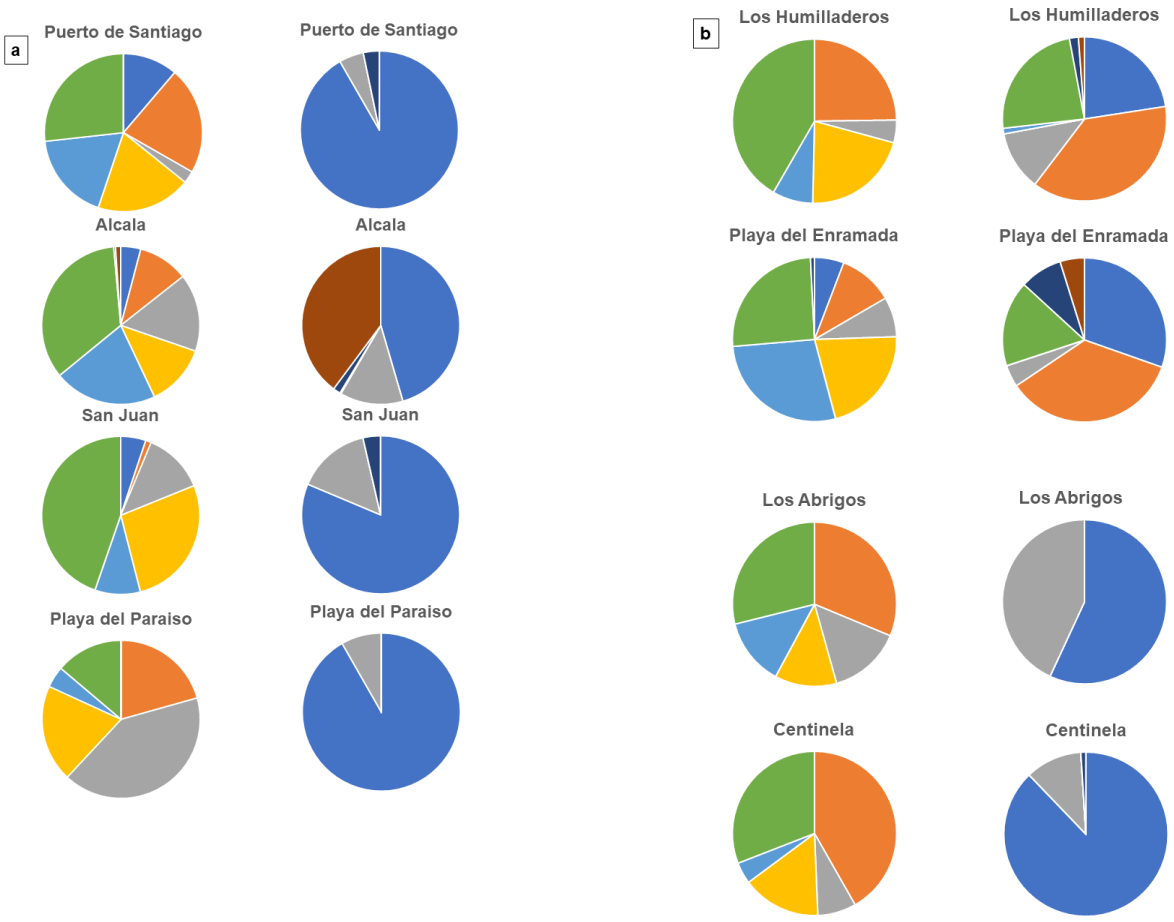


**Figure 4.** *Cont.*

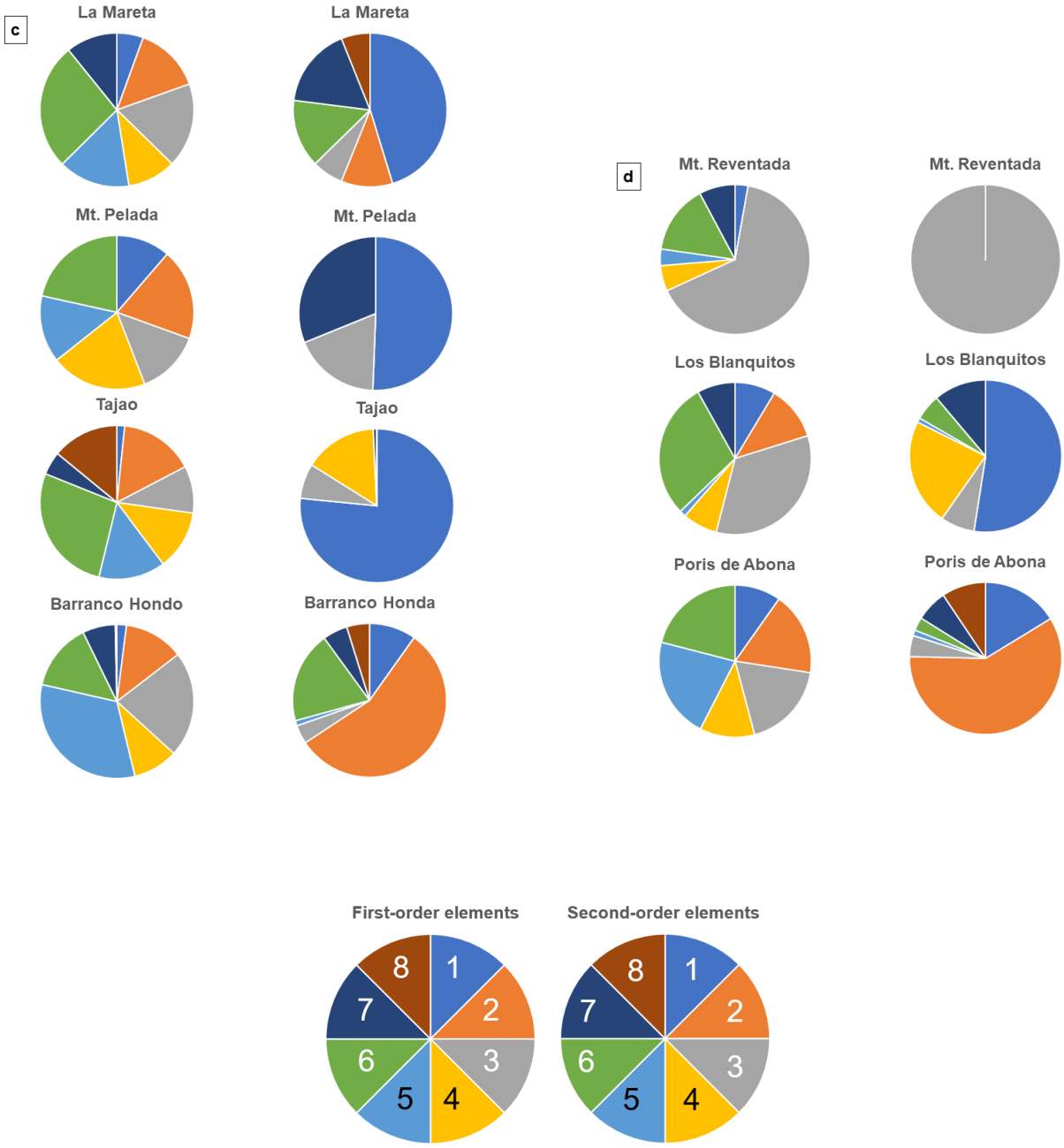


**Figure 4.** Rare elements of the first and second-order mineral assemblages at the various sites. (**a**) Puerto de Santiago, Alcala, San Juan, Playa del Paraiso. (**b**) Los Humilladeros, Playa del Enramada, Los Abrigos, Centinela. (**c**) La Mareta, Montaña Pelada, Tajao, Barranco Hondo. (**d**) Montana Reventada, Los Blanquitos, Poris de Abona plus legend: First-order elements (1) Be, (2) Zr, (3) F, (4) Ti, (5) Nb, (6) REE+Y, (7) Li+Cs, (8) Sn-W, Second-order elements (1) Mn, (2) Pb, (3) Fe, (4) U+Th, (5) As+Sb, (6) V, (7) S+B, (8) Cu+Zn+Mo+Au.

### *4.2. Landforms Hosting Critical Elements and Rare Minerals*

Reading the landscape that truncates the different volcanic and volcaniclastic bedrocks of the rare mineral occurrences enables geoscientists during this unconventional way of exploration to contour the shape of the body or structure at depth held accountable for the mineralization on the surface. It is most important to determine whether the landscape is made up predominantly of sculptural (Figure 5a–e) or structural landforms (Figure 5f) (Tables 1, 2 and 5). The major control on the shape and the outward appearance of structural landforms is exerted by endogenous forces (magmatism, tectonic, hypogene alteration),

mainly under higher pressure and/or temperature. Cinder cones, volcanic craters, domes, necks and plugs or lava lobes are attributed to this group of structural landforms. Structural landforms *sensu stricto* only occur in their *statu nascendi* such as a lava flow being quenched and starting to consolidate—see the Cumbre Vieja lava flowing into the Atlantic Ocean and forming some kind of volcano-sedimentary delta on September 2021 [77]. The older these structural landforms are, the more they are converted into a series of sculptural landforms and, on a small scale, into a landscape shaped by the climatic conditions. This transformation process occurs mainly via mass wasting (talus creep grading into sliding blocks, unconfined mass flows, volcaniclastic debris veneers boulder-strewn tops and upper hill slopes, triangular hill slopes (parautochthonous flatirons)). They are substituted by passing fluvial drainage systems, from rills and gullies to a full-blown drainage system, or, near the seaside, to coastal landforms when the gravitational processes becomes wetter and wetter (Figure 5a–e).

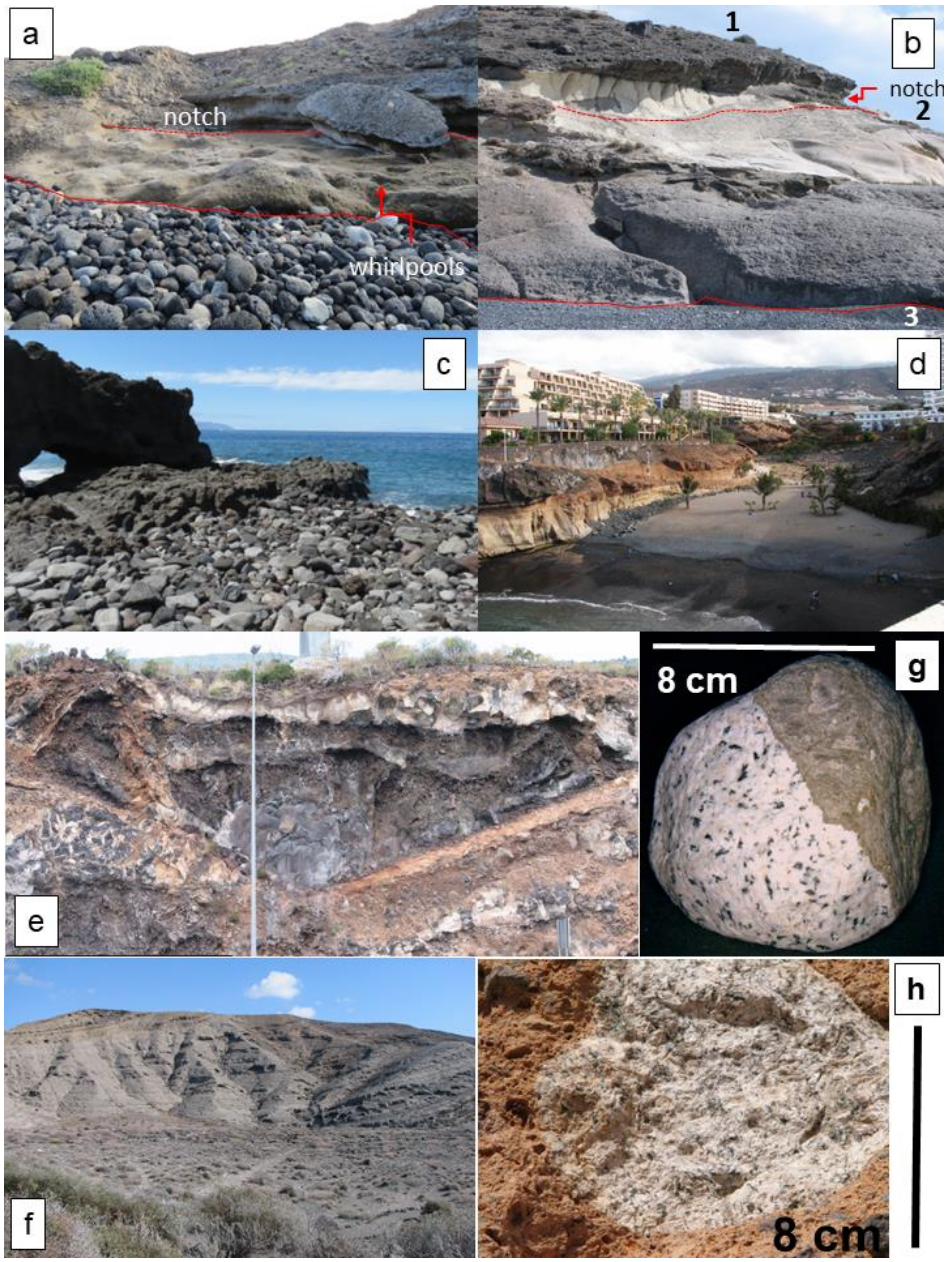


**Figure 5.** Landforms of sampling sites on the Isle of Tenerife, Spain (**a**) A wave-cut scarp with uplifted terrace and a gently seaward plunging erosional terrace bosselated with whirlpools passing along

a minor step into the recent depositional shore zone. The cliff was sculptured out of the Abrigo Ignimbrite. Locality: Alcala. (**b**) Linear cliff coast with shore zone (backshore plus foreshore) entirely made up of well-rounded volcanic gravel clasts with a staircase-like arrangement of three erosional and depositional terraces. The upper erosional terrace No. 2 has been dissected by modern coastal erosion caused by coastal and linear erosion of local drainage systems. The cliff of different slope angles formed in the Enramada Formation overlying the Morteros Formation. Locality: Playa del Enramada. (**c**) Wave-cut platform exposing volcanic rocks and providing host to the gravelly lithoclasts of the Adeje and San Juan Formations. The rocky coast shows remnants of a cliff retreat in form of caves and arches and protruding buttresses. Locality: Puerto de Santiago. (**d**) A linear volcanic–volcaniclastic shoreline coast is interrupted by a fluvial volcanic point-source coast representing the funnel-shaped mouth of the Barranco de las Galgas at Playa de Paraiso. A prominent traverse gravel bar marks the transition from the fluvial and mass wasting dominated barranco towards the sea. (**e**) Cross section through a channel filled with lava and pyroclastic flow deposits in a fluvial drainage system of Barranco Hondo. See pylon in the center of image for scale. (**f**) A typical structural landform, the morphology of which is primarily controlled by the endogenous eruptive forces. The outward appearance of this cone-shaped and well-bedded volcanic edifice is a smaller replica of its brethren Mt. Teide. Locality: Mt. Pelada. (**g**) Well-rounded beach gravel preserving the contact zone between syenite (white) and pyroclastic rock (brown) from the foreshore of Mt. Pelada (**h**) Syenite xenolith included in an ignimbrite matrix of the Morteros Formation at outcrop near Playa de la Enramada.

**Table 5.** Sculptural and structural volcanic landforms and their bedrocks (see also Figure 5).

| Geomorphology | Coastal Marine (CM) | Mass Wasting (MW) | Fluvial Drainage (FD) |
|---|---|---|---|
| Sampling sites | 1. Pto. d. Santiago<br>2. Alcala<br>3. San Juan (MW)<br>4. Pl. d. Paraiaso<br>6. Pl. d. Enramada | 7. Los Abrigos<br>8. Centinela<br>9. La Mareta<br>10. Mt. Pelada (CM)<br>11. Tajao<br>13. Mt. Reventada<br>14. Los Blanquitos<br>15. Poris de Abona | 5. Los Humilladeros<br>12. Barranco Hondo |
| Lithology | 1. Basanite, trachyte, foid-bearing monzodiorite/gabbro<br>2. Nepheline syenite, phonolite<br>3. Nepheline syenite, syenite, phonolite, foid-bearing monzodiorite/gabbro<br>4. Nepheline-syenite, trachyte, phonolite<br>6. Phonolite, tephrite, basanite | 7. Nepheline-syenite<br>8. Nepheline syenite, trachyte, phonolite<br>9. Syenite<br>10. Nepheline-monzodiorite<br>11. Phonolite<br>13. Foid-bearing monzodiorite/gabbro<br>14. Phonolite<br>15. Trachyte, phonolite | 5. Syenite<br>12. Foid-bearing monzodiorite/gabbro |

Pl. = Playa, Pto. = Puerto, Mt. = Montaña.

*Coastal landforms*: It goes without saying that in an archipelago like the Canary Islands, the coastal landforms play a significant part, not to say the most significant one (Figure 5a–d). The majority of cases present a rocky coast with steeply dipping wave-cut scarps and uplifted terraces gently dipping seaward. The erosional terraces are bosselated with whirlpools passing along minor steps in the recent narrow gravel-strewn depositional shore zone (Figure 5a). The linear shore zone (backshore plus foreshore) frequently shows a staircase arrangement of erosional and depositional terraces as a consequence of sea level changes (Figure 5b). Where the shore zone is under retreat, a wave-cut horizontal platform occurs scattered with gravelly lithoclasts (Figure 5c). The aforementioned landform series are linear siliciclastic shorelines, representative of a self-sufficient shore fed with lithoclasts to the littoral zone mainly by fall processes of mass wasting. Using volcanic flow deposits as guidelines, such a linear volcanic–volcaniclastic shoreline coast is interrupted by a fluvial volcanic point-source coast representing an introduction into the coastal zone and its lithoclasts reworked in a traverse gravel bar (Figure 5d). These estuarine fluvial–coastal landforms are the only one where a mixture of sand-sized mineral matter and gravelly lithoclasts occur side by side with each other.

*Mass wasting and fluvial landforms*: Barrancos (V-shaped deep gorges) are quite common and run subparallel to the volcanic and pyroclastic flow deposits. As ephemeral drainage systems, the channels are chocked with lithoclasts and only a small-sized fraction arrives to the coastal traps (Figure 5d,e). In the zone under consideration, gravity-driven landforming processes are mainly of the fall type (Figure 5d).

There are other landforms such as coastal dunes at Fuerteventura and Gran Canaria or lacustrine lands such as at La Gomera. They have only a minor local impact relative to the aforementioned ones and referred to here only for the sake of completeness. Every sculptural landform can be transformed into another structural landform when, after a period of volcanic quiescence, a new eruption takes place.

*Structural landforms*: Almost all near-shore lava deposits re-shaped by mass wasting and maritime processes still have some features of the well-preserved primary structural landforms. The most outstanding structural landforms are the cone-shaped volcanic edifices a replica of the Teide volcano (Figure 5e).

The landform is decisive regarding the delineation of the hidden magmatic body at depth when lithoclasts are encountered as xenoliths or marine and fluvial gravel has been released from the solid bedrock (Figure 5g,h). These sedimentological and geomorphological processes forming the landscape are targeted by a terrain analysis which is less compositional (mineralogy, petrography) than the current one and dealt with in a publication of its own. What this terrain analysis and landscape studies are based upon can be deduced from some comprehensive papers which have been used as a geoscientific platform [78–82].

### *4.3. From the Host Rock Lithology to the Mineral Texture*

In Table 5, the host rock lithologies are listed for every sampling site. As far as the coarse-grained igneous rocks are concerned, host rock lithologies straddle the A-P tie line in the double triangular diagram of [83,84] with most mineralogical compositions plotting in the foid-bearing territory, e.g., nepheline syenites, foid-bearing monzodiorite and gabbros (Figure 5g,h). There are also some finer-grained and porphyritic volcanic rocks such as porphyritic bassanites, trachytes and phonolites dependent upon the plagioclase-alkali feldspar ratio (Figure 6a,b). Many of them are intensively altered and may give way to first-order (Be, Zr, F, Ti, Nb, REE, Y, Li Cs, Sn and W) or second-order minerals (Mn, Pb, Fe, U, Th, As, Sb, V, S, B, C, Zn, Mo and Au) (Figure 4a,b).

The various lithologies are exposed in road cuts, in barrancos intersecting the lobes of lava flows, and in channelized pyroclastic flow deposits. The marker minerals occur among others in ignimbrites as xenoliths or as gravel covering the beach platforms (Figure 5g,h). Among these lithologies, the most promising target lithologies are the pyroclastic flow deposits, exemplified by the Abrigo Ignimbrite, which may contain xenoliths rife with rare minerals (Figures 5h and 7a, Table 4).

Not much scientific literature dealing particularly with the REE minerals and their associated minerals has been published about this area [2,85–90]. This is also valid for the categorization of the paragenetic associations and the characterization of textural types that have not yet been achieved in the region. The morphological analysis bridges the gap between the host rocks treated above and the compositional investigation of the 232 marker minerals, plus 15 zeolite species, and 7 clay minerals, plus boehmite in the succeeding sections (Table 4). Five textural types are established in the gravel-sized fragments of the marine and continental landforms.

*Mineral texture 1:* Radial oriented to palisade-shaped prismatic growth textures are rather rare and were only encountered in Centinela and the Barranco Hondo (Table 4). The basic minerals are Ca-silicates such as vesuvianite, grossularite and diopside with cuspidine and bixbyite (Figure 7b). They are encountered in the foid-bearing monzodiorite/gabbro clan widely exposed in the deeply eroded Miocene shield volcano stage. The texture results from high-temperature contact—from metamorphic to metasomatic processes.

*Mineral texture 2:* Granular and disseminated textures where the mineral constituents are randomly distributed are common to syenites of different grain size (Figure 7c). These syenitic xenoliths are found as armored relics among others in ignimbrites of the Morteros Fm. at outcrop at the Playa de la Enramada which is dated to have formed in the period 1.84 to 1.66 Ma ago [65]. They feature replacement textures of primary bastnaesite with perrierite-(Ce). Frequently, the REE minerals and their accompanying ones are disseminated in a medium- to coarse-grained syenitic matrix.

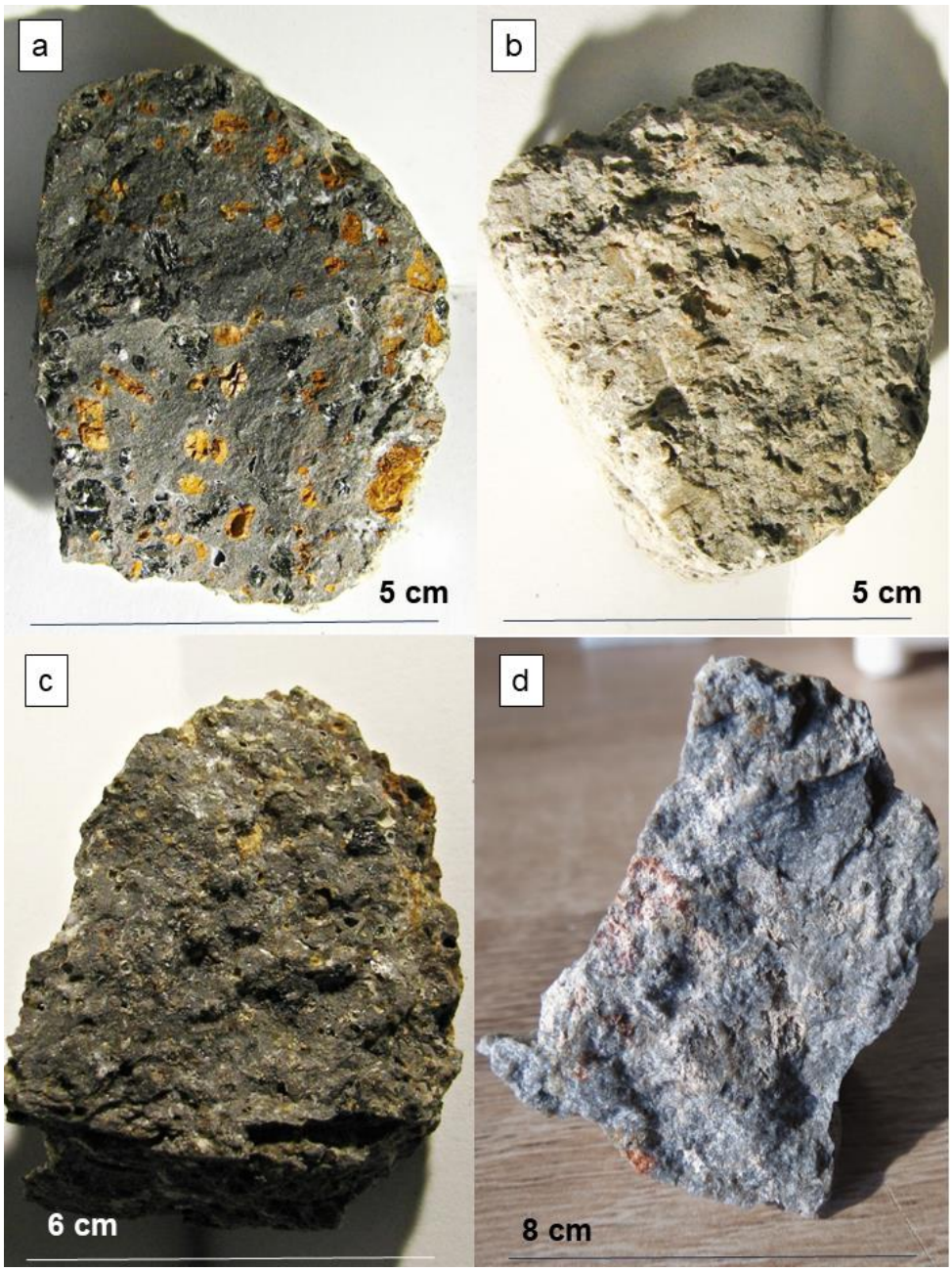


**Figure 6.** Host rock lithologies of rare minerals in hand specimen. (**a**) Altered basanite from the Playa de la Enramada. (**b**) Fine-grained amygdule-bearing phonolite from the Playa de la Enramada. (**c**) Hydrothermal alteration affecting a tephrite of the Playa de la Enramada. (**d**) Hydrothermal alteration affecting a syenite from the site Los Humilladeros.

*Mineral texture 3:* This vuggy mineralization comes into being as the matrix hosting the early-formed REE minerals is replaced. If alkaline igneous rocks become deprived of

part of their alkali elements during hypogene alteration, their groundmass will turn into a monzodioritic one and may take on a porous and permeable structure. It is the reverse process of what has been known from the epi-syenitisation when igneous rocks of the granite clan became deprived of their quartz content. This desilicification has been recorded from many areas mainly in the context of albitization and uranium mineralization [91–94]. In places, it does not only cause primary matrix minerals to become carved out but also gives rise to neomorphic minerals such as vinogradovite, which grow into in the newly created space. After a hiatus, secondary REE minerals can precipitate from mineralizing fluids to give rise to, e.g., aggregates of interwoven thin hairs of rhabdophane. According to the authors, this alteration likely proceeds at temperatures in the range 100 to 300 °C under high activity of alkalis.

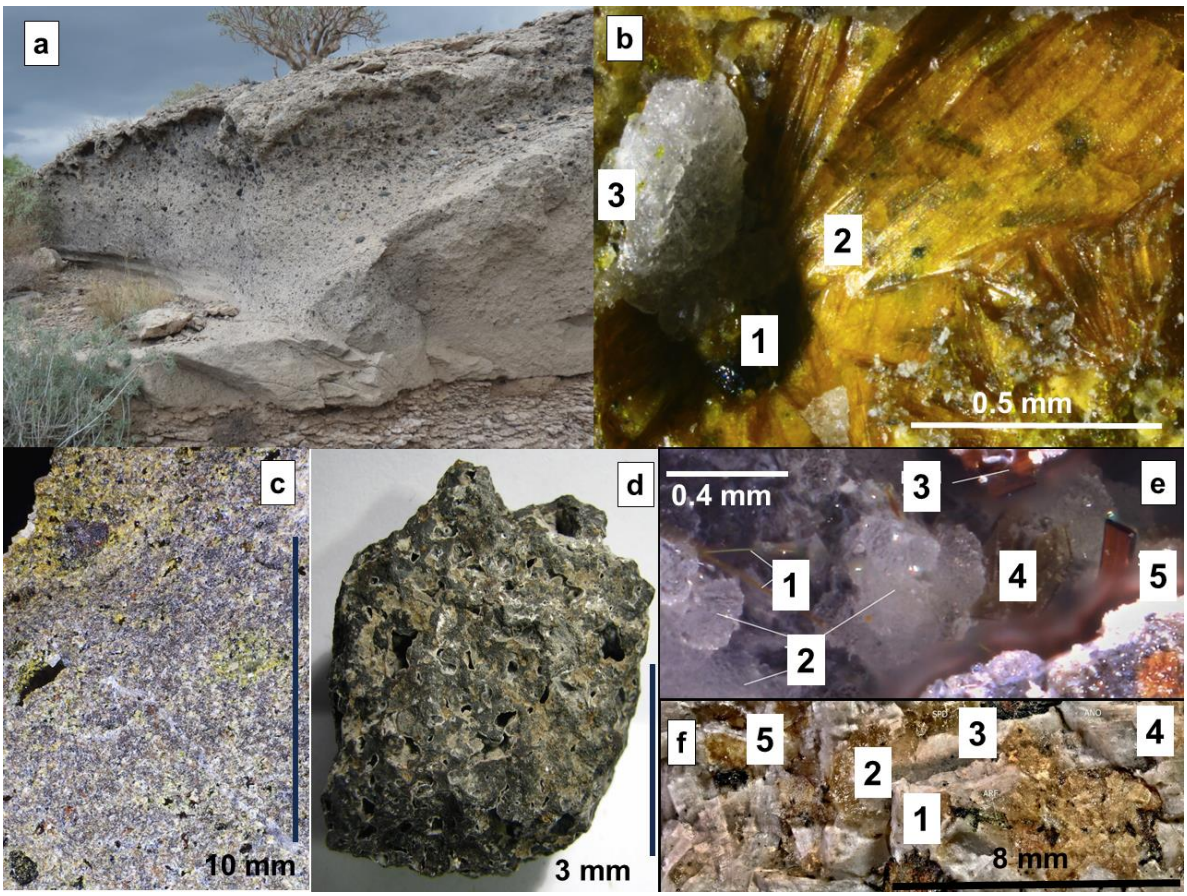


**Figure 7.** From the favorite outcrop to the most diagnostic textures. For the chemical composition of ore minerals spotted within the mineral assemblage of micro-mounts, see Table 4, unless given otherwise. The numerical labeling refers to the order of succession. (**a**) The most promising host rock lithology to be targeted for rare minerals is the pyroclastic flow deposit, for example, the Abrigo Ignimbrite. Locality: Los Abrigos. (**b**) A fan of acicular manganiferous vesuvianite (2) with aggregates of white cuspidine (3) and bixbyite (1) in kalsilite–leucite-bearing monzodiorite/gabbro from Barranco Hondo. (**c**) Strongly altered kalsilite–leucite-bearing monzodiorite/gabbro from Barranco Hondo. (**d**) Basalt peppered with amygdules. Locality: Mt. Pelada. (**e**) Vug in a nepheline syenite from Playa San Juan filled with ferroedenite (1) $[NaCa_2(Fe^{2+},Mg)_5(Si_7Al)O_{22}(OH)_2]$, thomsonite-Ca (2), emmerichite (3), chiavennite (4), and shcherbakovite (5). (**f**) Micro-pegmatitic syenite with anorthite (4), arfvedsonites (1), galaxite (3), hollandite (5) and the common lithium ore mineral spodumene (2) from La Mareta.

*Mineral texture 4:* Amygdules are filled with a multiple-phase mineral assemblage (Figure 7d). In Figure 7e, freely growing well-shaped crystals of chiavennite, emmerichite,

and shcherbakovite evolved in nepheline syenite from Playa de San Juan. The amount of mineralizing fluid was too low to fill the entire open space of the cavity. The process of creating space is phenomenological similar to that what has been described for episyenites, where skeletal textures are common.

*Mineral texture 5:* True pegmatites have not yet been mapped in the Canary Islands Archipelago but pegmatitic textured enclaves in peralkaline felsic and basic rocks are common (Figure 7f). It is a micro-pegmatitic intrusive rocks with anorthite, arfvedsonite, anorthoclase, galaxite, hollandite and the most common lithium ore mineral spodumene. It bridges the gap between the coarse-grained subvolcanic magmatic rocks and the alkaline rift-related pegmatites [21]. REE-, Be- and Zr pegmatites are often closely associated with carbonatites and considered a manifestation of subcrustal magmatic activity.

### *4.4. Minerals and Mineral Assemblages*

The minerals observed in the various landform series and bedrocks on the Isle of Tenerife are grouped into four categories:

1. Na-, K-, Ca-, Fe-, and Mg-bearing silicates (mainly tecto-silicates);
2. Ca- and Fe-bearing non-tectosilicates ("calcsilicate minerals");
3. Complex potentially economic Be-Zr-F-Ti-Nb-REE(+Y)-Li-Cs-W-Sn minerals;
4. Complex Mn-Fe-Pb-U-Th-As-Sb-V-Cr-S-B-Cu-Zn-Mo-Au minerals.

All four mineral categories provide a wealth of marker minerals and form the core of the so-called unconventional exploration model for critical elements. They are discussed in the following sections.

## 5. Discussion

### *5.1. Marker Minerals—From the Country Rock to the Rare Mineral Deposit*

#### 5.1.1. Petrology of Peralkaline Host Rocks and the Facies of Hydrothermal Alteration—Type I Mineral Assemblage

The Na-, K-, Ca-, Fe-, and Mg-bearing silicates of type I are the basis for the petrological classification of the rocks hosting the rare minerals in the study area, all of which pertain to the peralkaline suite according to the classification of [95] (Table 5). These magmatic rocks under study are silica-saturated, e.g., syenites and trachytes, or silica-undersaturated, e.g., nepheline syenites, foid-bearing monzodiorites, and phonolites [96–98]. The marker minerals for this classification are represented by K-, Na- and Ca feldspar modifications as well as by the feldspathoid group, the silica-undersaturated aluminosilicate equivalents of feldspar, e.g., nepheline, leucite, hauyne and kalsilite. The aerial distribution of these rocks and rock-forming minerals in the study area can be deduced from Table 5 and the geological map of Figure 3. Apart from these tecto-silicates, there are also sodic clinopyroxene such as aegirine, and sodic amphiboles such as arfvedsonite as well as aenigmatite (La Mareta), a combination of the two which corroborates the alkaline nature of the magmatic suite under consideration.

The zeolite group postdates the aforementioned feldspar group minerals and is a sensitive marker of hydrothermal post-eruptive alteration. In the current study, only the Ca- and Na sensitive ones are used for genetic discussion; the K-bearing ones are present only in minor quantities and irrelevant for deciphering the origin of rocks and mineral deposits. The sodic end members prevail (chabazite-Na, analcime, heulandite-Na, clinoptilolite-Na, natrolite, phillipsite-Na, stilbite-Na, gonnardite) over Ca-bearing end members (chabazite-Ca, laumontite, thomsonite-Ca, phillipsite-Ca, clinoptilolite-Ca, stilbite-Ca, offretite) in the zeolites of Tenerife, Spain (part c of Table 4).

In general, these silicates are of widespread occurrence in basic to intermediate volcanic and volcaniclastic rocks worldwide [99–102]. In the Canary Islands Archipelago, the aforementioned hydrothermal alteration was studied in detail on the Isle of Gran Canaria by [103,104] focusing on the non-welded ignimbrites of the Roque Nublo ignimbrites of the Pliocene age and the intracaldera facies of the Miocene Tejeda Caldera. The ignimbrites´ groundmass (K-feldspar, plagioclase, pyroxene, amphibole) has been

converted into adularia, zeolites and clay minerals. The emplacement of the alteration minerals is a direct consequence of the porosity and permeability of the pyroclastic flow deposits impeding the water vapor to be separated from the vitric fragments on transport. The altered tuffs have δD values that indicate an interaction with a meteoric water source and may have been produced in low-temperature steam fumaroles. It is a near-surface, epithermal fault-controlled hydrothermal system with fluid temperatures probably not exceeding 200–250 °C [104]. A similar maximum temperature range has been calculated for the three zeolite stages of the basic and ultrabasic rocks of the volcanic units of the Troodos Ophiolites, Cyprus ((1) laumontite-stilbite/stellerite, (2) natrolite-thomsonite-heulandite, (3) analcime-gmelinite), spreading a T range from 20 to 250 °C. Based on isotope studies of [71], zeolite mineralization formed from seawater with variable amounts of biogenic $CO_2$. Calcium-selective zeolites at depth and sodium-selective zeolites near the surface of the eruptive complex reflect a diminishing impact of seawater on the geothermal system with depth and an increase in biogenic $CO_2$ towards the seawater–rock interface.

Clay minerals are rather unevenly distributed across the Isle of Tenerife and not very diverse as compared with the varied mineralogy of the accompanying ore minerals (part a,b of Table 4). Similar to the findings published by [105] on La Palma, smectite is the most common clay mineral affecting the basic magmatic rocks. It is part of the late-stage, auto-hydrothermal alteration when meta-stable vitric material is replaced by these expandable 14 Å phyllosilicates. Vermiculite and chlorite s.s.s are less widespread than the expandable phyllosilicates montmorillonite and their Fe (III) analogue nontronite. The latter comes into being under oxidizing conditions in an acidic fluid regime similar to that of the kaolinite group minerals [106,107]. Kaolinite is, however, different regarding the pH of mineralizing fluids and the most widespread clay mineral that evolved along two trend lines. One linear trend is observed subparallel to the SW coast of Tenerife and another one in the NE-SW direction subparallel to the NW coast of the island where kaolinite occurs side by side with 7 Å and 10 Å halloysite in equal amounts together with saponite, hematite, goethite, magnetite and sanidine according to [108]. Saponite, a trioctahedral smectite group clay mineral, attests to a more reducing environment of formation along the NE–SW-striking KH-line because of bivalent Fe accommodated in its lattice instead of trivalent Fe. The kaolinite–halloysite clay mineralization was chronologically constrained to the period of 1.5 to 0.3 Ma and can be tracked towards the W into the hypogene Fe-sulfide-oxide-bearing mineralization in neighboring La Gomera Island [87,109]. An epithermal Fe-S-Cu association is found towards the SW at the Vallehermoso of La Gomera and towards the NE of the KH line at Taganana on Tenerife Island.

The clay mineral association along the KH-Line is the near-surface alteration zone of the hypogene Fe-sulfide-oxide mineralization: Fe sulfide ± magnetite → kaolinite 7 Å → halloysite 7 Å → halloysite 10 (Figure 3). By contrast, the enrichment of kaolinite group minerals around the S and SW coast of Tenerife coincides with the zeolite alteration, which unlike kaolinite, bears witness to a more alkaline fluid system. The succession zeolitization → kaolinization is evidence for a lowering of the pH value during fluid evolution. The zeolites show two hotspots, a first one at Puerto de Santiago at the point of intersection with the KH-Line, and a second one at Mt. Pelada.

#### 5.1.2. Calcsilicate Minerals and Skarnoid Alteration—Type II Mineral Assemblage

Wollastonite, vesuvianite, grossularite, monticellite, diopside and clinozoisite s.s.s. are characteristic contact-metamorphic and contact-metasomatic minerals (part a of Table 4) [110]. The close spatial relation between these skarnoid mineral assemblages and the syenitic to monzodioritic rocks suggests a genetic link between the emplacement of these intrusive magmatic rocks and carbonate and/or basic to ultrabasic host rocks at depth [111–114]. A similar skarn mineralization has been recorded from the Basal Complex of Fuerteventura, where it is associated with (meta) carbonatites [2]. At temperatures from 570 to 800 °C, wollastonite, monticellite, merwinite, forsterite, diopside and akermanite are stable at 100 MPa [110]. The mineral assemblage is typical of the shallow very-high T contact-

metamorphism of calcareous wall rocks. A similar mineral association with monticellite has also been encountered elsewhere in the carbonatite melts of the Oka Carbonatite Complex in Canada [115]. Vesuvianite is a silicate, which is stable over a wide temperature range and very sensitive to the $H_2O$ (high) and $CO_2$ contents (very low) in the system [116]. It converts together with clinozoisite/epidote, or tremolite and quartz into grossular, diopside and water. Hence, it can be used as a critical marker mineral for the boundary between the medium- and low-temperature contact-metamorphic/metasomatic facies (also called albite-epidote hornfels facies). The mineral association composed of wollastonite, monticellite, and vesuvianite is representative of the "hot spot" area in the skarn mineralization that stretches from the Roque del Conde Massif (11.6 to 3.5 Ma) to the Barranco Hondo parallel to the SE coast of Tenerife [117].

#### 5.1.3. The Cs-W-Sn-Bearing Be-Zr-F-Ti-Nb-REE(+Y)-Li-Cs-W-Sn Ore Minerals and Their Origin—Type III Mineral Assemblages

*Mineralogical mapping units:* Type III Cs-W-Sn-bearing Be-Zr-F-Ti-Nb-REE(+Y)-Li-Cs-W-Sn ore mineralizations constitute the framework for minero-stratigraphy and field mapping following the rules of [118]. The regional lithology and mineralogy allow for a subdivision into six mapping units: (1) sanidinite facies (monticellite, wollastonite), (2) high-grade contact-metamorphic facies equivalent to the pyroxene hornfels facies (wollastonite, vesuvianite, diopside), (3) low-grade contact-metamorphic facies equivalent to the amphibole-epidote hornfels facies (grossularite, clinozoisite), (4) zeolite facies zone, (5) kaolinization zone, and (6) auto-hydrothermal zone (Figure 8a,b, Table 4a,c).

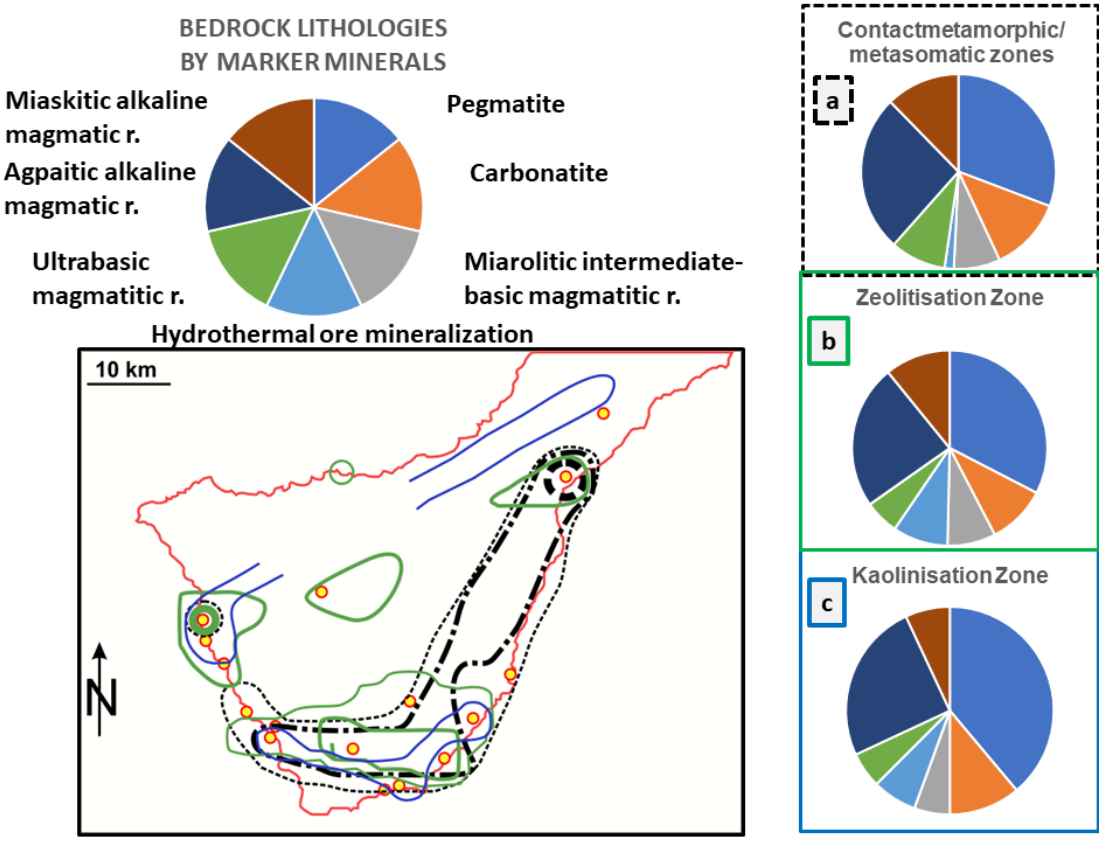


**Figure 8.** The distribution of hidden lithologies of Tenerife and alteration zones. See reference sector diagram. For regional geology and sampling sites, see Figure 3. (**a**) Sanidinite facies (black dashed bold line), high-grade/temperature (black dashed–dotted alternating medium line) and low-grade/temperature (black dotted thin line) contact-metamorphic/metasomatic facies. (**b**) Zeolitisation zones with grade (green bold full line: high grade, green medium full line: medium grade, green small full line: low grade). (**c**) Kaolinitisation zone (blue full line).

*Marker minerals for lithologies*: The type III minerals have been evaluated regarding whether they are useful as marker minerals and diagnostic of pegmatites, carbonatites, miarolitic intermediate to basic magmatic rocks, contact-metamorphic/metasomatic rocks, ultrabasic rocks, hydrothermal ore mineralization, and alkaline (Figure 8a). Some literature has been used in search of mineralogical and petrological reference sites to accomplish this goal, which is cited below: [32,119–154].

The approach to categorize the inferred magmatic rocks underneath the present-day volcanic landscape of Tenerife yields an overall pegmatite/carbonatite ratio of 2.70 and an agpaite/miaskite index of 2.53. The structural and lithological results enable us to model the hidden lithological body and denominate it as a syenitic pegmatite to pegmatitic syenite of predominantly agpaitic derivation with minor carbonatites. High-field-strength elements Ti, Zr, Nb, Ta, REE, Cl and F are typical of agpaitic and hyper-agpaitic rocks and ore deposits [155–159]. Nepheline syenites belonging to the miaskitic clan also present in the study area with their high-field-strength elements accommodated into zircon, titanite and Fe-Ti oxides. Even marker minerals of the hyper-agpaitic clan have been observed in the volcanic and volcaniclastic rocks of Tenerife at least in minor quantities such as steenstrupine-(Ce) and villiaumite [160,161]). There is a gradual increase in the agpaite/miaskite index from the sanidinite into the low -T skarn mineralization (2.00 → 2.13 → 2.50), which, according to [136], is controlled by the activities of F and Cl (Figure 8a). The zeolite and kaolinite zones reveal an increasing quantity of pegmatitic and agpaitic lithologies in the deeper parts of Tenerife towards the NW (Figure 8b).

Based upon the minerals observed at each sampling site, the relative amounts of elements have been calculated and illustrated by sector diagrams (Figure 9). They allow four characteristic element assemblages to be established.

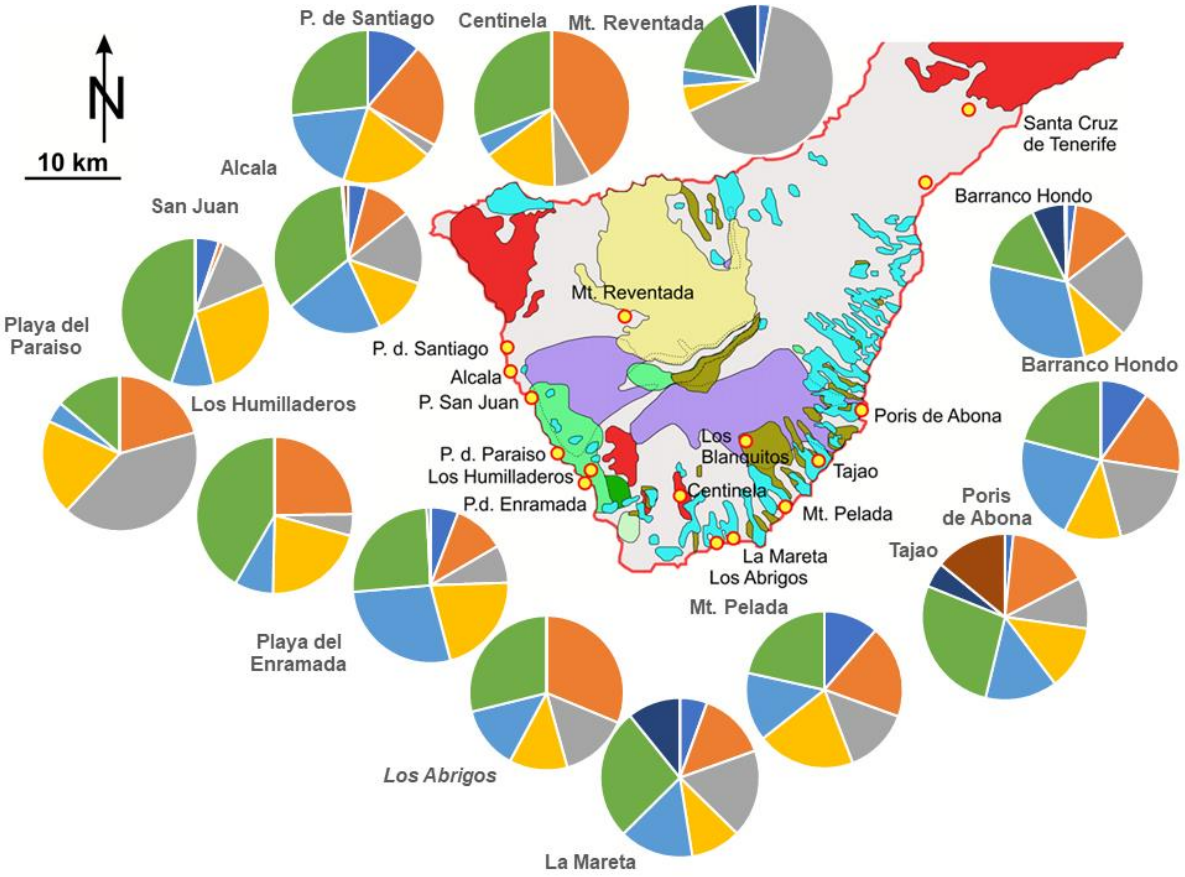


**Figure 9.** First-order assemblages of the inferred hidden rare element deposits. Sector diagrams of elements for each sampling site. For legend of geology see Figure 3 and for the sector diagrams see Figure 4.

- Nb-F-Ti-REE-Zr assemblage;
- Be-Nb-Ti-Zr-REE-F assemblage;
- Be-Li-Cs-F-Ti-Nb-Zr-REE(+Y) assemblage;
- W-Sn-Be-Li-Cs-Ti-Zr-REE(+Y)-F-Nb assemblage.

*Nb-F-Ti-REE-Zr assemblage*: This mineral assemblage evolved on the southern tip of Tenerife and represents the most primitive stage with only five marker elements Nb, F, Ti, REE and Zr arranged in order of increasing quantities that show up in different minerals (Figure 9, Table 4a). The inferred intrusive body is located underneath the oldest massif of the Isle of Tenerife, called the Roque del Conde Massif, chronologically constrained to the interval 11.6 to 3.5 Ma [162]. As far as the Zr hosts are concerned, there are Zr oxides, (baddeleyite), mixed Zr-Ti oxides (zirconolite), Zr silicates (zircon), mixed Zr-Ti silicates (dalyite), F- and hydroxyl-group-bearing Zr silicates (normandite, låvenite), and eventually hydrated mixed Zr silicates (elpidite) indicative of carbonatites and ultrapotassic veins in mantle xenoliths, with prevailing Ba- and Zr-enriched alkaline pegmatites and nepheline syenites [85,122,136,141,147,163].

Rare earth elements are second in the row in this assemblage. These are not monazite and bastnaesite, which are the most common REE-ore minerals but burbankite and loparite-(Ce), which rank first, followed by a second batch of minerals made up of allanite-(Ce), rinkite-(Ce), lucasite-(Ce) and a HREE host, xenotime. Burbankite is one of the earliest REE mineral to precipitate [164–166]. It is rarely preserved and its hexagonal crystals are mostly pseudomorphed by different REE phosphates such as monazite. The widespread occurrence of this LREE carbonate relative to monazite attests to a young mineralization in full agreement with the idea that hydrothermal processes could not lead their actions to full completeness and eradicate burbankite. Furthermore, the carbonate anion points to carbonatites where burbankite is cogenetic with calcite in calcio-carbonatites, which is proven by C- and O isotope studies. Loparite-(Ce) acts as a marker mineral for alkaline igneous rocks at depth, as described from agpaitic magmatic provinces elsewhere [85,167]. Lucasite characterizes the hydrothermal alteration of pegmatites at Khibiny, Kola Peninsula, Russia, and rinkite-(Ce) agpaitic alkaline complexes, as exemplified by the Late Cretaceous Poços de Caldas potassic alkaline complex, Brazil [140,168]. Xenotime, followed by a wide margin by allanite, is the most common host of HREE besides adamsite-(Y), aeschinite-(Y), churchite-(Y), and fergusonite-(Y), and it is present in all mineral suites. The rare mineral association extends towards the SW and across the sea into La Gomera (Figure 2).

*Be-Nb-Ti- Zr-REE-F assemblage*: This mineralization sees fluorine become the leading element instead of Zr and reveals the appearance of beryllium. The top representers are the simple and complex halogenides, e.g., fluorite and cryolite. Bastnaesite and rock-forming phosphate, e.g., fluorine apatite, are also contained in one of the most common REE minerals. These are most widespread as substitutes for the hydroxyl group in pyrochlore s.s.s. and minerals such as janhaugite and låvenite, which already appeared among the Zr minerals. One of the most significant minerals for minero-stratigraphic purposes is cuspidine or niocalite-cuspidine s.s.s, which were recorded by [129] from the natrocarbonatite at Oldoinyo Lengai, Tanzania, together with monticellite, and from the calcite carbonatite of the Oka Complex, Canada, by [169].

The mineral association is also common in the central parts of Fuerteventura, Spain, the second largest island of the archipelago. Syenitic intrusions occur in domes while ring dyke complexes are exposed near Betancuria adjacent to the Ajui-Solapa carbonatite district [2,170]. At Fuerteventura, an alkaline complex dominated by REE-bearing calcite carbonatites is at outcrop and inferred from this meticulous study of marker minerals at subcrop on the Isle of Tenerife. Between the two islands, there is a marked difference among the type III mineral association in quantity and quality. The mineral association of Fuerteventura is less variegated in terms of quality but much stronger in terms of quantity concerning the REE and Ti minerals (e.g., britholite, monazite, apatite, bastnaesite, allanite, titanite, perovskite) (Table 4a) [2,171]. Gran Canaria is still inferior to both of them in terms the variety of rare minerals (Table 4a) [90].

Another critical metal enriched in this volcanic setting is beryllium with hambergite and bertrandite ranking first, whereas beryl, the main Be host in many deposits worldwide, is absent in Tenerife. At around 200 °C, phenakite and bromellite hydrate to bertrandite and behoite, respectively. Bromellite does not exist in this system, and only behoite comes up later. Beryl in pegmatites decomposes in the course of hydration to a wide range of Be minerals, including, among others, hambergite [172].

*Be-Li-Cs-F-Ti-Nb-Zr-REE(+Y) assemblage:* Another set of minerals appears on the scene accommodating the couple lithium–cesium in their structure (Figure 9). The most frequent Li-Cs minerals are griceite, holmquisite, and pollucite with the strongest concentration at La Mareta [173]. The above cited authors described griceite from the Mont Saint-Hilaire Area, Canada, where between 133 and 120 Ma old plutonic intrusions (gabbro, nepheline syenite, diorite, monzonite, albitite dikes, marble xenoliths) are exposed, rife with very exotic minerals. The zone critical for the wealth of minerals consists of agpaitic pegmatites, and contact-metasomatic and contact-metamorphic zones marginal to the intrusives [174]. Another Li host, holmquisite, a common metasomatic replacement mineral in the distal zone of lithium-rich pegmatites, corroborates this environment of formation described above [147]. Apart from petalite and spodumene hydrated species bikitaite, Li-Al phosphates (montebrasite), complex hydrous Li-HREE phosphate-carbonates (peatite-Y), occur (Table 4a). These describe the main period of pegmatite formation succeeded by some subsequent hydrothermal alteration [14]. Peatite-(Y) is a late-stage mineral recorded from the Poudrette Pegmatites of the Mont Saint-Hilaire Area, Canada. Their marble is known in xenoliths and as a potential source for carbonate. Underneath Tenerife, carbonatite is assumed as a carbonate source [175]. There are other complex mineral phases with different metals under consideration typical of syenite pegmatites. Tainiolite is a rare Li phyllosilicate of the biotite group resulting from fluorine-enriched solutions and typical of early mineralizing events, whereas lepidolite and polylithionite are lithium micas widespread in the granitic pegmatites poor in phosphates [14]. Lintisite and lithiotantite are oxides that formed together with Ta and Nb, respectively. The first-mentioned mineral is known from the hydrothermal alteration of pegmatites of nepheline–sodalite syenite [176,177]. The metal Cs rarely shows up in minerals of its own like pollucite and garmite. Pollucite is a zeolite-group mineral which is said to be associated with chabazite and harmotome in pegmatites from the Czech Moldanubian basement and is enriched in the southern zeolite zone of Tenerife [178]. Garmite is the Cs-enriched analogue of taniolite, a mica-group phyllosilicate which was described for the first time from the Darai-Piyoz Alkaline Massif, Tajikistan [179,180].

*W-Sn-Be-Li-Cs-Ti-Zr-REE(+Y)-F-Nb assemblage:* The element couple Sn-W is observed at the Tajao outcrop, where it is accompanied by Be and Li-Cs, the minerals of the original mineralization (Figure 9). There are only two minerals scheelite common to skarn deposits and cassiterite, which occurs in a great many deposits running the gamut from strongly fractionated granites through pegmatites into subvolcanic ones [9]. In the latter type of the so-called subvolcanic Sn deposits (e.g., Montserrat, Bolivia), it is mainly Sn sulfides that represent an isomorphous series of minerals, such as teallite and herzenbergite, which may be hydrated to form hydrocassiterite and hochschildite. In the low-T subvolcanic Sn deposits in Bolivia, Sn sulfosalts, e.g., kylindrite, franckeite, and canfieldite, were found locally in concentrations that render the mining of these sulfosalts for Sn viable. Cassiterite occurs mainly as collomorphous "wood tin. By and large, this subvolcanic type of W-Sn mineralization can be ruled out for Tenerife and a genetic link to felsic intrusives is the only alternative.

#### 5.1.4. Accompanying Mn-Fe-Pb-U-Th-As-Sb-V-Cr-S-B-Cu-Zn-Mo-Au Minerals and Their Origin—Type IV Mineral Assemblages

There are four type IV mineral assemblages:

1. Mn-Fe assemblage;
2. V-Pb-Sb-As-S assemblage;

3. Th-U mineral assemblage;
4. Cu-Mo-Zn-Au assemblage.

Chromium is substituted with vanadium and titanium in oxides like byrudite and vuorelainenite, and boron is accommodated into the lattice of Be minerals like berborite and hambergite (Table 4, Figure 10). These elements are treated on their own on account of their minor quantity.

*Mn-Fe mineral assemblage*: There are 59 minerals containing Mn, from 72 wt.% Mn (hausmannite) to 2.4 wt.% Mn (babingtonite), which are ubiquitous across the island (Figure 10). The most frequent Mn minerals in the study area are bixbyite, pyrophanite and serandite, which are present in more than half of the sampling sites and older than the Be-Zr-F-Ti-Nb-REE minerals of type III and the skarn minerals of type II. Serandite and the Mn borate tinzenite are the only ones that show a direct link to the type III minerals in agpaitic pegmatites, phonolites, carbonatites and skarn deposits situated around the southern tip of Tenerife, while the less widespread rhodochrosite points to carbonatites at depth [181–187]. Bixbyite has been recorded as a cavity filling in rhyolites as well as in karst landforms [188–191]. Pyrophanite, the Mn analogue of ilmenite, is rather rare but occurs in a series of environments together with hollandite known from, e.g., iron formation deposits of Precambrian age, low-grade metamorphic deposits, A-type granites, mixed-type pegmatites and carbonatites [133,168,192–195]. Low-grade metamorphosed and highly oxidized Mn sedimentary deposits are typical Mn host rocks, as shown by the Mn phyllosilicate namansilite [196]. This variegated image drawn by the environments of Mn deposition can only be accounted for by the rifting area in NW Africa, the mirror image of which can still be seen at the eastern edge of the African continent, which is compared with the current one. The variegated Mn mineralizations at the NE edge of the African Continent evolved in a triple junction formed by the NE Egypt Rift, the Najd-Strike-Slip Zone and the Jordan-Valley Rift (620–520 Ma) more than 500 million years ago [112]. The rifting system there developed to a great extent in sedimentary environments with minor alkaline granite, whereas the reference type at Tenerife is exclusively of volcanic to pyroclastic origin with a rather moderate variety of Mn minerals (18 mineral types). The Mn-Fe mineralization mirrors the incipient rifting underneath the Tenerife volcanic edifice. Its supercritical (skarn) and subcritical hydrothermal fluids are accountable for the majority of the marker minerals. Furthermore, the polyvalent character of manganese is a favorable indicator for all those processes sensitive to the redox regime. Pervasive supergene processes and the build-up of a thick metalliferous regolith cannot be seen on Tenerife due to the continuous modern volcanic activity during the Neogene and Quaternary. They cause a lack of long-term hiatuses during the Quaternary that is detrimental to the built-up a thick regolith, as is the case with the rugged mountainous landscape on the volcanic islands [197,198]. In stark contrast to that, on the Isle of Fuerteventura, such hiatuses occur and favor the exhumation of the carbonatites. Lead is present among the second-order mineral assemblages but never shows up on the volcanic island in combination with Mn to precipitate as coronadite, which is the most common sediment-hosted Pb-Mn oxide under near-ambient conditions. It gives rise to pyrobelonite instead, which is common in Fe deposits, where it has been derived from coulsonite [199–201].

Bivalent Mn-V minerals, e.g., ronneburgite, and the Mn sulfide alabandite are found in organic matter-bearing sediments, a lithology in the study area where only an immigration of bituminous matter along fissures and faults is the most plausible explanation for their presence [202,203]. The complex Mn sulfate shigaite is nothing but the replacement product of the aforementioned bivalent Mn minerals [199]. The hydrothermal oxidation led to an increase in the valence state of S, yet not of Mn, excluding the possibility of any simple supergene oxidation processes having an influence on the Mn system.

*V-Pb-As-Sb-S assemblage*: This mineral assemblage needs to be split into different subfacies types for quantitative and qualitative reasons: one subfacies is abundant in V, and another one strongly enriched in Pb. Both of them are concentrated along the southern

coast of Tenerife. No direct genetic link to the Type III first-order rare element association is revealed (Figures 9 and 10, part a,b of Table 4).

*Pb-enriched S-based subfacies*: Galena is the only Pb sulfide in the study area, present in a considerable amount of 80% within the V-Pb-As-Sb-S mineral assemblage. Without any doubt, it is the primary source of Pb and developed in a reducing regime. Undergoing oxidation provokes this sulfide to convert in a couple of plumbiferous oxide-bearing compounds such as anglesite, cerussite, and pyromorphite depending upon the soluble anion complexes to react with Pb. Vanadinite bridges the gap into the V-enriched subfacies [204]. Pyromorphite is the latest mineral in the succession and resulted from the supergene adjustment of the aforementioned sulfidic, sulfatic, and carbonatic Pb compounds to the most recent Cenozoic climate providing P [200].

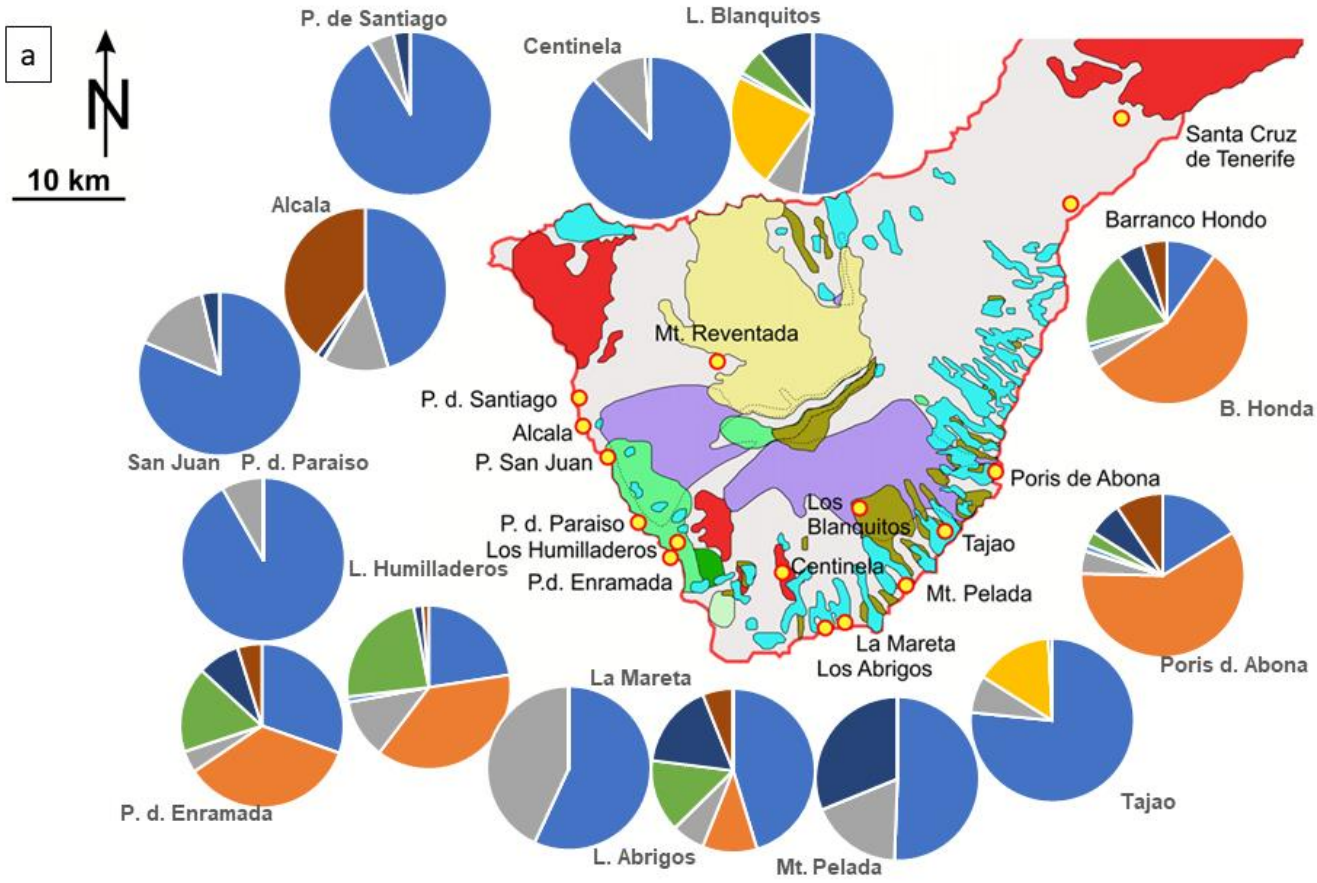


**Figure 10.** *Cont.*

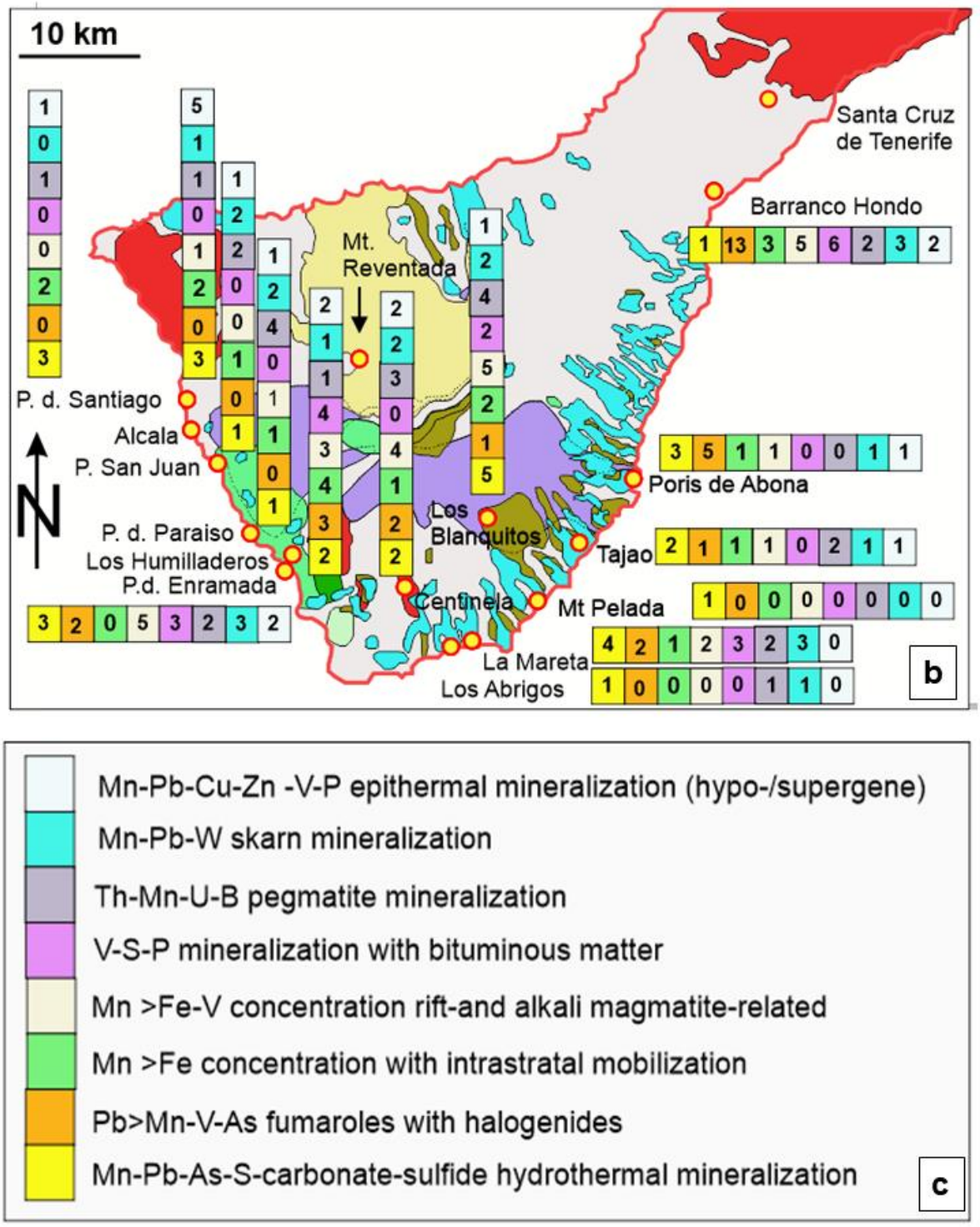


**Figure 10.** Second-order assemblages accompanying the hidden rare element deposits (Figure 9). (**a**) Sector diagrams of elements for each sampling site (for regional geology see Figure 3). (**b**) Columnar diagrams showing the mineralizing processes for each sampling site (see color code and Figure 10c). The Arabic numerals denote the relative intensity of the different mineralization processes at each sampling site. (**c**) Key showing the color code of each mineralization process.

*Pb-enriched halogenide subfacies*: There is another string where chlorine and fluorine are accommodated into the same lattice of Pb-bearing compounds in places in hydrated forms, e.g., laurionite, paralaurionite, matlockite, and cotunnite. Cotunnite may occur in salcretes under arid conditions in sabkhas and, as a result of anthropogenic post-mining

mineralization, in abandoned adits and shafts. Some show up as a byproduct of smelting while coating ancient slags such as fiedlerite [205]. These anthropogenic as well as geogenic environments quoted above can be ruled out and precipitates from fumaroles, as they were described from volcanoes of Kamchatka, Russia, are likely to have been responsible instead [206,207]. This is also valid for the chlorine-bearing Pb arsenates which can also be attributed to the group of fumaroles and were active in the aftermaths of volcanic eruptions [208]. Undergoing further oxidation leads Pb oxides to be found only in coal-fires on waste dumps and in slags [72]. The only link of these Pb oxides to any Type III host rock lithologies is known from natrocarbonatites. This type of carbonatite is, however, very unlikely to have formed in the present geodynamic situation [209]. This mineral succession only contains two minerals where type III and IV elements share the same crystal. It is stolzite and macedonite which occur in syenite pegmatites, the first one late in the succession of Pb minerals, whereas macedonites formed at the beginning of this Pb-bearing mineral assemblage [132].

*Vanadiniferous spinel subfacies*: This vanadiferous mineral assemblage is of more widespread occurrence than a plumbiferous one and it has the closest genetic link to the Fe-Mn association, which acts as a marker for the initial rifting period (Figure 10b). The initial subfacies is characterized by spinel-type oxides with coulsonite (Fe), magnesiocoulsonite (Mg), and vuorelainenite (Mn, Cr, V). They are common to massive sulfide base-metal deposits, metamorphosed pyrite deposits, meta-igneous rocks and pegmatites [201]. Schubnelite is a hydrated late form of coulsonite and also ranks among this vanadiferous subfacies [210]. The quoted vanadiferous subfacies is more widespread and closer to the rifting zone than its Pb counterpart (Figure 10a).

The sulfur analogue of the vanadiferous subfacies is a replica of the famous Ragra Mine, in the Huayllay District, Pasco Province, Peru, a vanadium mine which was closed in 1944 [211]. This shale-hosted vanadium deposit has fault-bound, lens-shaped V concentrations with quiesqueite, a bitumen coke, patronite, montroseite, minasragrite, and hewettite. Some of the V minerals, such as patronite, fernandinite, melanovanadite, hewettite, ronneburgite, pascoite minasragrite, and stanleyite, found on the Isle of Tenerife are analogous to the Pb-S and Pb-S-O paragenesis. The unique V deposit evolved from the interaction of V-bearing hydrothermal fluids with hydrocarbon-related sulfur. It may sound optimistic and daring to hold this assemblage as a marker of hydrocarbon immigration from elsewhere into the deeper levels of the volcanic edifice and a byproduct of rare metal exploration with unconventional methods.

There are also vanadiferous hydrothermal solutions devoid of hydrocarbons characterized by the pentavalent V-Mn minerals ansermetite and schaeferite [212,213].

*Th-U mineral assemblage*: The Th-U ratio in the study area is always greater than one with the exception of Los Blanquitos where only coffinite has been detected. The more Th predominates over U in the element composition of Th- and U-bearing intrusive rocks, the more likely it becomes that a strong interference with subcrustal material has taken place.

A-type or mantle-derived alkaline magmatic and pegmatitic rocks like those at Ilimaussaq, Greenland, are supposed to occur at depth on the Isle of Tenerife. Coffinite acts as the easternmost representative of the U-Th mineral assemblage and forms part of a hydrothermal mineralization [214].

*Cu-Mo-Zn-Au mineral assemblage*: The Cu minerals native copper and cuprite are part of a shallow near-ambient mineralization. This reflects moderately oxidizing conditions. Copper sulfides and the commonly ubiquitous Fe sulfides are absent. Molybdenite and gold are seldom encountered, and their genetic attribution can only be achieved in combination with other rare metals—see next section.

### *5.2. The Evolution of the Inferred Hidden Rare Element and Rare Mineral Occurrences on the Isle of Tenerife and the New REE Discovery at La Gomera*

The evolution of the Tenerife volcanic island and their mineral deposits is subdivided into seven stages, the origin of which is based on the environmental analysis of their marker

mineral assemblages and the terrain analysis unravelling the host landforms and the morpho-tectonic structural elements acting as pathways for the magma and the hydrothermal solutions and assisting in delineating the inferred rock and ore bodies (Figures 11 and 12a–g). The tripartite scheme reveals the basic structural and physical changes throughout mineralization, as well as their orientation (Figure 12g). The figure at the end of this succession illustrates the outcrop and subcrop setting of the six stages and their temporal and spacious relationship to each other (Figure 12h).

5.2.1. Stage 1—The Initial Rifting Stage

Tenerife features a triple junction with three rift arms, highlighted in the recent landscape by the Roque del Conde, Teno, and Anaga Massifs, each at the ends. The younger Teide Volcano is erected from the center of this triple junction and covers a lot of the older massifs with its lava deposits and pyroclastic sediments [59,60,62,215] (Figure 11). It is the NNE- and ENE-striking rift arms that are relevant for the evolution of the incipient stage of mineralization (Figures 3 and 11). On a regional scale, the Canary Island Archipelago reveals through its morph-tectonic elements where the active and inactive structures during the rifting event are and thus directs our view to the sites where the potential ore shoots for rare element deposits might be situated.

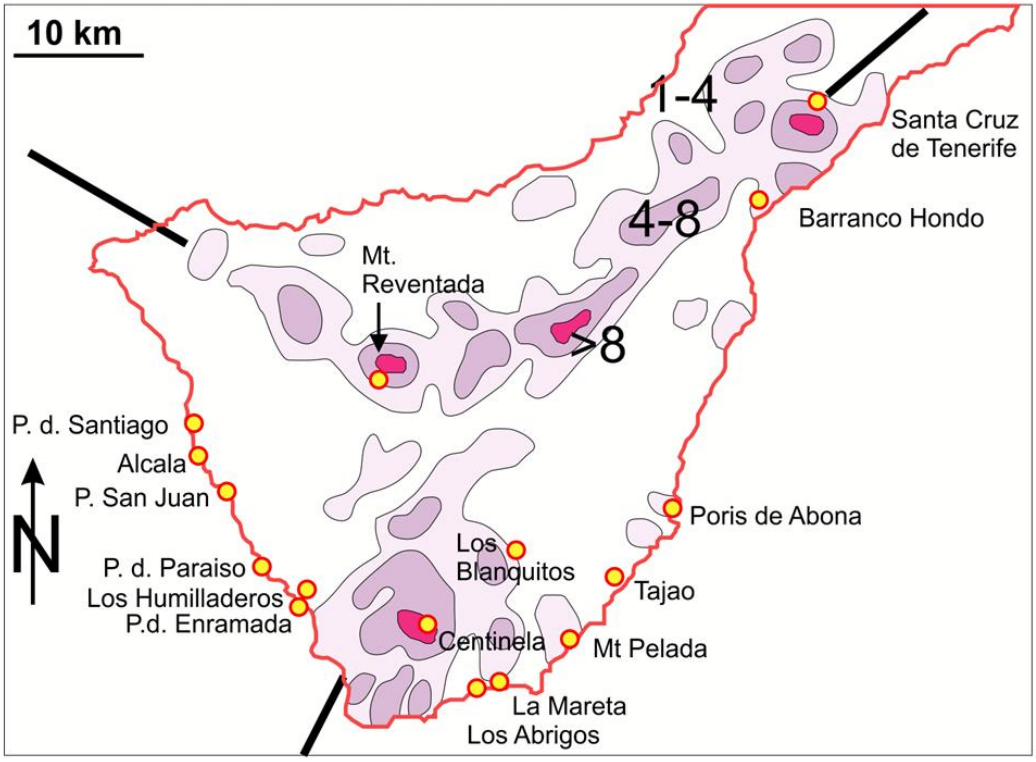


**Figure 11.** Hotspot volcanism close to a passive continental margin zooming in on the Isle of Tenerife, Spain (modified from [215]). The map shows the three rift arms marked by the three massifs and the distribution of eruptive events given by the number of vents per km$^2$. See the tripartite scale: >8, 8–4, 4–1 (upper right).

The carbonatite-bound REE mineralization at the NW edge of Fuerteventura, the eastern sister island of Tenerife, took place syn- to post-kinematically along NNE-running master faults. Contrary to this, the NE-striking arms on the same island and the paired island Lanzarote following the same strike are non-productive because these deep-seated faults did not provide accommodation space to either vent carbonatitic magma or concentrate REE. According to the current compositional studies at Tenerife, investigations of the structural geology on the remaining islands have been performed which identified the NNE structures as feather joints, creating the accommodation space necessary for

the emplacement of several mineralized carbonatites in the central and northern parts of Fuerteventura and, presumably, the hidden alkaline magmatite–carbonatite system at depth on Tenerife (Figure 11).

The fertile one on Tenerife ends in the Roque del Conde Massif at the southern tip of the island. The NE-striking rift arm is representative of the strike-slip master fault that did not open up during this initial rifting stage. The feeder channels for the rare metal mineralization are confined to the NNE end echelon structures around this massif. The stress pattern is part of a compression in the NW-SE direction between the Iberian Peninsula and the West African Continent. This complex geodynamic process is responsible for the occurrence of the mineralizations under study in the southern part of Tenerife.

The current variegated Mn mineralization at the NNW corner of the African Continent has a mirror image at NE edge of the African Continent, which also evolved in a triple junction formed by the NE Egypt Rift, the Najd-Strike-Slip Zone, and the Jordan-Valley Rift (620–520 Ma) through more than 500 million years ago [9]. The NNE-rifting system developed to a great extent in sedimentary environments with minor alkaline granite with a rather moderate variety of Mn minerals (18 mineral species), whereas the reference type at Tenerife is exclusively volcanic to pyroclastic in origin and well-endowed with a plethora of Mn minerals. The Mn-Fe mineralization mirrors the incipient rifting underneath the Tenerife volcanic edifice.

The embryonic mineralizing events are characterized by the Mn > Fe-V concentrations linked to the NNE-tending rift structures and connected to alkali-magmatic intrusive processes which grade into hydrothermal MFe intrastratal mobilization towards the NW during subsequent phases (Figures 10a–c and 12a). The Mn minerals of this stage are concentrated around the Roque del Conde Massif with a NE-SW trend (Figure 12a).

The marker ore minerals are typical of un-metamorphosed-to-low-grade regional-metamorphosed Mn deposits and vanadiferous Mn oxides which are typical of alkaline magmatic rocks, see Mn-Fe and V-Pb-Sb-As-S assemblages. Minerals typical of manganese nodules, e.g., lithiophorite, which was recorded from the low-temperature, shallow-water hydrothermal vent mineralization of the recent submarine eruption of the Tagoro volcano near El Hierro, Spain, by [216], are absent from Tenerife. The Fe-Mn marker minerals are more akin to basic-to-ultrabasic source rocks known from Fuerteventura, Spain [2]. It shows a "Hockey-Stick Pattern" which denotes a rifting mineralization and the beginning of an alkali-magmatic ensimatic intrusion accompanied by rare-metal pegmatites (Figure 12a).

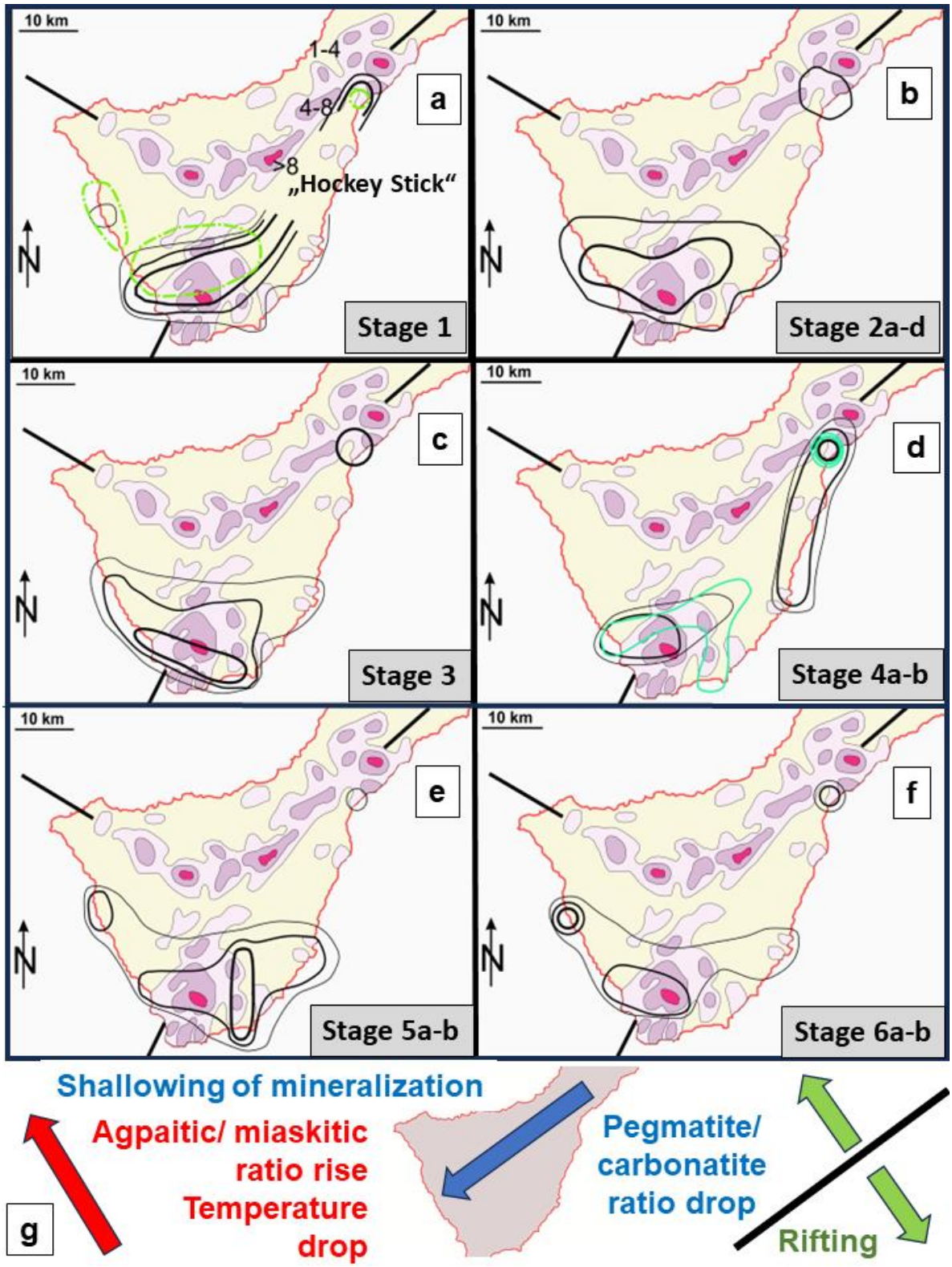


**Figure 12.** *Cont*.

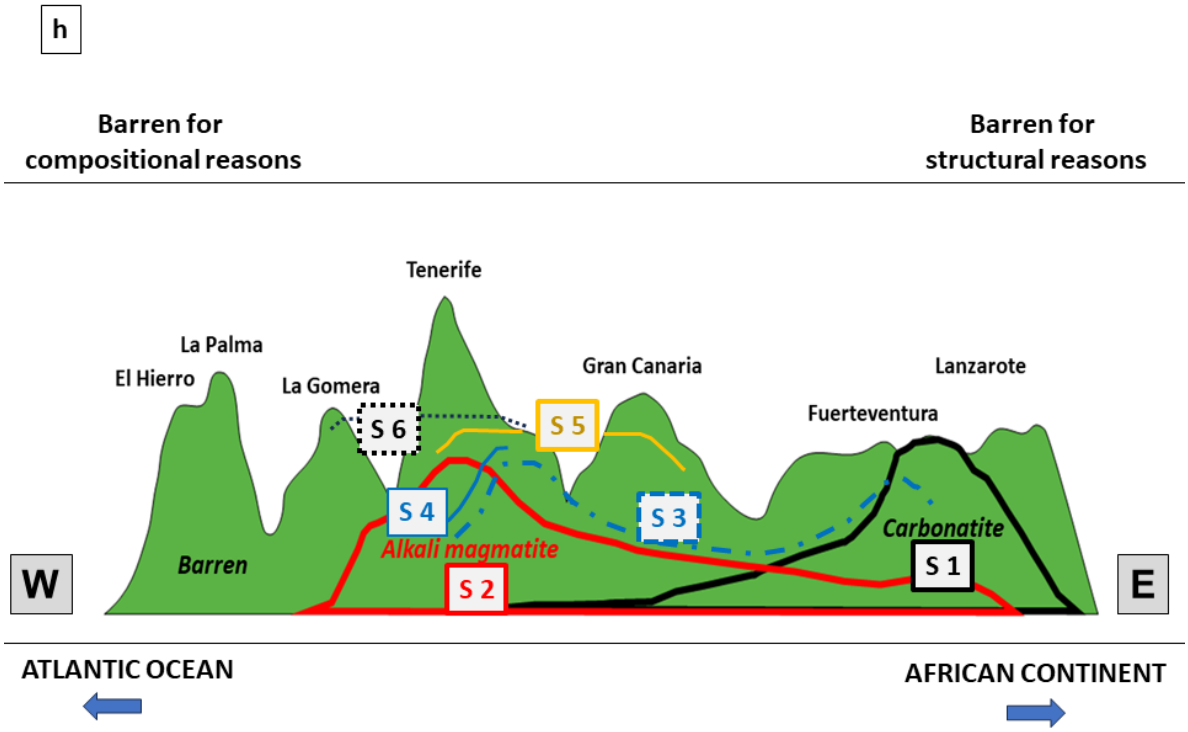


**Figure 12.** The metallogenic evolution of the inferred second-order mineralization at Tenerife which forms the structurally related framework for the first-order mineralization. The thickness and type of the contours denote the intensity of the mineralization based on the data of Figure 10b,c. The number of vents per km$^2$ is only marked in Figure 12a for reasons of clarity. See also the tripartite scale: >8, 8–4, 4–1 (Figure 11). For more detailed information, see Table 6. (**a**) Stage 1: Mn > Fe-V concentration rift-/alkali magmatite-related (black lines), Mn > Fe concentration as intrastratal mobilization (green line). "Hockey stick" depicts the shape of the distribution pattern. (**b**) Stage 2: Th-Mn-U-B pegmatite mineralization and alkali magmatites. For more details on this stage of first-order mineralization, see Figure 13 where fine-tuning of its zonation is achieved. (**c**) Stage 3: Mn-Pb-W skarn mineralization. (**d**) Stage 4: V-S-P mineralization + carbonaceous matter (stage 4a green line), Pb>Mn-V-As fumaroles (stage 4b black line). (**e**) Stage 5: Mn-Pb-As-sulfide-carbonate-zeolite hydrothermal mineralization. (**f**) Stage 6: Mn-Pb-Cu-Zn-V-P epithermal (hypo-/supergene) mineralization. (**g**) The basic structural and physical changes throughout mineralization. Green pattern: opening of the rift system NW-SE, red pattern: (2) mineralogy (the temperature drop towards the NW), blue pattern: economic geology: indicates a shallowing (blue pattern towards the SW of the metallogenic axis which plunges towards the NE. (**h**) The bipolar alkali magmatite—carbonatite mineralization and its stages of formation 1 to 6 at depth and at outcrop (see Table 6 for more details).

**Table 6.** Metallogenetic evolution of the inferred rift-related rare-element syenite–pegmatite system below the present-day volcanic landscape of Tenerife, Spain, based upon mineralogical micro-mount mapping supplemented by the study of zeolites and clay minerals.

| Stage | Assemblage | Environment | Orientation | Mineralizing Processes | Lithology | Site |
|---|---|---|---|---|---|---|
| **Proto-stage 1** | Mn > Fe-(V) | Incipient phases of rifting and magmatism | "Hockey stick" NNE+ENE | Volcano-sedimentary (+hydrother-mal intra-stratal mobilization) | Basic to ultra-basic source rocks (=s.r.) | Rocque del Conde (=RdC) Hernandez Group + Flank Basalts |
| **2a** | Zr > REE-Ti-F-Nb-Th-Mn-U-B | Differentiation residue + minor in-situ mobilization ("paleosome") | Latent "Hockey stick" Cluster | Intrusive-pegmatitic/ensin | Intermediate (to felsic) s.r. | RdC |

**Table 6.** *Cont.*

| Stage | | Assemblage | Environment | Orientation | Mineralizing Processes | Lithology | Site |
|---|---|---|---|---|---|---|---|
| **2b** | | F > +Be | Differentiation product moderately self-intrusive ("leucosome") | Latent "Hockey stick" Cluster | Intrusive-pegmatitic/ensin | Intermediate (to felsic) s.r. | RdC |
| **2c** | | REE + Y > +Li-Cs | Differentiation product moderately self-intrusive ("leucosome") | Latent "Hockey stick" Cluster | Intrusive-pegmatitic/ensin | Intermediate (to felsic) s.r. | RdC |
| **2d** | | REE + Y > +W-Sn | Differentiation product moderately self-intrusive ("leucosome") | Latent "Hockey stick" Cluster | Intrusive-pegmatitic/ensin -greisen | Intermediate (to felsic) s.r. | RdC |
| **3 (2b,c, d overlap with 3)** | | REE + Y-Nb-Ti-F-Zr-Be-Sn-W-Li-Cs + Pb-Mn + calcsilicate minerals | Alkali-magmatite-carbonatite reaction(skarn) | "Hockey stick" NNE+ENE | Contact-metamorphic contact-metasomatic | Intermediate (to felsic)—carbonatite | Temperature trend Anaga (A) > RdC |
| **4a** | | V > S-P-(C?) | Hydrocarbon immigration (?) | NE → NNE (RdC) | Contact-metasomatic hydrothermal | Intermediate (to felsic)—carbonatite | Temp. trend A > RdC |
| **4b** | | Pb > Mn-V-As (Au) (+halogens) | Fumaroles | NNE near A ENE near RdC | Hydrothermal | Mainly basic volcanic and pyroclastic rocks | Temp. trend A > RdC |
| **Shallow low-temperature mineralization** | 5a | Mn-Fe-Pb-As-V-(Cu-Zn) sulfides-carbonates | Remobilization of primary mineralization | N-S NE-SWENE-WSW | Hydrothermal deep level pH ≥ 7 Eh ≤ 0 ⇒ Eh ≥ 0 | Mainly basic volcanic and pyroclastic rocks | Temp. trend RdC > A RdC > T |
| | **5b** | REE-Be-Mn zeolites | Remobilization of primary mineralization and zeolitization | E-W NW-SE NE-SW Triangular cluster | Hydrothermal basic deep level pH ≥ 7 Eh ≤ 0 ⇒ Eh ≥ 0 | Mainly basic volcanic and pyroclastic rocks | Temp. trend Teno (T) > A T > RdC |
| | **6** | Mn-Pb-Cu-Zn-V-P-(S)-LREE kaolinite-group minerals + boehmite | Mineralization and kaolinization | E-W NE-SW | Hydrothermal/e shallow level pH < 7 Eh > 0 (hypo-gene/supergene) mineralization | Mainly basic volcanic and pyroclastic rocks | Temp. trend: no aerial extension, confined to the KH line NE-SW |
| **7** | | Mn | Topomineralic mineralization | no | Autohydrotherm | Basic volcanic + pyroclastic rocks | no |

#### 5.2.2. Stage 2—The Syenite–pegmatite Intrusion

Stage 2, encompassing the alkaline intrusive rocks and their pegmatitic affiliates, is the crucial phase in the concentration of the rare and critical elements Be, Zr, F, Ti, Nb, REE, and Y, the marker minerals of which have been dealt with as Type III mineral assemblages (Figure 12b). This is also underscored by the in-depth discussion of their zonation on display in Figure 13 and the origin of their individual subfacies.

*Stage 2a*: This stage consists of primitive and very homogeneous facies of the syenite–pegmatite intrusion, with the rare element assemblage made up of Nb, F, Ti, and REE and dominated by Zr. They are accompanied by the radioactive elements U and Th, with a Th/U ratio greater than 1 that attests to an ensimatic origin (Figures 9 and 13, part a,b of Table 4). In moderately-to-highly fractionated granitic host rocks such as granitic pegmatites, Zr is said to be concentrated mainly in Nb-Ta-oxide minerals. The highest quantity was recorded from wodginite followed by columbite s.s.s. [217]. Depolymerization of highly fractionated, (F, B, P)- and $H_2O$-rich pegmatite-forming melts decreases the role of zircon relative to that of the Nb-Ta-oxide minerals. In the syenite–pegmatite intrusion, none of the cited host minerals occur, and baddeleyite, zircon, calcio-catapleite, elpidite, woehlerite, dalyite, (ferro) kentbrooksite, låvenite, zirconolite, eudyalite, and steenstrupine-(Ce) develop instead. Zirconium-scandium

phosphate-silicates have also been found in the Hagendorf–Pleystein Pegmatite Province in the incipient stages of pegmatite evolution [14]. The Strange Lake pegmatite, Canada, is a (Li-Zn-Th-F-Nb-Ta)-Be-REE-Zr pegmatite-aplite—see Section 4.2—with similar Zr minerals, e.g., calcio-catapleite, elpidite, dalyite, and eudyalite [29,31]. The stage-2a mineralization took place during the early phases of the syenite–pegmatite fractionation, and the mineralization is cast into the role of a differentiation residue or paleosome. Consequently, the following stages, 2b and 2c, are representative of the highly mobilized neosome (Figure 13). In peralkaline miaskitic rocks, Zr is incorporated in minerals like zircon, sphene, and ilmenite, suggesting stage 2a to be a miaskitic residue of differentiation [32].

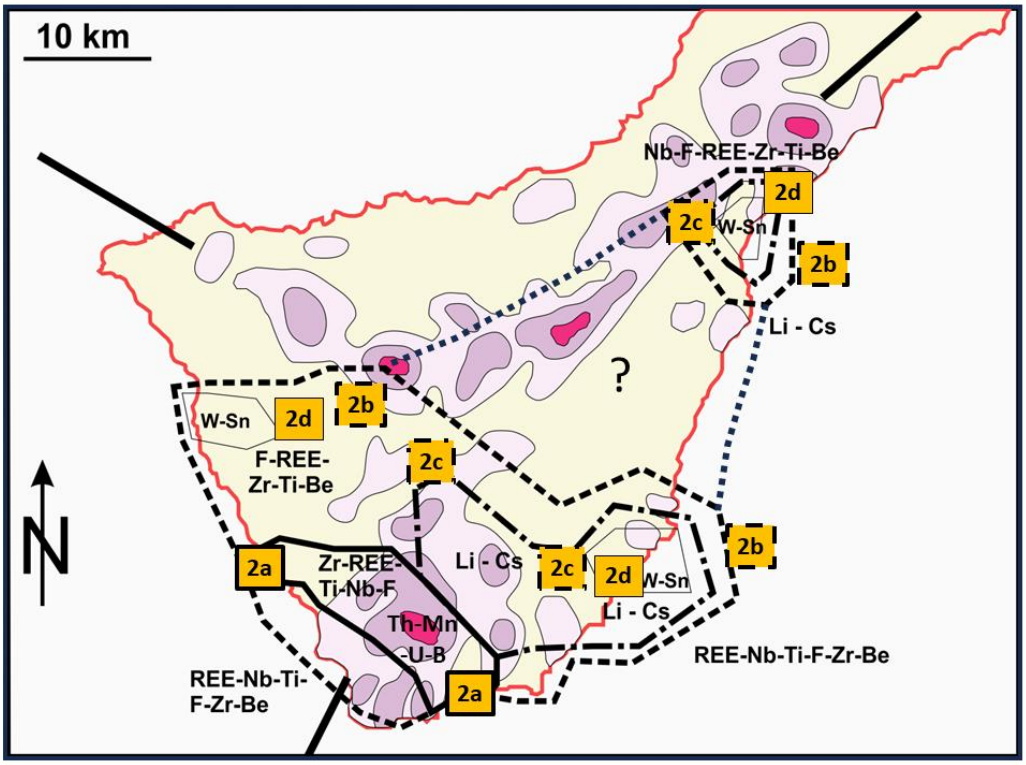


**Figure 13.** Close-up view of the evolution of the inferred syenite–pegmatite system and the zonation of the first-order elements shown in Figure 12b. See also Table 6. The areas framed with different bold lines denote the distribution of the different mineral assemblages the numbers of which are given by the orange boxes from 2a to 2d. The prevailing elements in each of these mineral assemblages are given.

*Stage 2b*: Beryllium, regarding its source, is a subcrustal element. It is frequently present in many pegmatites as beryl, but not so at Tenerife, where this Be mineral is absent and substituted for by a varied group of beryllium-bearing minerals appearing during different periods [14]. When displayed in a triplot of $SiO_2$-BeO-$Al_2O_3$, some common Be minerals reveal their facies-diagnostic features, which are part of the current composite study [20] (Figure 14). Helvine shows up very early on in the mineral succession among the hosts of Be, together with eudidymite and bertrandite. Beryllium is bound to deep fault zones and often assembled with another subcrustal derivate, vanadium, used as a chromophore to create gemmy Be silicates, e.g., Madagascar [21]. The element Be is a typical marker of mantle origin, rifting, and hotspot magmatic activity. It is not surprising to find it present side by side with Mn minerals such as rhodonite, bixbyite, pyrophanite, and pyroxmangite. The Be minerals characterize the transition from an intrusive-pegmatitic to a (sub) volcanic phase. Helvine is the only Mn-bearing Be mineral pointing towards the predecessor rift-related stage 1, which is exceptionally enriched in Mn minerals. On the opposite side of stage 2b, the skarn mineralization of stage 3 is looming with typical minerals such as pyroxmangite, pyrophanite, rhodonite, leucophoenicite and hedenbergite.

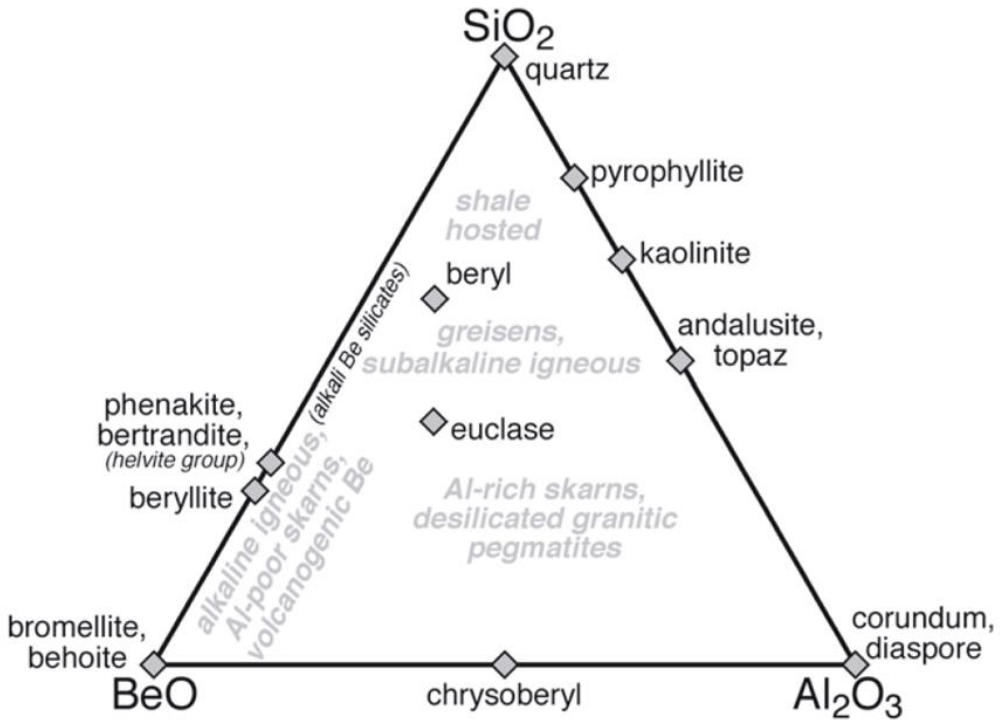


**Figure 14.** Chemography of the principal solid phases in the BeO-$Al_2O_3$-$SiO_2$ (projected from $H_2O$-$F_2O$) with some generalized fields for some of the major types of occurrences (slightly modified from [20]).

*Stage 2c*: Lithium follows suit with the cited Be mineral assemblage in that its protagonist of pegmatitic Li concentration spodumene accompanied by bikitaite is directly connected in time and space with Mn-bearing minerals such as galaxite, bixbyite, braunite, and hollandite, as well as the Zr host of stage 2a, dalyite, in the pegmatite-(skarn). Holmquisite comes up later and develops from the replacement of aegirine, while being itself replaced by lintisite. The postdating rare Li mineral tainiolite has also been recorded from carbonatites attesting to the looming stage 3 skarn mineralization [41] (part a of Tables 4 and 6).

*Stage 2d*: The Sn-W mineralization is only of minor importance in Tenerife, manifesting the waning stages of the syenite–pegmatite intrusion (Figure 13). Its presence can be taken as a hint to some greisen.

#### 5.2.3. Stage 3—Alkali-Magmatite-Carbonatite Skarn

Pegmatite skarn is not uncommon and it is known from W, Sn, REE, U, and Th mineralizations. The intracrustal setting of W, Sn and U is described as a frontal part of nappes and recorded from collisional geodynamic environments. Only REE and Th show a mantle affiliation while being bound to deep-seated lineaments and rifts, as is the case with Tenerife [14,114]). In Tenerife and Fuerteventura, the carbonate-bearing country rocks are not found among calcareous sediments or marbles but only among carbonatites, which formed in the Basal Complex between 28.1 ± 4.3 and 26.9 ±1.0 Ma, associated in time and space with older syenites aged 36.3 ± 1.7 Ma to 30.9 ± 1.2 Ma. The adjacent syenites of the Vega de Rio Palmas Ring Complex belong to a younger intrusion series spanning an interval of formation from 18.7 ± 0.8 Ma to 16.05 ± 0.04 Ma and are held accountable for the skarn mineralization and the denomination of the carbonatites of Fuerteventura as metacarbonatites [218].

A similar temporal relationship is also assumed for the hidden syenite–pegmatites and the parent material of the exoskarn at depth of Tenerife is inferred to be carbonatites (Figure 12c). The hottest point in Tenerife has been located in the environs of the Barranco Hondo where the same marker minerals, monticellite, wollastonite, and cuspidine,

came into being as in the Basal Complex of Fuerteventura. In Fuerteventura, the calcio-carbonatites have been exhumed by landslides and fluvial drainage systems. Similar erosional land-forming processes are missing at Tenerife in quantity and quality.

The bimodal couple alkali magmatite–carbonatite productive in terms of rare metals is also present in Tenerife, yet with a reversed carbonatite/alkali magmatite ratio. It has been tremendously shifted towards the agpaitic magmatic rocks, whereas the carbonatites have completely been wiped out and converted into a skarn by the younger syenites. They did not only provide the heat for the contact-metamorphism but also the varied portfolio of rare and critical elements for the contact-metasomatism (see stage 2). Carbonate minerals bearing $CO_3$–anion complexes have been found in stages 2 and 3, such as burbankite, cordylite-(Ce), kukharenkoite-(Ce), adamsite-(Y), ankylite-(Ce-La), bastnaesite, ankerite, rhodochrosite, niveolanite and sabinaite. There are productive mineralizations exemplified by the Y-Th-REE-Nb-Zr-Be pegmatite mineralization elsewhere that are genetically related to peralkaline magmatic activity, e.g., the Two Tom Lake deposit which is associated with metasyenites hosting barylite, eudidymite, niobophyllite and pyrochlore [219].

#### 5.2.4. Stage 4—Alkali-Magmatite-Carbonatite-Related Metasomatic-Hydrothermal Mineralizations

*Stage 4a*: Stage 4a is characterized by V, S, P and C and confined to trachytes (Figure 12d). It is a rare mineral assemblage known only from the Minas Ragra mineralization in the Peruvian Andes [211]. The reference deposit suggests the interaction of V-bearing hydrothermal fluids with hydrocarbon-related sulfur. Such an enrichment of carbonaceous matter in geyserite and calcareous brine deposits is common in rift zones according to [220], who studied the origin of these carbon concentrations in the Baikal Rift Zone, Russia. The authors determined the formation temperatures to be above 400 °C for the carbonaceous matter from well-crystallized graphite to alpha-carbyne and bitumen. They reported a low-pressure poly-condensation of hydrocarbons at free growth in open space from oversaturated solutions and/or a gas phase, which reported as the waning hydrothermal stages of the contact-metasomatic processes during stage 3. There are also mineral assemblages devoid of this conspicuous "Minas Ragra Facies" in Tenerife.

*Stage 4b*: The chlorine-bearing Pb-Mn-V-As mineral assemblage is representative of organic-matter-free fumaroles closely related to volcanoes (Figure 12d) [221–225]. Minerals like cotunnite and phosgenite can be of anthropogenic origin such as from slags at smelting sites and from post-mining mineralization in abandoned shafts and galleries given the climate is rather dry or of geogene origin when salars or spill-overs from breakers and the surf in the coastal zone occur. None of these arguments can be put forward for the areas on Tenerife where neither the climate nor the cultural evolution of the ancient Canarians support any of these ideas. Hot brines in the aftermath of volcanic activity are more likely to have brought about these minerals at temperatures of less than 50 °C [222].

Both mineralizations discussed above show similar trends of their formation temperatures decreasing from the Anaga towards the Roque del Conde Massif, with the "hot spot" being situated in the Barranco Hondo region. The preference of the NNE and NE direction during these mineralizations provides evidence of late-stage rift movements creating a line of magma eruptions like pearls on string and sparking hot brines that ascend in the aftermaths of those magma ascent. The line of eruption centers runs parallel to the Hernandez Fm., which was emplaced in the interval >0.37–0.19 Ma, and the magma of which made contact with intrusives and/or tapped into subvolcanics at depth.

Native gold has been found in the south-eastern part of Tenerife, Spain. Therefore, this precious metal can only be attributed to one of these local stages displaying a temperature trend of A > RdC. It belongs either to stage 3 or 4, heralding a transition from contact-metasomatic to hydrothermal processes (Table 6). There are various mineralizing processes that need to be discussed for its emplacement: (1) pyrometasomatic Au skarn, (2) shallow Cu-Au-Ag mineralization of different degrees of sulfidation, (3) alkaline igneous rock with Au-Ag-Te enrichments, and (4) carbonate-hosted disseminated Au-Ag deposits

(Carlin-type) [9]. A seamount-hosted tellurium deposit has been found 500 km from the Canary Islands: *Samples brought back to the surface contain the scarce substance tellurium in concentrations 50,000 times higher than in deposits on land To* [226]. Pigeonholing as performed in many textbooks and reviews is necessary to constrain the possible modes of concentration, but, in practice, it is mostly a complex telescoping of different concentration processes. In the current geological–mineralogical setting, only type 4 can definitely be ruled out on the aforementioned selection (Table 6).

#### 5.2.5. Stage 5—Hydrothermal Mineralization and Zeolitization

Stage 5 marks a turning of the tides regarding the orientation of the fault systems used by magma and hydrothermal fluids alike, unravelling the direction of the temperature drop, and the compositional changes in the mineral assemblages involved (Table 6, Figure 12e). These are the criteria to split stage 5 into two substages 5a (Mn-Pb-As-V-S carbonate) and 5b (zeolites-Be) and suggest a combination with stage 6 named "Shallow low-temperature mineralization", which is transitional from hypogene into supergene (Table 6). Type II contact-metasomatic/contact-metamorphic minerals no longer play a part as indicator minerals for the temperature during this period of mineralization. It is the type I silicates that have a controlling effect on the mineralization during the waning metallogenesis between the Anaga Massif (NE Tenerife) and the Garajonay volcanic-core-failure caldera of the "Alto de Garajonay" (NE La Gomera) where the KH-Line as a tie line hits the Isle of La Gomera (Figure 2).

*Stage 5a*: Stage 5a is representative of a remobilization of metals under a sulfidic and carbonatic regime by basic to neutral fluids at the transition from reducing (galena, alabandite, kutnohorite, ankerite) to oxidizing conditions (reppaite, bixbyite, hollandite, tiragalloite) at low temperature, affecting all previous stages as exemplified by the varied element spectrum of stage 5a. The stage 5a mineralization resembles the oxide and sulfide mineralization in the islands of Tenerife and La Gomera recorded by [87], although its less variegated spectrum composed of magnetite, ilmenite, pyrite, pyrrhotite and Cu-Zn sulfides bound to intrusive rocks in the Basal Complex of La Gomera and in the Anaga Massif of Tenerife (Figure 2, Table 6).

*Stage 5b*: Like in its predecessor, stage 5a, the zeolites of stage 5b precipitated from alkaline to neutral fluids. They affected all kinds of eruptive volcanic rocks and depleted them of their Na, K, Ca, and Mg primarily accommodated in the lattice of feldspar, Na pyroxene and Na amphibole (chabazite-Na, analcime, heulandite-Na, clinoptilolite-Na, natrolite, phillipsite-Na, stilbite-Na, gonnardite) over Ca-bearing end members (chabazite-Ca, laumontite, thomsonite-Ca, phillipsite-Ca, clinoptilolite-Ca, stilbite-Ca, offretite (Table 4c). The temperature trend controlling zeolitization, however, reversed during stage 5b, shifting the T hotspot towards the Teno Massif (Figure 8, Table 6). Along with this zeolitization, LREE and HREE are redeposited into rhabdophane and churchite, respectively. Secondary beryllium minerals such as behoite, bavenite, chiavennite, gugiaite, hambergite, and tvedalite postdate the formation of zeolites, e.g., phillipsite-K. Heulandite-K is replaced by hollandite and ranceite, attesting to an overall oxidizing regime during stage 5b. Other minerals like shcherbakovite or sazhinite-(Ce) belong to this stage but cannot be attributed to one or the other zeolite species.

Stage 5 formed from hydrothermal solution in the range 20 to 250 °C. It has offshoots in Gran Canaria, Tenerife, and La Gomera and is representative of the deep level of what might be called a mixed or intermediate epithermal system with marker minerals such as Fe-Cu-Zn sulfides, kaolinite group minerals and APS minerals, while the latter category of minerals is only present at the far end of the KH Line on La Gomera in stage 6, where the newly discovered florencite-(Ce) occurrence is situated.

#### 5.2.6. Stage 6—Hypogene–Supergene Mineralization and Kaolinization

Regarding its structure and ore mineralization, stage 6 is a replica of stage 5, yet with a marked change in the group silicates from tectosilicates to phyllosilicates. A conspicuous

kaolinization involving kaolinite, halloysite 7 Å and 10 Å mainly in the NE–SW direction between Barranco Hondo and Alcala is typical of this stage (Figure 12f). The mineral association Fe sulfide ± magnetite → kaolinite 7 Å → halloysite 7 Å → halloysite 10 Å is, according to [227], interpreted as advanced argillitization, which can penetrate down to a depth of as much as 600 m. Other minerals trail behind kaolinite group clay minerals by a wide margin. It is saponite, hematite, goethite, magnetite and sanidine which are chronologically constrained to the period 1.5 to 0.3 Ma [108]. Chlorite, vermiculite, smectite and nontronite occur in minor quantities. Nontronite formed during a low-temperature alteration in sulfide-bearing felsic metavolcanics and in epithermal copper-gold-silver deposits of high- and low-sulfidation type, which closely resembles the so-called "Shallow low-T mineralization" [228,229] (Table 6). Saponite present along the KH Line has derived from the ubiquitous mafic minerals, e.g., sodium-enriched pyroxene and amphibole at shallow depth underneath the zone of oxidation at temperatures below 100–150 °C in the pH range from pH 7 to pH 5.5. Boehmite has only been found at two locations, at the southernmost and northwesternmost sampling sites, attesting to an oxidic marginal facies of probably supergene origin.

In the Garajonay volcanic-core-failure caldera of La Gomera, the florencite mineralization is immediately associated with kaolinite and halloysite. A calculation based upon the bulk chemical analysis at La Gomera yields a kaolinite content between 75 and 80%. It is the only in situ REE mineralization at the surface related to the kaolinization. Unlike neighboring Tenerife, the volcanic activity at La Gomera ceased around 2 Ma ago and thus the REE mineralization persisted until the present completely untouched by younger volcanic processes [63].

#### 5.2.7. Stage 7—Auto-Hydrothermal Mineralization in Volcanic and Volcaniclastic Rocks

Stage 7 mineralization is neither structurally related nor does it exhibit any temperature trends enabling us to correlate it with a special heat center. It is therefore named topomineralic; in other words, it is related to the place and type of magmatic rocks. The prototype for this (sub)recent mineralization is the complex manganese silicate mendigite that was named after a town in one of the largest volcanic fields, Niedermendig, Germany [230] (part a,b of Table 4).

A set of sketches at the end of the sixfold succession of maps of Figure 12 allows for a briefing combining geodynamics (1) the opening of the rift system (green pattern: NW-SE), (2) mineralogy (the temperature drop (red pattern: towards the NW)) and (3) economic geology. The latter indicates a shallowing (blue pattern: towards the SW) of the metallogenic axis, which plunges towards the NE. The shallowing of the axis accounts for the discovery of the new florencite-(Ce)-kaolinite-halloysite occurrence in the Garajonay slope failure caldera of La Gomera island, off Tenerife (Figures 1b and 12g). It proves the effectiveness of this holistic approach grouped around the mineralogy.

### *5.3. From rare Minerals in Volcanics and Xenoliths to the Critical Element Deposits—A Conditio Sine Qua Non for the Use of Modern Technologies*

#### 5.3.1. From Classical Chemical to Mineralogical Exploration

Chemical exploration has been since long ago the technique of choice to define prominent anomalies of chemical compounds and elements in order to delineate a metal concentration [231]. This was either carried out using bare rocks (lithochemical—primary exploration) or unconsolidated rocks subjected to weathering and transport, e.g., stream sediments, soil samples, water samples, soil gas or plants (biochemical exploration and geobotanical exploration (marker plants)). The litho-geochemical anomalies are caused by primary processes when an ore deposit was emplaced under high T and P conditions. Secondary anomalies come into existence as an ore deposit is exposed by weathering and erosion and the constituent minerals and trace elements are dispersed and transported downstream.

Mineralogical exploration using, e.g., heavy minerals and lithoclasts, gives an overview of the dispersion of rocks and minerals at surface [27,76]. These methods need mineralogical and sedimentological knowledge and experience in climate geomorphology. These methods are confined to rocks and minerals resistant to attrition on transport and weathering under certain climates. These are also method that give a clue regarding the origin of the source rock.

Micromounts have so far been objects collected only for the showroom, for the sake of beauty and to find new minerals. To also be useful for exploration, one needs both mineralogical experience and sedimentological and geomorphological experience to study landforms and "read" the landscapes. In the present case of a modern volcanic landscape, it is volcano-morphology that has a strong say when it comes to mineralogical, quantitative mapping. It is the only one giving an insight into what might have happened at depth and at the surface.

Summarized in a more succinct expression, one can say: "Geochemical exploration gives you a whisper whereas mineralogical mapping tells you a story from the early beginning".

The current "story" is not taken as the blueprint for a deep drill hole at the heart of the volcanic island of Tenerife, maybe sunken in the midst of one of the many tourist resorts about 10 km deep, to strike the potential source and bedrocks of Late Jurassic age and penetrate an intrusive core of agpaitic and miaskitic descend. The same holds true for a shaft or gallery on the island.

The minero-stratigraphy within the archipelago extended into the submarine environment at the brink between the continental shelf and the open ocean. The first positive result obtained from this mineralogical mapping was the discovery of a florencite-bearing occurrence in the basal complex of the neighboring island of La Gomera along the KH-Line and a promising open view into the submarine region through the finding of tellurium [226] (Figure 2). There is much more potential in the submarine environment between the islands and the many seamounts around the Canary Islands Archipelago which have been mapped but not yet tested in such a way [232,233]. With this in mind, many archipelagos elsewhere in the world endowed with volcanic islands are awaiting reference mineralogical mapping on land and follow-up submarine mapping.

The prerequisites for this holistic approach to be taken successfully in economic geology are a (1) a low maturity of the landscapes in the target area and (2) Cenozoic (Late Cretaceous?) ages; in other words, a target area where endogenous and exogenous processes are intertwined and force mineralogy to steadily keep pace with the sedimentological, geomorphological and volcano-tectonic variations.

The exploration tool for mineral deposits put forward in this composite study can be successfully applied to find mineral accumulations in the course of a mineralogical terrain analysis as exemplified by the La Gomera's findings. It is, however, primarily designed as a strategic rather than tactical or operative tool in terms of the military chain of command. It can be translated into exploration terminology and common tripartite reserve designation arranged in order of decreasing security as (1) proved/measured, (2) probable/indicated and (3) possible/inferred [8]. This is also signaled by the timeframe of the current "micromount exploration" on Tenerife and its sister islands, which is rated as more than ten years. Given this fact, this "*advanced-level terrain analysis*" can successfully be applied in geological surveys, international organizations and large metal-mining enterprises for their strategic planning rather than a short-term exploration campaign with a quick return of investment (Figures 15 and 16).

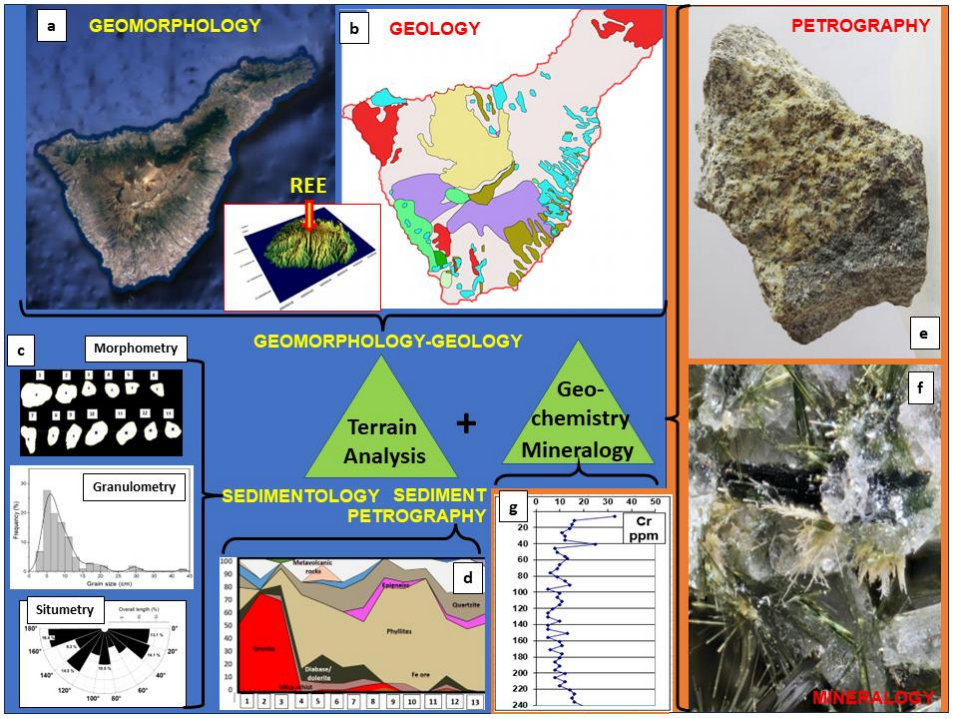


**Figure 15.** Figure to show the disciplines interlocked with each other in the project of the "Mineralogical Terrain Analyses" consisting of the terrain analysis (blue background) and the mineralogical modifier (brown background). The inset between (**a**) and (**b**) denotes the 3D digital terrain model of the Garajonay volcanic-core-failure caldera on the flanks of the "Alto de Garajonay", La Gomera Spain and the REE discovery throughout this study. (**a**) Geomorphology (e.g., satellite image of Tenerife, Spain-Source Google Maps). (**b**) Geological map (e.g., geological map of Tenerife, Spain-modified from [65]). (**c**) Sedimentology (e.g., morphometry of gravel, granulometry of gravel, situmetry/orientation of gravel). (**d**) Sediment petrography (e.g., variation in lithoclasts along the talweg as function of fluvial and mass wasting transport). (**e**) Petrography (e.g., altered nepheline-syenite). (**f**) Mineralogy (e.g., vuggy groundmass with låvenite and aegerite). (**g**) Geochemistry (e.g., DDH chemical analysis of a chromium project).

#### 5.3.2. Critical Elements—Low Grade–Low Quantity and High Quality–High Impact

From whatever angle you may look at modern high-tech devices, be it as a defense analyst, a specialist on fossil and renewables energies, their availability, transport, storage, and use, as a nano-technologist or as a medical engineer, there are many devices that need low quantities of high-purity critical elements to work at all. Where the dissipative use of such an element is the only application, the constant availability of such elements is paramount. Substitution of the critical elements and recycling them may mean that these swiftly reach their limits due to the aforementioned reasons.

In economic geology, another third type of mineral commodity needs to be defined in addition to the two existing end-member types. The high-unit value mineral commodities (e.g., diamonds, platinum-group minerals) and high-place value commodities (e.g., silica sand and gravel). The third one in this categorization scheme is the "have-it-or-leave-it commodity"; the presence of a critical element is decisive for its use, a *conditio sine qua non* for the entire production of special high-tech devices. And obtaining such "have-it-or-leave-it commodities" justifies the application of the most exotic exploration methods to achieve this goal.

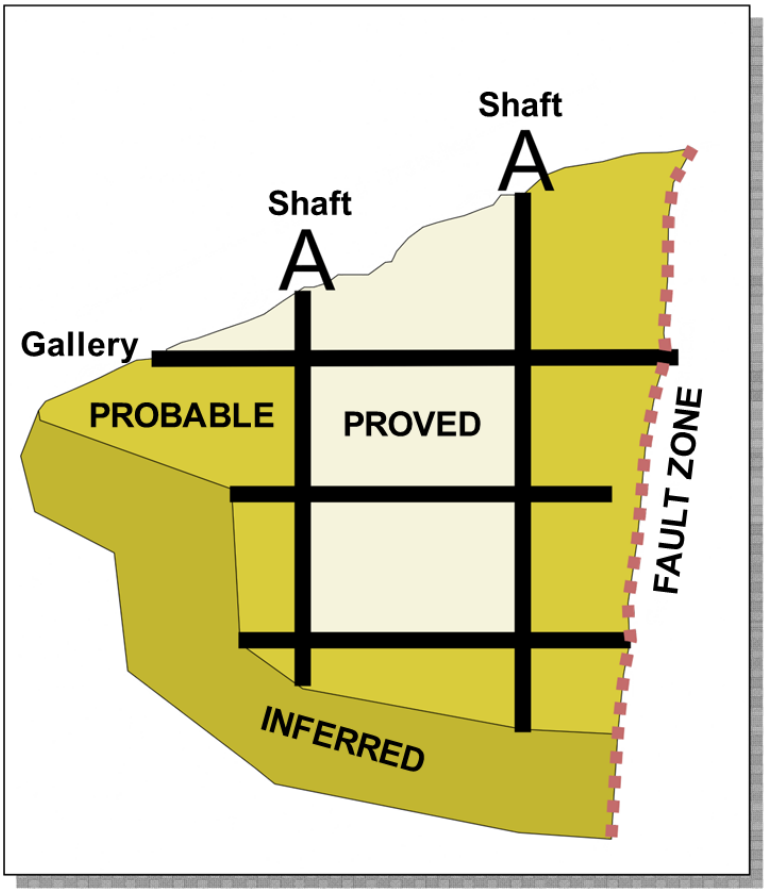


**Figure 16.** Figure outlining reserves modified from [8]. It is used to visualize the confidence level of an "inferred mineral deposit" as dealt with in the current study in relation to indicated and proved equivalent ones.

### *5.4. Synopsis and Exploration Using an Advanced Level of Terrain Analysis*

Mineral exploration using a mineralogical terrain analysis is a holistic approach in the true sense of the word (Figure 15). The mineralogical part is the topic of the current publication, and the terrain analysis *sensu stricto* is more complex and planned to be discussed in a separate paper. The terrain analysis is designed to provide the spatial framework in which the mineralogical field and laboratory studies are embedded. In essence, the terrain analysis is the core of this composite study in applied economic geology to which different geoscientific disciplines can be attached according to needs and wants. Alternatively applied geophysics and geochemistry can stand in for mineralogical mapping simply by capturing digital data in the field. Apart from measuring magnetic susceptibility, using gamma spectrometry and micro-electrical conductivity (SER method), the determination of the electromagnetic spectrum at the surface can be very helpful [234]. SWIR and NIR spectrometry cannot replace detailed XRD runs in the laboratory to identify the minerals but these can constrain the sampling area in the field significantly and fill in the gap between field-based and laboratory-based mineral identification as shown using a UV–Vis–NIR (250–2500 nm range) spectroradiometer [235] This also holds true for laser-induced plasma spectroscopy (LIPS) [236]. These hand-held devices can be used in the terrain analysis but they cannot substitute a precise mineralogical and petrographic study.

## 6. Conclusions

- Critical elements, in this case history of Tenerife, such as beryllium, fluorine, lithium, niobium (tantalum), zirconium (hafnium), and rare earth elements are decisive in

many high-tech products to find out if a device can economically be operated or not. Their availability is a *conditio sine qua non* for the final products (Figures 1 and 15).

- For discovering new deposits of these critical elements, unconventional quantitative mineralogical mapping has proved to assist in delineating lithological intrusive/subvolcanic bodies, varied alteration zones and potential ore deposits using xenoliths (Figures 5–7, 12 and 13).
- Two types of critical element concentrations, carbonatites and pegmatites bound to agpaitic intrusive rocks, are genetically closely interlocked with each other in rift zones and associated with hotspots and, hence, these govern the evolution of volcanic island archipelagos near passive continental margins (Figure 12g,h).
- There are multiple mineralizing processes: rifting, differentiation, contact-metasomatic/hydrothermal mineralization, hydrothermal remobilization and zeolitization hypogene–supergene transitional kaolinization, and auto-hydrothermal–topomineralic mineralization (Figures 8, 11, 12a–f and 13, Table 6).
- The prerequisites for this holistic approach in economic geology are a low maturity of the landscapes in the target area, Cenozoic (Late Cretaceous?) ages of endogenous and exogenous processes amenable to sedimentological, geomorphological, volcanotectonic and quantitative mineralogical investigations (Figures 3 and 5, Table 5).
- The volcanic island mineralogical mapping of Tenerife, Spain, is not primarily designed as a pre-well-site study. It is a reference study area for minero-stratigraphic inter-island correlation (land–land) and land–sea when investigating the seabed and seamounts around volcanic archipelagos worldwide in search of critical elements (Figures 2 and 12h, part a–c of Table 4).

**Author Contributions:** H.G.D.: Conceptualization, writing the text and illustrations; K.A.R.: mineralogical mapping. All authors have read and agreed to the published version of the manuscript.

**Funding:** This research received no external funding.

**Data Availability Statement:** Data will be made available on request.

**Acknowledgments:** We acknowledge with gratitude the helpful comments of two anonymous reviewers made to our manuscript and the academic editor's handling of our paper submitted to *Minerals*.

**Conflicts of Interest:** The authors declare no conflict of interest.

## References

1. Wagner, C.; Mokhtari Deloule, E.; Chabaux, F. Carbonatite and Alkaline Magmatism in Taourirt (Morocco): Petrological, Geochemical and Sr–Nd Isotope Characteristics. *J. Petrol.* **2003**, *44*, 937–965. [CrossRef]
2. Casillas, R.; Demény, A.; Nagy, G.; Ahijado, A.; Fernández, C. Metacarbonatites in the Basal Complex of Fuerteventura (Canary Islands). The role of fluid/rock interactions during contact metamorphism and anatexis. *Lithos* **2011**, *125*, 503–520.
3. Bea, F.; Montero, P.; Haissen, F.; El Archi, A. 2.46 Ga kalsilite and nepheline syenites from the Awsard pluton, Reguibat Rise of the West African Craton, Morocco. Generation of extremely K-rich magmas at the Archean–Proterozoic transition. *Precambrian Res.* **2013**, *224*, 242–254. [CrossRef]
4. Benaouda, R.; Kraemer, D.; Sitnikova, M.; Goldmann, S.; Schwarz-Schampera, U.; Errami, A.; Mouttaqi, A.; Bau, M. Discovery of high-grade REE-Nb-Fe mineralization associated with calciocarbonatite in south Morocco. *Ore Geol. Rev.* **2020**, *124*, 103631. [CrossRef]
5. Benaouda, R.; Kraemer, D.; Bejtullahu, S.; Mouttaqi, A.; Bau, M. Occurrence of high-grade LREE allanite-pegmatites and calcite carbonatite dykes in the Ediacaran complex of Aghracha, Oulad Dlim Massif (South Morocco). *J. Afr. Earth Sci.* **2022**, *196*, 104727. [CrossRef]
6. Haissen, F.; Montero, P.; Cambeses, A.; Bea, F.; Molina, J.F.; Mouttaqi, A.; Gonzalez- Lodeiro, F.; Sadki, O.; Errami, A. Petrogenesis of Derraman peralkaline granite (Oulad Dlim massif, west African Craton margin, Morocco): New constraints from zircon Hf and O isotopic compositions. *Compt. Rendus Geosci.* **2018**, *350*, 236–244. [CrossRef]
7. Maham, E.S.; Ouali, H.; Jébrak, M.; Ouabid, M. 2021 Contribution to the study of carbonatite complex of the Richat Dome (Mauritania). In Proceedings of the EGU General Assembly 2021, Online, 19–30 April 2021; p. EGU21-12995. [CrossRef]
8. Carr, D.D.; Herz, N. *Concise Encyclopedia of Mineral Resources*; Pergamon Press: Oxford, UK, 1989; p. 426.

9. Dill, H.G. The "chessboard" classification scheme of mineral deposits: Mineralogy and geology from aluminum to zirconium. *Earth Sci. Rev.* **2010**, *100*, 1–420. [CrossRef]
10. Dill, H.G.; Buzatu, A.; Balaban, S.-I.; Rüsenberg, K.A. A mineralogical-geomorphological terrain analysis of hotspot volcanic islands—The missing link between carbonatite- and pegmatite Nb-F-Zr-Li-Be-bearing REE deposits and new tools for their exploration (Canary Islands Archipelago, Spain). *Ore Geol. Rev.* **2023**. *in print*.
11. Monster, M.W.L.; van Galen, J.; Kuiper, K.F.; Dekkers, M.J.; de Groot, L.V. A late-Quaternary full-vector geomagnetic record from El Golfo section, El Hierro, Canary Islands. *Geophys. J. Int.* **2018**, *215*, 1701–1717. [CrossRef]
12. Paris, R.; Guillou, H.; Carracedo, J.C.; Pérez-Torrado, F.J. Volcanic and morphological evolution of La Gomera (Canary Islands), based on new K–Ar ages and magnetic stratigraphy: Implications for oceanic island evolution. *J. Geol. Soc. Lond.* **2005**, *162*, 501–512. [CrossRef]
13. Sagan, M.; Heaman, L.M.; Pearson, D.G.; Luo, Y.; Stern, R.A. Removal of continental lithosphere beneath the Canary archipelago revealed from a U/Pb age and Hf/O isotope study of modern sand detrital zircons. *Lithos* **2020**, *362–363*, 105448. [CrossRef]
14. Dill, H.G. Pegmatites and aplites: Their genetic and applied ore geology. *Ore Geol. Rev.* **2015**, *69*, 417–561. [CrossRef]
15. Sørensen, H. *Beryllium Minerals in a Pegmatite in the Nepheline Syenites of Ilimaussaq, South West Greenland*; Report, 21st Session, Norden, Part 17; International Geological Congress: Buffalo, NY, USA, 1960; pp. 31–35.
16. Novák, M.; Černý, P.; Uher, P. Extreme variation and apparent reversal of Nb-Ta fractionation in columbite-group minerals from the Scheibengraben beryl-columbite granite pegmatite, Marsikov, Czech Republic. *Eur. J. Mineral.* **2003**, *15*, 565–574. [CrossRef]
17. Groat, L.A.; Giuliani, G.; Marshall, D.D.; Turner, D. Emerald deposits and occurrences: A review. *Ore Geol. Rev.* **2008**, *34*, 87–112. [CrossRef]
18. Uher, P.; Bačík, P.; Ozdín D Števko, M. Beryl in granitic pegmatites of the Western Carpathians (Slovakia): Compositional variations, mineral inclusions and breakdown products. *Acta Mineral. Petrographica. Abstr. Ser.* **2012**, *7*, 144.
19. Lyalina, L.M.; Selivanova, E.A.; Zozulya, D.R.; Ivanyuk, G.Y. Beryllium Mineralogy of the Kola Peninsula, Russia—A Review. *Minerals* **2018**, *9*, 42. [CrossRef]
20. Barton, M.D.; Young, S. Non-pegmatitic Deposits of Beryllium: Mineralogy, geology, phase equilibria and origin. *Rev. Mineral. Geochem.* **2002**, *50*, 591–692. [CrossRef]
21. Dill, H.G. *The Hagendorf-Pleystein Pegmatite Province, SE Germany: The Center of Pegmatites in an Ensialic Orogen (Modern Approaches in Solid Earth Sciences)*; Springer: Dortrecht, The Netherlands; Berlin/Heidelberg, Germany; London, UK; New York, NY, USA, 2015; p. 343. ISBN 978-3-319-18805-8.
22. Lindsey, D.A. Beryllium deposits at Spor Mountain, Utah. In Proceedings of the 35th forum on the geology of industrial mineral—The International West Forum 1999, Salt Lake City, UT, USA, 1 January 1999; Bon, R.L., Riordan, R.F., Tripp, B.T., Krukowski, S.T., Eds.; Utah Geological Survey Miscellaneous Publication 01-2: Salt Lake, UT, USA, 2001; pp. 73–77.
23. Ludwig, K.R.; Lindsey, D.A.; Zielinski, R.A.; Simmons, K.R. U-Pb ages of uraniferous opals and implications for the history of beryllium, fluorine, and uranium mineralization at Spor Mountain. *Utah Earth Planet. Sci. Lett.* **1980**, *46*, 221–232. [CrossRef]
24. Hou, B.; Keeling, J.; Frakes, L.; Alley, N.; Luo, X. Evolution and exploration of palaeochannels/palaeoshorelines, South Australia: A decade on-MRD-12 Fluvial palaeo-systems. In *Evolution and Mineral Deposits*; International Geological Congress: Oslo, Norway, 2008.
25. Benisek, A.; Finger, F. Factors controlling the development of prism faces in granite zircons: A microprobe study. *Contrib. Mineral. Petrol.* **1993**, *114*, 441–451. [CrossRef]
26. Bingen, B.; Davis, W.J.; Austrheim, H. Zircon U–Pb geochronology in the Bergenarc eclogites and their Proterozoic protoliths, and implications for the pre- Scandian evolution of the Caledonides in western Norway. *Geol. Soc. Am. Bull.* **2001**, *113*, 640–649. [CrossRef]
27. Dill, H.G.; Weber, B.; Klosa, D. Crystal morphology and mineral chemistry of monazite–zircon mineral assemblages in continental placer deposits (SE Germany): Ore guide and provenance marker. *J. Geochem. Explor.* **2012**, *112*, 322–346. [CrossRef]
28. Gübelin, E.; Erni, F. *Gemstones, Symbols of Beauty and Power*; Geoscience Press: Tucson, AZ, USA, 2000; p. 240.
29. Salvi, S.; Williams-Jones, A.E. Zirconosilicate phase relations in the Strange Lake (Lac Brisson) pluton, Quebec–Labrador, Canada. *Am. Mineral.* **1995**, *80*, 1031–1040. [CrossRef]
30. Kerr, A.; Rafuse, H. Rare-earth element (REE) geochemistry of the Strange Lake deposits: Implications for resource estimation and metallogenic models. *Nfld. Labrador Dep. Nat. Resour. Curr. Res.* **2012**, 39–60.
31. Gysi, A.P.; Williams-Jones, A.E. Hydrothermal mobilization of pegmatite-hosted REE and Zr at Strange Lake, Canada: A reaction path model. *Geochim. Cosmochim. Acta* **2013**, *122*, 324–352. [CrossRef]
32. Doroshkevich, A.; Sharygin, V.V.; Belousova, E.A.; Izbrodin, I.A.; Prokopyev, I.R. Zircon from the Chuktukon alkaline ultramafic carbonatite complex (Chadobets uplift, Siberian craton) as evidence of source heterogeneity. *Lithos* **2021**, *382–383*, 105957. [CrossRef]
33. Tichomirowa, M.; Whitehouse, M.J.; Gerdes, A.; Götze, J.; Schulz, B.; Belyatsky, B.V. Different zircon recrystallization types in carbonatites caused by magma mixing: Evidence from U–Pb dating, trace element and isotope composition (Hf and O) of zircons from two Precambrian carbonatites from Fennoscandia. *Chem. Geol.* **2013**, *353*, 173–198. [CrossRef]
34. Jago, B.C.; Gittins, J. The role of fluorine in carbonatite magma evolution. *Nature* **1991**, *349*, 56–58. [CrossRef]
35. Alvin, M.P.; Dunphy, J.M.; Groves, D.I. Nature and genesis of a carbonatite-associated fluorite deposit at Speewah, East Kimberley region, Western Australia. *Mineral. Petrol.* **2004**, *80*, 127–153. [CrossRef]

36. Samson, I.M.; Wood, S.A.; Finucane, K. Fluid inclusion characteristics and genesis of the fluorite–parisite mineralization in the Snowbird Deposit, Montana. *Econ. Geol.* **2004**, *99*, 1727–1744. [CrossRef]
37. Kontak, D.J.; Ansdell, K.; Dostal, J.; Halter, W.; Martin, R.; Williams-Jones, A.E. The nature and origin of pegmatites in a fluorine-rich leucogranite, East Kemptville Tin Deposit, Nova Scotia, Canada. *Trans. R. Soc. Edinb. Earth Sci.* **2001**, *92*, 173–200. [CrossRef]
38. Bastos Neto, A.C.; Pereira, V.P.; Ronchi, L.H.; Lima, E.F.; Frantz, J.C. The world-class Sn, Nb, Ta, F (Y, Ree, Li) deposit and the massive cryolite associated with the albite-enriched facies of the Madeira A-type granite, Pitinga Mining District, Amazonas State, Brazil. *Can. Mineral.* **2009**, *47*, 1329–1357. [CrossRef]
39. Dixon, C.J. *Atlas of Economic Mineral Deposits*; Chapman and Hall: London, UK, 1979.
40. Novák, M.; Cerný, P. Distinctive compositional trends in columbite–tantalite from two segments of the lepidolite pegmatite at Rozná, western Moravia, Czech Republic. *J. Czech Geol. Soc.* **2001**, *46*, 1–8.
41. Cooper, A.F.; Paterson, L.A.; Reid, D.L. Lithium in carbonatites-consequence of an enriched mantle source? *Mineral. Mag.* **1995**, *59*, 401–408. [CrossRef]
42. Dias, M.B.; Wilson, W.E. Famous mineral localities: The Alto Ligonha pegmatites (Mozambique). *Mineral. Rec.* **2000**, *31*, 459–497.
43. Selway, J.B.; Breaks, F.W.; Tindle, A.G. A review of rare-element (Li–Cs–Ta) pegmatite exploration techniques for the Superior Province, Canada, and large worldwide tantalum deposits. *Explor. Min. Geol.* **2005**, *14*, 1–30. [CrossRef]
44. Neiva, A. Feldspars, micas and columbite–tantalite minerals from the zoned granitic lepidolite-subtype pegmatite at Namivo, Alto Ligonha, Mozambique. *Eur. J. Mineral.* **2013**, *25*, 967–985. [CrossRef]
45. Chakhmouradian, A.R.; Sitnikova, M.A. Radioactive minerals in murmanite–lorenzenite-tinguaite at Mt. Selsurt, Lovozero complex, Kola Peninsula. *Eur. J. Mineral.* **1999**, *11*, 871–878. [CrossRef]
46. Chakhmouradian, A.R.; Mitchell, R.H. New data on pyrochlore- and perovskite-group minerals from the Lovozero alkaline complex, Russia. *Eur. J. Mineral.* **2002**, *14*, 821–836. [CrossRef]
47. Woolley, A.R.; Church, A.A. Extrusive carbonatites: A brief review. *Lithos* **2005**, *85*, 1–14. [CrossRef]
48. Kanazawa, Y.; Kamitani, M. Rare earth minerals and resources in the world. *J. Alloys Compd.* **2006**, *408–412*, 1339–1343. [CrossRef]
49. Hong-Rui, F.; Yi-Han, X.; Kai-Yi, W.; Wilde, S.A. Methane-rich fluid inclusions in skarn near the giant REE–Nb–Fe deposit at Bayan Obo, Northern China. *Ore Geol. Rev.* **2004**, *25*, 259–283.
50. Ni, P.; Zhou, J.; Chi, Z.; Pan, J.-Y.; Li, S.-N.; Ding, J.-Y.; Han, L. Carbonatite dyke and related REE mineralization in the Bayan Obo REE ore field, North China: Evidence from geochemistry, C-O isotopes and Rb-Sr dating. *J. Geochem. Explor.* **2020**, *215*, 106560. [CrossRef]
51. She, H.-D.; Fan, H.-R.; Yang, K.-F.; Li, X.-C.; Wang, Q.-W.; Zhang, L.-F.; Liu, S.; Li, X.-H.; Dai, Z.-H. In situ trace elements of magnetite in the Bayan Obo REE-Nb-Fe deposit: Implications for the genesis of Mesoproterozoic iron mineralization. *Ore Geol. Rev.* **2021**, *139*, 104574. [CrossRef]
52. Tian, P.; Xiaoyong, Y. Wanming Yuan Formation and preservation of the Bayan Obo Fe-REE-Nb deposit, Inner Mongolia: Insights from evidences of petrogenesis, geochemistry and apatite fission track dating. *Solid Earth Sci.* **2021**, *6*, 228–245. [CrossRef]
53. Tian, P.; Xiaoyong, Y.; Yulun, X.; Wanming, Y.; Zifei, H. In Situ Monazite U-Pb Ages in Thin Sections from the Giant Bayan Obo Fe–REE–Nb Deposit, Inner Mongolia: Implications for Formation Sequences. *Minerals* **2022**, *12*, 1237. [CrossRef]
54. Wei, C.W.; Xu, C.; Deng, M.; Song, W.L.; Shi, A.; Li, Z.; Fan, C.; Kuang, G. Origin of metasomatic fluids in the Bayan Obo rare-earth-element deposit. *Ore Geol. Rev.* **2022**, *141*, 104654. [CrossRef]
55. Philpotts, J.; Tatsumoto, M.; Li, X.; Wang, K. Some Nd and Sr isotopic systematics for the REE-enriched deposit at Bayan Obo, China. *Chem. Geol.* **1991**, *90*, 177–188. [CrossRef]
56. Conrad, J.E.; McKee, E.H. 40Ar/30Ar dating of vein amphibole from the Bayan Obo iron-rare earth element-niobium deposit, Inner Mongolia, China; constraints on mineralization and deposition of the Bayan Obo Group. *Econ. Geol.* **1992**, *87*, 185–188. [CrossRef]
57. Wang, J.; Tatsumoto, M.; Li, X.; Premo, W.R.; Chao, E.C.T. A precise 232Th-208Pb chronology of fine grained monazite: Age of the Bayan Obo REE-Fe-Nb ore deposit, China. *Geochim. Et Cosmochim. Acta* **1994**, *58*, 3155–3169. [CrossRef]
58. Walter, T.R.; Schmincke, H.-U. Rifting, recurrent landsliding and Miocene structural reorganization on NW-Tenerife (Canary Islands). *Int. J. Earth Sci.* **2002**, *91*, 615–628. [CrossRef]
59. Acosta, J.; Uchupi, E.; Muñoz, A.; Herranz, P.; Palomo, C.; Ballesteros, M.; ZEE Working Group. Geologic evolution of the Canarian Islands of Lanzarote, Fuerteventura, Gran Canaria and La Gomera and comparison of landslides at these islands with those at Tenerife, La Palma and El Hierro. In *Geophysics of the Canary Islands*; Clift, P., Acosta, J., Eds.; Springer: Dordrecht, The Netherlands, 2005.
60. Pittari, A.; Cas, R.A.F.; Edgar, C.J.; Nichols, H.J.; Wolff, A.J.; Marti, J. The influence of paleotopography on facies architecture and pyroclastic flow processes of a lithic-rich ignimbrite in a high gradient setting: The Abrigo ignimbrite, Tenerife, Canary Islands. *J. Volcanol. Geotherm. Res.* **2006**, *152*, 253–315. [CrossRef]
61. Clarke, H.; Troll, V.R.; Carracedo, J.C. Phreatomagmatic to Strombolian eruptive activity of basaltic cinder cones: Montaña Los Erales, Tenerife, Canary Islands. *J. Volcanol. Geotherm. Res.* **2009**, *180*, 225–245. [CrossRef]
62. Dávila-Harris, P. Explosive ocean-island volcanism: The 1.8–0.7 Ma explosive eruption history of Cañadas volcano recorded by the pyroclastic successions around Adeje and Abona, southern Tenerife, Canary Islands. Ph.D. Thesis, University of Leicester, Leicester, UK, 2009; p. 311, *unpublished*.

63. Ancochea, E.; Hernán, F.; Huertas, M.J.; Brändle, J.L.; Herrera, R. A new chronostratigraphical and evolutionary model for La Gomera: Implications for the overall evolution of the Canarian Archipelago. *J. Volcanol. Geotherm. Res.* **2006**, *157*, 271–293. [CrossRef]
64. Von Suchodoletz, H.; Blanchard, H.; Hilgers, A.; Radtke, U.; Fuchs, M.; Dietze, M.; Zöller, L. TL and ESR dating of Middle Pleistocene lava flows on Lanzarote island, Canary Islands (Spain). *Quat. Geochronol.* **2012**, *9*, 54–64. [CrossRef]
65. Cas, R.A.F.; Wolff, J.A.; Martí, J.; Olin, P.H.; Edgar, C.J.; Pittari, A.; Simmons, J.M. Tenerife, a complex end member of basaltic oceanic island volcanoes, with explosive polygenetic phonolitic calderas, and phonolitic-basaltic stratovolcanoes. *Earth Sci. Rev.* **2022**, *230*, 103990. [CrossRef]
66. Samonova, O.A.; Aseyeva, E.N.; Kasimov, N.S. Metals in soils of erosional systems in forest zone in the central part of European Russia. *J. Geochem. Exploration.* **2014**, *144*, 247–259. [CrossRef]
67. Novoselov, A.A.; Hodson, M.E.; Tapia-Gatica, J.; Dovletyarova, E.A.; Yáñez, C.; Neaman, A. The effect of rock lithology on the background concentrations of trace elements in alluvial soils: Implications for environmental regulation. *Appl. Geochem.* **2022**, *146*, 105440. [CrossRef]
68. Qiao, Y.; Wang, X.; Han, Z.; Tian, M.; Wang, Q.; Wu, H.; Liu, F. Geodetector based identification of influencing factors on spatial distribution patterns of heavy metals in soil: A case in the upper reaches of the Yangtze River. *China Appl. Geochem.* **2022**, *146*, 105459. [CrossRef]
69. Gent, M.R.; Alvarez, M.M.; Iglesias, J.J.M.G.; Álvarez, J.T. Offshore occurrences of heavy-mineral placers, Northwest Galicia, Spain. *Mar. Georesources Geotechnol.* **2005**, *23*, 39–59. [CrossRef]
70. Jacob, J.; Ward, J.D.; Bluck, B.J.; Scholz, R.A.; Frimmel, H.E. Some observations on diamondiferous bedrock gully trap sites on Late Cainozoic, marine-cut platforms of the Sperrgebiet, Namibia. *Ore Geol. Rev.* **2006**, *28*, 493–506. [CrossRef]
71. Dill, H.G. Grain morphology of heavy minerals from marine and continental placer deposits, with special reference to Fe–Ti oxides. *Sediment. Geol.* **2007**, *198*, 1–27. [CrossRef]
72. Dill, H.G. Geogene and anthropogenic controls on the mineralogy and geochemistry of modern alluvial-(fluvial) gold placer deposits in man-made landscapes in France, Switzerland and Germany. *J. Geochem. Explor.* **2008**, *99*, 29–60. [CrossRef]
73. Dill, H.G.; Ludwig, R.-R. Geomorphological—Sedimentological studies of landform types and modern placer deposits in the savanna (Southern Malawi). *Ore Geol. Rev.* **2008**, *33*, 411–434. [CrossRef]
74. Philander, C.; Rozendaal, A. Geology of the Cenozoic Namakwa Sands Heavy Mineral Deposit, West Coast of South Africa: A World-Class Resource of Titanium and Zircon. *Econ. Geol.* **2015**, *110*, 1577–1623. [CrossRef]
75. Bern, C.R.; Shah, A.K.; Benzel, W.M. Lowers HA The distribution composition of REE-bearing minerals in placers of the Atlantic Gulf coastal plains, U.S.A. *J. Geochem. Explor.* **2016**, *162*, 50–61. [CrossRef]
76. Hou, B.; Keeling, J.; Van Gosen, B.S. Geological and exploration models of beach placer deposits, integrated from case-studies of Southern Australia. *Ore Geol. Rev.* **2017**, *80*, 437–459. [CrossRef]
77. Instituto Geográfico Nacional. 2022. Available online: https://igme.maps.arcgis.com/home/webmap/viewer.html?webmap=44df600f5c6241b59edb596f54388ae4 (accessed on 3 August 2022).
78. Knighton, D.A. *Fluvial Forms and Processes: New Perspective*; Routledge: Arnold, London, 1998; p. 400.
79. Bird, E.C.F. *Coastal Geomorphology: An Introduction*; John Wiley & Sons: Chichester, UK, 2008; p. 411.
80. Nichols, G. *Sedimentology and Stratigraphy*; Wiley-Blackwell: Hoboken, NJ, USA, 2009; p. 432.
81. Lancaster, N.; Baas, A.C.W.; Sherman, D.J. Aeolian geomorphology: Introduction. In *Treatise on Geomorphology*; Aeolian Geomorphology, Shroder, J., Lancaster, N., Sherman, D.J., Baas, A.C.W., Eds.; Academic Press: San Diego, CA, USA, 2013; Volume 11, pp. 1–6.
82. Barudžija, U.; Velic, J.; Malvic, T.; Trenc, N.; Matovinovic´ Božinovic´, N. Morphometric characteristics, shapes and provenance of Holocene pebbles from the Sava River gravels (Zagreb, Croatia). *Geosciences* **2020**, *10*, 92. [CrossRef]
83. Streckeisen, A.L. To each plutonic rock its proper name. *Earth-Sci. Rev.* **1976**, *12*, 1–33. [CrossRef]
84. Le Maitre, R.W.; Bateman, P.; Dudek, A.; Keller, J.; Lameyre, J.L.; Bas, M.J.; Sabine, P.A.; Schmid, R.; Sorensen, H.; Streckeisen, A.; et al. *A Classification of Igneous Rocks and Glossary of terms: Recommendations of the International Union of Geological Sciences Subcommission on the Systematics of Igneous Rocks*; Blackwell Scientific Publications: Oxford, UK, 1989.
85. Ferguson, A.K. The occurrence of ramsayite, titan-låvenite and a fluorine-rich eucolite in a nepheline-syenite inclusion from Tenerife, Canary Islands. *Contrib. Mineral. Petrol.* **1978**, *66*, 15–20. [CrossRef]
86. Mangas, J.; Perez-Torrado, F.J.; Regulion, R.M.; Martin-Izard, A. Rare earth minerals in carbonatites of basal complex of Fuerteventura (Canary Islands, Spain), Mineral Deposits. In Proceedings of the 4th Biennial SGA Meeting, Turku, Finland, 11–13 August 1997; pp. 471–478.
87. Rodriguez-Losada, J.A.; Martinez-Frias, J. Ancient oxide- and sulphide-mineralization in the islands of Tenerife and La Gomera (Canary Archipelago, Spain). *Miner. Depos.* **1998**, *33*, 639–643. [CrossRef]
88. Ahijado, A. Características mineralógicas de una sövita pirofanítica de la Pta. del Peñón Blanco, Fuerteventura, Canarias. *Geogaceta* **1992**, *12*, 81–82.
89. Rüsenberg, K.A. Mineralien in den Pyroklastiten von Teneriffa, Kanarische Inseln. *Aufschluss* **2016**, *67*, 301–324.
90. Menéndez, I.; Campeny, M.; Quevedo-González, L.; Mangas, J.; Llovet, X.; Tauler, E.; Barrón, V.; Torrent, J.; Méndez-Ramos, J. Distribution of REE-bearing minerals in felsic magmatic rocks and paleosols from Gran Canaria, Spain: Intraplate oceanic islands as a new example of potential, non-conventional sources of rare-earth elements. *J. Geochem. Explor.* **2019**, *204*, 270–288. [CrossRef]

91. Hecht l Thuro, K.; Plinninger, R.; Cuney, M. Mineralogical and geochemical characteristics of hydrothermal alteration and episyenitization in the Königshain granites, northern Bohemian Massif, Germany. *Int. J. Earth Sci.* **1999**, *88*, 236–252. [CrossRef]
92. Boulvais, P.; Ruffet, G.; Cornichet, J.; Mermet, M. Cretaceous albitization and dequartzification of Hercynian peraluminous granites in the Salvezines Massif (French Pyrénées). *Lithos* **2007**, *93*, 89–106. [CrossRef]
93. Dosbaba, M.; Novák, M. Quartz replacement by "kerolite" in graphic quartz–feldspar intergrowths from the Věžná I pegmatite, Czech Republic: A complex desilication process related to episyenitization. *Can. Mineral.* **2012**, *50*, 1609–1622. [CrossRef]
94. Petersson, J.; Eliasson, T. Mineral evolution and element mobility during episyenitization (dequartzification) and albitization in the postkinematic Bohus granite, southwest Sweden. *Lithos* **1997**, *42*, 123–146. [CrossRef]
95. Marks, M.A.W.; Markl, G. A global review on agpaitic rocks. *Earth-Sci. Rev.* **2017**, *173*, 229–258. [CrossRef]
96. Le Maitre, R.W. International Union of Geological Sciences. Subcommission on the systematics of igneous rocks. In *A Classification of Igneous Rocks and Glossary of Terms*; Blackwell Scientific Publications: Oxford, UK, 2003; p. 193.
97. Frost, B.R.; Frost, C.D. A geochemical classification for feldspathic igneous rocks. *J. Petrol.* **2008**, *49*, 1955–1969. [CrossRef]
98. Frost, B.R.; Frost, C.D. On ferroan (A-type) granitoids: Their compositional variability modes of origin. *J. Petrol.* **2010**, *52*, 39–53. [CrossRef]
99. Gottardi, G.; Galli, E. *Natural Zeolites*; Springer: Berlin/Heidelberg, Germany; New York, NY, USA; Tokyo, Japan, 1985; p. 409.
100. Tschernich, R.W. *Zeolites of the World*; Geoscience Press: Phoenix, Arizona, 1992; p. 563.
101. Coombs, D.S.; Alberti, A.; Armbruster, T.; Artioli, G.; Colella, C.; Galli, E.; Grice, J.D.; Liebau, F.; Mandarino, J.A.; Minato, H.; et al. Recommended nomenclature for zeolite minerals: Report of the subcommittee on zeolites of the International Mineralogical Association, Commission on New Minerals and Mineral Names. *Can. Mineral.* **1997**, *35*, 1571–1606.
102. Neuhoff, S.; Fridriksson, T.; Bird, D.K. Zeolite parageneses in the north Atlantic igneous province: Implications for geotectonics and groundwater quality of basaltic crust. *Int. Geol. Rev.* **2000**, *42*, 15–44. [CrossRef]
103. Pérez-Torrado, F.J.; Martí, J.; Queralt, I.; Mangas, J. Alteration processes of the Roque Nublo ignimbrites (Gran Canaria, Canary Islands). *J. Volcanol. Geotherm. Res.* **1995**, *65*, 191–204. [CrossRef]
104. Donoghue, E.; Troll, V.R.; Harris, C.; O'Halloran, A.; Walter, T.R.; Pérez, F.J. Torrado Low-temperature hydrothermal alteration of intra-caldera tuffs, Miocene Tejeda caldera, Gran Canaria, Canary Islands. *J. Volcanol. Geotherm. Res.* **2008**, *176*, 551–564. [CrossRef]
105. Garcıa-Romero, E.; Vegas, J.; Baldonedo, J.L.; Marfil, R. Clay minerals as alteration products in basaltic volcaniclastic deposits of La Palma (Canary Islands, Spain). *Sedim. Geol.* **2005**, *174*, 237–253. [CrossRef]
106. De Oliveira, M.T.G.; Furtado, S.M.A.; Formoso, M.L.L.; Eggleton, R.A.; Dani, N. Coexistence of halloysite and kaolinite-a study on the genesis of kaolin clays of Campo Alegre Basin, Santa Catarina State, Brazil. *An. Acad. Bras. Ciências* **2007**, *79*, 665–681. [CrossRef]
107. Churchman, G.J.; Pontifex, I.R.; McClure, S.G. Factors influencing the formation and characteristics of halloysites or kaolinites in granitic and tuffaceous saprolites in Hong Kong. *Clays Clay Miner.* **2010**, *58*, 220–237. [CrossRef]
108. Schwaighofer, B. Zur Verwitterung vulkanischer Gesteine—Ein Beitrag zur Halloysit-Genese. *Mitteilungen Geol. Ges.* **1974**, *66/67*, 221–236.
109. Rodriguez-Losada, J.A.; Martinez-Frias, J. The felsic complex of the Vallehermoso Caldera: Interior of an ancient volcanic system (La Gomera, Canary Islands). *J. Volcanol. Geotherm. Res.* **2004**, *137*, 261–284. [CrossRef]
110. Bucher, K.; Grapes, R. *Petrogenesis of Metamorphic Rocks*; Springer: Berlin/Heidelberg, Germany; Dortrecht, The Netherlands; London, UK; New York, NY, USA, 2011; p. 428.
111. Castorina, F.; Masi, U. REE and Nd-isotope evidence for the origin of siderite from the Jebel Awam deposit (Central Morocco). *Ore Geol. Rev.* **2008**, *34*, 337–342. [CrossRef]
112. Dill, H.G.; Botz, R.; Berner, Z.; Abu Hamad, A.M.B. The origin of pre-and syn-rift, hypogene Fe-P mineralization during the Cenozoic along the Dead-Sea-Transform Fault, Northwest Jordan. *Econ. Geol.* **2010**, *105*, 1301–1319. [CrossRef]
113. Dill, H.G.; Kolb, J. Carbonate-related metallic and non-metallic mineralization within and proximal to granites (Fichtelgebirge Pluton, Germany): Mantle-crust marker mineralization. *Ore Geol. Rev.* **2019**, *104*, 46–71. [CrossRef]
114. Meinert, L.D. Dipple and Nicolescu, G.M. World Skarn Deposits. In *Economic Geology 100th Anniversary Volume 1905–2005*; Hedenquist, J.W., Thompson, J.F.H., Goldfarb, R.J., Richards, J.P., Eds.; Elsevier Science: Amsterdam, The Netherlands, 2005; Volume 1905–2005, pp. 299–336.
115. Chen, W.; Simonetti, A. Evidence for the multi-stage petrogenetic history of the Oka Carbonatite Complex (Quebec, Canada) as recorded by perovskite and apatite. *Minerals* **2014**, *4*, 437–476. [CrossRef]
116. Patel, S.C.J. Vesuvianite-wollastonite-grossular-bearing calc-silicate rock near Tatapani, Surguja district, Chhattisgarh. *J. Earth Syst. Sci.* **2007**, *116*, 143–147. [CrossRef]
117. Ancochea, E.; Huertas, M.J.; Cantagrel, J.M.; Coello, J.; Fúster, J.M.; Arnaud, N.; Ibarrola, E. Evolution of the Cañadas edifice and its implications for the origin of the Cañadas Caldera (Tenerife, Canary Islands). *J. Volcanol Geotherm Res.* **1999**, *88*, 177–199. [CrossRef]
118. Duff, D. *Holmes Principles of Physical Geology*; Routledge: Cheltenham, UK, 1993; p. 832.
119. Raade, G.; Mladeck, M.H. Janhaugite, $Na_3Mn_3Ti_2Si_4O_{15}(OH,F,O)_3$, A new mineral from Norway. *Am. Mineral.* **1983**, *68*, 1216–1219.
120. Wagner, C.; Velde, D. Davanite, $K_2TiSi_6O_{15}$, in the Smoky Butte (Montana) lamproites. *Am. Mineral.* **1986**, *71*, 1473–1475.

121. Chesner, C.A.; Ettlinger, A.D. Composition of volcanic allanite from the Toba Tuffs, Sumatra, Indonesia. *Am. Mineral.* **1989**, *74*, 750–758.
122. Hornig, I.; Wörner, G. Zirconolite-bearing ultra-potassic veins in a mantle-xenolith from Mt. Melbourne Volcanic Field, Victoria Land, Antarctica. *Contrib. Mineral. Petrol.* **1991**, *106*, 355–366. [CrossRef]
123. Keller, J.; Williams, T. Niocalite and Woehlerite from the alkaline and carbonatite rocks at Kaiserstuhl, Germany. *Mineral. Mag.* **1995**, *59*, 561–566. [CrossRef]
124. Chakhmouradian, A.R.; Zaitsev, A.N. Calcite–amphibole–clinopyroxene rock from the Afrikanda complex, Kola Peninsula, Russia: Mineralogy and a possible link to carbonatites. *I. Oxide Miner. Can. Mineral.* **1999**, *37*, 177–198. [CrossRef]
125. Traversa, G.; Gomes, C.B.; Brotzu, P.; Buraglini, N.; Morbidelli, L.; Principato, M.S.; Ronca, S.; Ruberti, E. Petrography and mineral chemistry of carbonatites and mica-rich rocks from the Araxá complex (Alto Paranaíba Province, Brazil). *An. Acad. Bras. Ciências* **2001**, *73*, 71–98. [CrossRef]
126. Petersen, O.V.; Giester, G.; Brandstätter, F.; Niedermayr, G. Nabesite, a new mineral species from the Ilimaussaq alkaline complex. *Can. Mineral.* **2002**, *40*, 173–181. [CrossRef]
127. Poitrasson, F. In situ investigations of allanite hydrothermal alteration: Examples from calc-alkaline and anorogenic granites of Corsica (southeast France). *Contrib. Mineral. Petrol.* **2002**, *142*, 485–500. [CrossRef]
128. Chukanov, N.V.; Pekov, I.V.; Rastsvetaeva, R.K.; Chilov, G.V.; Zadov, A.E. Clinobarylite, $BaBe_2Si_2O_7$, a new mineral from Khibiny massif, Kola peninsula. *Zap. Vser. Miner. Obshch.* **2003**, *132*, 2937. (In Russian)
129. Mitchell, R.H.; Belton, F. Niocalite-cuspidine solid solution and manganoan monticellite from natrocarbonatite, Oldoinyo Lengai, Tanzania. *Mineral. Mag.* **2004**, *68*, 787–799. [CrossRef]
130. Pekov, I.V.; Chukanov, N.V.; Ferraris, G.; Gula, A.; Pushcharovsky, D.Y.; Zadov, A.E. Tsepinite–Ca,$(Ca,K,Na,\square)_2(Ti,Nb)_2(Si_4O_{12})(OH,O)_2 \cdot 4H_2O$, a new mineral of the labuntsovite group from the Khibiny alkaline massif, Kola Peninsula–Novel disordered sites in the vuoriyarvite-type structure. *Neues Jahrb. Für Mineral. Monatshefte* **2003**, *2003*, 461480.
131. Pekov, I.V.; Chukanov, N.V.; Lebedeva Yu, S.; Pushcharovsky DYu Ferraris, G.; Gula, A.; Zadov, A.E.; Novakova, A.A.; Petersen, O.V. Potassic-Arfvedsonite a K-dominant Amphibole of the Arfvedsonite-series from agpaitic pegmatites. *Neues Jahrb. Mineral. Monatshefte* **2004**, *12*, 555–574. [CrossRef]
132. Liferovich, R.P.; Mitchell, R.H.; Zozulya, D.R.; Shpachenko, A.K. Paragenesis and composition of banalsite, stronalsite, and their solid solution in nepheline syenite and ultramafic alkaline rocks. *Can. Mineral.* **2006**, *44*, 929–942. [CrossRef]
133. Costanzo, A.; Moore, K.R.; Wall, F.; Feely, M. Fluid inclusions in apatite from Jacupiranga calcite carbonatites: Evidence for a fluid-stratified carbonatite magma chamber. *Lithos* **2006**, *91*, 208–228. [CrossRef]
134. Azarova, Y.V.; Shlyukova, Z.V.; Zolotarev, A.A., Jr.; Organova, N.I. Burovaite-Ca, (Na, K) $_4Ca_2$ (Ti, Nb) $_8$ [Si4$O_{12}$] $_4$ (OH, O) $_8 \cdot 12H_2O$, a new labuntsovite-group mineral species and its place in low-temperature mineral formation in pegmatites of the Khibiny pluton, Kola Peninsula, Russia. *Geol. Ore Depos.* **2009**, *51*, 774–783. [CrossRef]
135. Berger, V.I.; Singer, D.A.; Orris, G.J. *Carbonatites of the World, Explored Deposits of Nb and REE—Database and Grade and Tonnage Models*; U.S. Geological Survey Open-File Report 2009–1139, 17 p. and database; US Geological Survey: Reston, VA, USA, 2009.
136. Andersen, T.; Erambert, M.; Larsen, A.O.; Selbekk, R.S. Petrology of nepheline syenite pegmatites in the Oslo Rift, Norway: Zirconium silicate mineral assemblages as indicators of alkalinity and volatile fugacity in mildly agpaitic magma. *J. Petrol.* **2010**, *51*, 2303–2325. [CrossRef]
137. Valentini, L.; Moore, K.R.; Chazot, G. Unravelling carbonatite–silicate magma interaction dynamics: A case study from the Velay province (Massif Central, France). *Lithos* **2010**, *116*, 53–64. [CrossRef]
138. Chernysheva, E.A.; Kharin, G.S. Melilitites in the alkaline volcanic succession of the Gorringe bank, Southwestern Portugal. *Geochem. Int.* **2012**, *50*, 54–62. [CrossRef]
139. Larsen, A.O. Contributions to the mineralogy of the syenite pegmatites in the Larvik Plutonic complex. *Nor. Bergverksmus. Skrifter.* **2013**, *50*, 101–109.
140. Pekov, I.V.; Nikolaev, A.P. Minerals of the pegmatites and hydrothermal assemblages of the Koashva deposit (Khibiny, Kola Peninsula, Russia). *Mineral. Alm.* **2013**, *189*, 765.
141. Chakhmouradian, A.R.; Reguir, E.P.; Kressall, R.D.; Crozier, J.; Pisiak, L.K.; Sidhu, R.; Yang, P. Carbonatite-hosted niobium deposit at Aley, northern British Columbia (Canada): Mineralogy, geochemistry and petrogenesis. *Ore Geol. Rev.* **2015**, *64*, 642–666. [CrossRef]
142. Novák, M.; Čopjaková, R.; Dosbaba, M.; Galiová, M.V.; Všianský, D.; Staněk, J. Two paragenetic types of cookeite from the Dolní Bory-Hatě Pegmatites, Moldanubian Zone, Czech Republic: Proximal and distal alteration productions of Li-bearing sekaninaite. *Can. Mineral.* **2015**, *53*, 1035–1048. [CrossRef]
143. Downes, P.J.; Dunkley, D.J.; Fletcher, I.R.; McNaughton, N.J.; Rasmussen, B.; Jaques, A.L.; Verrall, M.; Sweetapple, M.T. Zirconolite, zircon and monazite-(Ce) U-Th-Pb age constraints on the emplacement, deformation and alteration history of the Cummins Range Carbonatite Complex, Halls Creek Orogen, Kimberley region, Western Australia. *Mineral. Petrol.* **2016**, *110*, 199–222. [CrossRef]
144. Torró, L.; Villanova, C.; Castillo, M.; Campeny, M.; Gonçalves, A.O.; Melgarejo, J.C. Melgarejo Niobium and rare earth minerals from the Virulundo carbonatite, Namibe, Angola. *Mineral. Mag.* **2012**, *76*, 393–409. [CrossRef]

145. Amores-Casals, S.; Melgarejo, J.C.; Bambi, A.; Gonçalves, A.O.; Morais, E.A.; Manuel, J.; Buta Neto, A.; Costanzo, A.; Molist, J.M. Lamprophyre-Carbonatite Magma Mingling and Subsolidus Processes as Key Controls on Critical Element Concentration in Carbonatites—The Bonga Complex (Angola). *Minerals* **2019**, *9*, 601. [CrossRef]
146. Buchholz, T.; Falster, A.; Simmons, W. A rediscovered pegmatite in the Stettin Complex, Wausau Syenite Complex, Marathon County, Wisconsin. *Rocks Miner.* **2019**, *94*, 184–185.
147. Gonçalves, A.O.; Melgarejo, J.C.; Alfonso, P.; Amores, S.; Paniagua, A.; Neto, A.B.; Eduardo, A.M.; Camprubí, A. The Distribution of Rare Metals in the LCT Pegmatites from the Giraúl Field, Angola. *Minerals* **2019**, *9*, 580. [CrossRef]
148. Galliski, M.Á.; Márquez-Zavalía, M.F.; Roquet, M.B. Los minerales de Nb-Ta-U de la pegmatita María Elena, Sierra de San Luis, Argentina. *Rev. Asoc. Geológica Argent.* **2021**, *78*, 355–367.
149. Mitchell, R.H.; Dawson, J.B. Mineralogy of volcanic calciocarbonatites from the Trig Point Hill debris flow, Kerimasi volcano, Tanzania: Implications for the altered natrocarbonatite hypothesis. *Mineral. Mag.* **2021**, *85*, 484–495. [CrossRef]
150. Mikhailova, J.A.; Kalashnikov, A.O.; Sokharev, V.A.; Pakhomovsky, Y.A.; Konopleva, N.G.; Yakovenchuk, V.N.; Bazai, A.V.; Goryainov, P.M.; IvanyukIvanyuk, G.Y. 3D mineralogical mapping of the Kovdor phoscorite–carbonatite complex (Russia). *Miner. Depos.* **2016**, *51*, 131–149. [CrossRef]
151. Doroshkevich, A.; Prokopyev, I.; Kruk, M.; Sharygin, V.; Izbrodin, I.; Starikova, A.; Ponomarchuk, A.; Izokh, A.; Nugumanova, Y. Age and petrogenesis of ultramafic lamprophyres of the Arbarastakh alkaline-carbonatite complex, Aldan-Stanovoy shield, South of Siberian Craton (Russia): Evidence for ultramafic lamprophyre-carbonatite link. *J. Petrol.* **2022**, *63*, egac073. [CrossRef]
152. Hutchinson, M.; Slezak, P.; Wendlandt, R.; Hitzman, M. Rare Earth Element Enrichment in the Weathering Profile of the Bull Hill Carbonatite at Bear Lodge, Wyoming, USA. *Econ. Geol.* **2022**, *117*, 813–831. [CrossRef]
153. Zaitsev, V.A.; Chukanov, N.V.; Aksenov, S.M. Chlorine-Deficient Analog of Taseqite from Odikhincha Massif (Russia): Genesis and Relation with Other Sr-Rich Eudialyte-Group. *Minerals* **2022**, *12*, 1015. [CrossRef]
154. Cook, N.J.; Ciobanu, C.L.; Wade, B.P.; Gilbert, S.E.; Alford, R. Mineralogy and distribution of REE in oxidized ores of the Mount Weld laterite deposit. *West. Aust. Miner.* **2023**, *13*, 656.
155. Kogarko, L.N. Ore-forming potential of alkaline magmas. *Lithos* **1990**, *26*, 167–175. [CrossRef]
156. Sørensen, H. Agpaitic nepheline syenites: A potential of rare elements. *Appl. Geochem.* **1992**, *7*, 417–427. [CrossRef]
157. Sørensen, H. The agpaitic rocks—An overview. *Mineral. Mag.* **1997**, *61*, 485–498. [CrossRef]
158. Sørensen, H.; Larsen, L.M. The hyper-agpaitic stage in the evolution of the llimaussaq alkaline complex, South Greenland. In: Sørensen, H. The llimaussaq Alkaline Complex, South Greenland: Status of Mineralogical Research with New Results. *Geol. Greenl. Surv. Bull.* **2001**, *190*, 83–94. [CrossRef]
159. Marks, M.A.W.; Hettmann, K.; Schilling, J.; Frost, B.R.; Markl, G. The mineralogical diversity of alkaline igneous rocks: Critical factors for the transition from miaskitic to agpaitic phase assemblages. *J. Petrol.* **2011**, *52*, 439–455. [CrossRef]
160. Khomyakov, A.P.; Sørensen, H. Zoning in steenstrupine-(Ce) from the llimaussaq alkaline complex, South Greenland: A review and discussion. *Geol. Greenl. Surv. Bull.* **2001**, *190*, 109–118. [CrossRef]
161. Andersen, T.; Friis, H. The transition from agpaitic to hyperagpaitic magmatic crystallization in the llimaussaq alkaline complex, South Greenland. *J. Petrol.* **2015**, *56*, 1343–1364. [CrossRef]
162. Carracedo, J.C.; Rodriguez Badiola, E.; Guillou, H.; Paterne, M.; Scaillet, S.; Perez Torrado, F.J.; Paris, R.; Fra-Paleo, U.; Hansen, A. Eruptive and structural history of the Teide Volcano and rift zones of Tenerife, Canary islands. *Geol. Soc. Ameri. Bull.* **2007**, *119*, 1027–1051. [CrossRef]
163. Chakhmouradian, A.R.; Mitchell, R.H. The mineralogy of Ba- and Zr-rich alkaline pegmatites from Gordon Butte, Crazy Mountains (Montana, USA): Comparisons between potassic and sodic agpaitic pegmatites. *Contrib. Mineral. Petrol.* **2002**, *143*, 93–114. [CrossRef]
164. Broom-Fendley, S.; Brady, A.E.; Horstwood, M.S.A.; Woolley, A.R.; Mtegha, J.; Wall, F.; Dawes, W.; Gunn, G. Geology, geochemistry and geochronology of the Songwe Hill carbonatite, Malawi. *J. Afr. Earth Sci.* **2017**, *134*, 10–23. [CrossRef]
165. Broom-Fendley, S.; Brady, A.E.; Wall, F.; Gunn, G.; Dawes, W. REE minerals at the Songwe Hill carbonatite, Malawi: HREE-enrichment in late-stage apatite. *Ore Geol. Rev.* **2017**, *81*, 23–41. [CrossRef]
166. Wall, F.; Zaitsev, A.N. *Phoscorites and Carbonatites from Mantle to Mine: The Key Example of the Kola Alkaline Province*; The Mineralogical Society Series 10; British Mineralogical Society: London, UK, 2004; p. 498.
167. Khomyakov, A.P.; Nechelyustov, G.N.; Rastsvetaeva, R.K. Aqualite, $(H_3O)_8(Na,K,Sr)_5Ca_6Zr_3Si_{26}O_{66}(OH)_9Cl$, a new eudialyte-group mineral from Inagli alkaline massif (Sakha-Yakutia, Russia), and the problem of oxonium in hydrated eudialytes. *Proc. Russ. Mineral. Soc.* **2007**, *136*, 39–55.
168. Guarino, V.; Lustrino, M.; Zanetti, A.; Tassinari, C.C.; Ruberti, E.; de'Gennaro, R.; Melluso, L. Mineralogy and geochemistry of a giant agpaitic magma reservoir: The Late Cretaceous Poços de Caldas potassic alkaline complex (SE Brazil). *Lithos* **2021**, *398*, 106330. [CrossRef]
169. Chakhmouradian, A.R. On the development of niobium and rare-earth minerals in monticellite-calcite carbonatite of the Oka Complex, Quebec. *Can. Mineral.* **1996**, *34*, 479–484.
170. Oteo, G.D. REE Geochemical Exploration in Magmatic Felsic Rocks and Carbonatites of Oceanic Intraplate Volcanic Islands (the Island of Fuerteventura). Master's Thesis, Universidad Las Palmas de Gran Canaria, Las Palmas, Spain, 2020; p. 38.
171. Carnevale, G.; Caracausi, A.; Correale, A.; Italiano, L.; Rotolo, S.G. An Overview of the Geochemical characteristics of oceanic carbonatites: New insights from Fuerteventura Carbonatites (Canary Islands). *Minerals* **2021**, *11*, 203. [CrossRef]

172. O'Donoghue, M. *Gems their Sources, Descriptions and Identification*; Elsevier: Amsterdam, The Netherlands, 2006; p. 873.
173. Van Velthuizen, J.; Chao, G.Y. Griceite, LiF, a new mineral species from Mont Saint-Hilaire, Quebec. *Can. Mineral.* **1989**, *27*, 125–127.
174. Grice, J.D. Mont Saint-Hilaire, Quebec: Canada's Most Diverse Mineral Locality. In *Famous Mineral Localities of Canada*; Fitzhenry & Whiteside Limited & the National Museum of Natural Sciences: Markham, ON, Canada, 1989; p. 190.
175. McDonald, A.M.; Back, M.E.; Gault, R.A.; Horváth, L. Peatite-(Y) and ramikite-(Y), two new Na-Li-Y{+/−}Zr phosphate-carbonate minerals from the Poudrette pegmatite, Mont Saint-Hilaire, Québec. *Can. Mineral.* **2013**, *51*, 569–596. [CrossRef]
176. Voloshin, A.V.; Pakomovskii, Y.A.; Stepanov, V.I.; Tyusheva, F.N. Lithiotantite, Li, $(Ta,Nb)_3O_8$, a new mineral from granite pegmatites of Eastern Kazakhstan. *Mineral. Zhurnal* **1983**, *5*, 91–95.
177. Yakovenchik, V.N.; Ivaniuk GYu Pakhomovsky, Y.A.; Selivanova, E.A.; Men'shikov, Y.P.; Korchak, J.A.; Krivovichev, S.V.; Spiridonova, D.V.; Zalkind, O.A. Punkaruaivite, $Li\{Ti_2(OH)_2[Si_4O_{11}(OH)]\}$. $H_2O$, a new mineral species from hydrothermalites of Khibiny and Lovozero alkaline massifs (Kola Peninsula, Russia). *Can. Mineral.* **2010**, *48*, 41–50. [CrossRef]
178. Teertstra, D.K.; Černý, P.; Novák, M. Compositional and textural evolution of pollucite in pegmatites of the Moldanubicum. *Mineral. Petrol.* **1995**, *55*, 37–51. [CrossRef]
179. Pautov, L.A.; Agakhanov, A.A.; Pekov, I.V.; Karpenko, V.Y.; Siidra, O.I.; Sokolova, E.; Hawthorne, F.C.; Faiziev, A.R. Garmite, IMA 2017-008. *Mineral. Mag.* **2017**, *81*, 737–742.
180. Pautov, L.; Agakhanov, A.; Pekov, I.; Karpenko, V.; Siidra, O.; Sokolova, E.; Hawthorne, F.; Fayziev, A.R. Garmite, $CsLiMg_2(Si_4O_{10})F_2$, a New mica-group mineral from "Quartz Lumps" of the Darai-Piyoz Alkaline Massif, Tajikistan. *Geol. Ore Depos.* **2022**, 95894. [CrossRef]
181. Gold, D.P.; Eby, G.N.; Valleé, M. Carbonatites, diatremes and ultra-alkaline rocks in the Oka area. In *Fieldtrip Guidebook 21*; GAC/MAC Meeting: Ottawa, ON, Canada, 1986; p. 51.
182. Mitchell, R.H.; Liferovich, R.P. Ecandrewsite-zincian pyrophanite from lujavrite. Pilanesberg alkaline complex, South Africa. *Can. Mineral.* **2004**, *42*, 1169–1178. [CrossRef]
183. Pekov, I.V.; Podlesnyi, A.S. Kukisvumchorr Deposit: Mineralogy of Alkaline Pegmatites and Hydrothermalites. *Mineral. Alm.* **2004**, *7*, 140.
184. Škoda, R.; Čopjaková, R. Herzenbergite and Sn-bearing tinzenite from the NYF Pegmatite in Třebíč Pluton, Moldanubicum, Czech Republic. *Acta Miner. Petrograph. Abstr. Ser.* **2006**, *5*, 107.
185. Tucker, R.D.; Belkin, H.E.; Schulz, K.J.; Peters, S.G.; Horton, F.; Buttleman, K.; Scott, E.R. A major light rare-earth element (LREE) resource in the Khanneshin carbonatite complex, southern Afghanistan. *Econ. Geol.* **2012**, *107*, 197–208. [CrossRef]
186. Chakrabarty, A.; Mitchell, R.H.; Ren, M.; Pal, S.; Pal, S.; Sen, A.K. Nb–Zr–REE re-mobilization and implications for transitional agpaitic rock formation: Insights from the Sushina Hill Complex, India. *J. Petrol.* **2018**, *59*, 1899–1938. [CrossRef]
187. Holtstam, D.; Cámara, F.; Skogby, H.; Karlsson, A. Hjalmarite, a new Na–Mn member of the amphibole supergroup, from Mn skarn in the Långban deposit, Värmland, Sweden. *Eur. J. Mineral.* **2019**, *31*, 565–574. [CrossRef]
188. Ibrahim, E. Sedimentary origin of the Mn-Fe Ore of Um Bogma, Southwest Sinai: Geochemical and Paleomagnetic Evidence. *Econ. Geol.* **2000**, *95*, 607–620.
189. Cabral, A.R.; Moore, J.M.; Mapani, B.S.; Koubová, M.; Sattler, C.D. Geochemical and mineralogical constraints on the genesis of the Otjosondu ferromanganese deposit, Namibia: Hydrothermal exhalative versus hydrogenetic (including snowball-earth) origins. *S. Afr. J. Geol.* **2011**, *114*, 57–76. [CrossRef]
190. Jones, S.; McNaughton, N.J.; Grguric, B. Structural controls and timing of fault-hosted manganese at Woodie, East Pilbara, Western Australia. *Ore Geol. Rev.* **2013**, *50*, 52–82. [CrossRef]
191. Bonzi, W.M.E.; Van Lichtervelde, M.; Vanderhaeghe, O.; André-Mayer, A.S.; Salvi, S.; Wenmenga, U. Insights from mineral trace chemistry on the origin of NYF and mixed LCT + NYF pegmatites and their mineralization at Mangodara, SW Burkina Faso. *Miner. Depos.* **2023**, *58*, 75–104. [CrossRef]
192. Horváth l Gault, R.A. The mineralogy of Mont Saint-Hilaire. *Mineral. Rec.* **1990**, *21*, 281–359, 330–331.
193. Cabral, A.R.; Sattler, C.-D. Alteration of pyrophanite: Transition in chemical composition to a manganese analogue of pseudorutile-evidence from the Quadrilatero Ferrifero of Minas Gerais, Brazil. *N. Jb. Mineral. Monatsh.* **2004**, *3*, 97–103. [CrossRef]
194. Goss, S.C.; Wilde, S.A.; Wu, F.; Yang, J. The age, isotopic signature and significance of the youngest Mesozoic granitoids in the Jiaodong Terrane, Shandong Province, North China Craton. *Lithos* **2010**, *120*, 309–326. [CrossRef]
195. Xie, L.; Wang, R.C.; Wang, D.Z.; Qiu, J.S. A survey of accessory mineral assemblages in peralkaline and more aluminous A-type granites of the southeast coastal area of China. *Mineral. Mag.* **2006**, *70*, 709–729. [CrossRef]
196. Gu, X.; Yang, H.; Xie, X.; Van Nieuwenhuizen, J.; Downs, R.; Evans, S. Lipuite, a new manganese phyllosilicate mineral from the N'Chwaning III mine, Kalahari Manganese Fields, South Africa. *Mineral. Mag.* **2019**, *83*, 645–654. [CrossRef]
197. Goudie, A.S.; Viles, H. Weathering processes and forms. In *Quaternary and Recent Processes and Forms*; Burt, T.P., Chorley, R.J., Brunsden, D., Cox, N.J., Goudie, A.S., Eds.; Landforms or the Development of Geomorphology Geological Society: London, UK, 2008; pp. 129–164.
198. Taylor, G.; Eggleton, R.A. *Regolith Geology and Geomorphology*; John Wiley & Sons: Hoboken, NJ, USA, 2009; p. 375.
199. Pring, A.; Francis, G.; Birch, W.D. Pyrobelonite, arsenoklasite, switzerite and other recent finds at Iron Monarch, South Australia. *Aust. Mineral.* **1989**, *4*, 49–55.

200. Dill, H.G.; Berner, Z.A. Sedimentological and structural processes operative along a metalliferous catena from sandstone-hosted to unconformity-related Pb-Cu-Zn deposit in an epicontinental basin, SE Germany. *Ore Geol. Rev.* **2014**, *63*, 91–114. [CrossRef]
201. Gomes, C.A.L.; Neiva, A.M. Tourmalines in the Namacotche Li-Cs-Ta granitic pegmatite group, Mozambique: Crystal chemistry and origin. Cadernos do Laboratorio Xeolóxico de Laxe. *Rev. De Xeol. Galega E Do Hercínico Penins.* **2022**, *44*, 132–153.
202. Manrique, J.; Guaman, G.; Guartan, J. Geochemical prospecting study of the Vanadium-Uranium Mineralization of Puyango, Ecuador (No. IAEA-CN--261). In Proceedings of the International Symposium on Uranium Raw Material for the Nuclear FuelCycle: Exploration, Mining, Production, Supply and Demand, Economics and Environmental Issues (URAM-2018), Vienna, Austria, 25–29 June 2018.
203. Witzke, T.; Zhen, S.; Seff, K.; Doering, T.; Nasdala, L.; Kolitsch, U. Ronneburgite, $K_2MnV_4O_{12}$, a new mineral from Ronneburg, Thuringia, Germany: Description and crystal structure. *Am. Mineral.* **2001**, *86*, 1081–1086. [CrossRef]
204. Szczerba, M.; Sawłowicz, Z. Remarks on the origin of cerussite in the Upper Silesian Zn-Pb deposits, Poland. *Mineralogia* **2009**, *40*, 54–64. [CrossRef]
205. Zubkova, N.V.; Chukanov, N.V.; Pekov, I.V.; Pushcharovsky DYu Katerinopoulos, A.; Voudouris, P.; Magganas, A. New data on fiedlerite-1A from ancient slags of Lavrion, Greece: Crystal structure and H-bonding. *Dokl. Akad. Nauk* **2019**, *486*, 83–87.
206. Bulakh, M.O.; Pekov, I.V.; Koshlyakova, N.N.; Sidorov, E.G. Ludwigite and Yuanfuliite from Fumarolic Exhalations of the Tolbachik Volcano, Kamchatka, Russia. *Geol. Ore Depos.* **2022**, *64*, 607–621. [CrossRef]
207. Pekov, I.V.; Zubkova, N.V.; Britvin, S.N.; Yapaskurt, V.O.; Chukanov, N.V.; Lykova, I.S.; Sidorov, E.; Pushcharovsky, D.Y. New zinc and potassium chlorides from fumaroles of the Tolbachik volcano, Kamchatka, Russia: Mineral data and crystal chemistry. III., Cryobostryxite, $KZnCl_3 \cdot 2H_2O$. *Eur. J. Mineral.* **2015**, *27*, 805–812. [CrossRef]
208. Rüsenberg, K.A. Mineralparagenesen in den Schlacken von Lavrion und ihre Entstehung. *Aufschluss* **2001**, *52*, 25–44.
209. Kaminsky, F.V.; Ryabchikov, I.D.; Wirth, R. A primary natrocarbonatitic association in the Deep Earth. *Mineral. Petrol.* **2015**, *110*, 387–398. [CrossRef]
210. Foord, E.E.; Jensen, M.; Rota, J.C. The Gold Quarry Mine, Carlin-Trend, Eureka County, Nevada. *Mineral. Rec.* **1995**, *26*, 449–469.
211. Haggan, T.; Parnell, J. Hydrocarbon-metal associations in the Western Cordillera, Central Peru. *J. Geochem. Explor.* **2000**, *69–70*, 229–234. [CrossRef]
212. Brugger, J.; Berlepsch, P.; Meisser, N.; Armbruster, T. Ansermetite, $MnV_2O_6 \cdot 4H_2O$, a new mineral species with $V^{5+}$ in five-fold coordination from Val Ferrera, Eastern Swiss Alps. *Can. Mineral.* **2003**, *41*, 1423–1431. [CrossRef]
213. Schäfer, C. Armalcolit und Schäferit vom Weinberg bei Nickenich. *Der Aufschluß* **2021**, *72*, 170–176.
214. Števko, M.; Uher, P.; Ondrejka, M.; Ozdín, D.; Bačík, P. Quartz-apatite-REE phosphates-uraninite vein mineralization near Čučma (eastern Slovakia): A product of early Alpine hydrothermal activity in the Gemeric superunit, Western Carpathians. *J. Geosci.* **2014**, *59*, 209–222. [CrossRef]
215. Carracedo, J.C.; Day, S.; Guillou, H. Hotspot volcanism close to a passive continental margin: The Canary Islands. *Geol. Mag.* **1998**, *135*, 591604. [CrossRef]
216. González, F.J.; Rincón-Tomás, B.; Somoza, L.; Santofimia, E.; Medialdea, T.; Madureira, P.; López-Pamo, E.; Hein, J.R.; Marino, E.; de Ignacio, C.; et al. Low-temperature, shallow-water hydrothermal vent mineralization following the recent submarine eruption of Tagoro volcano (El Hierro, Canary Islands. *Mar. Geol.* **2020**, *430*, 106333. [CrossRef]
217. Cerný, P.; Ercit, T.S.; Groat, L.A.; Chapman, R. Zirconium and hafnium in minerals of the columbite and wodginite groups from granitic pegmatites. *Can. Mineral.* **2007**, *45*, 185–202. [CrossRef]
218. Mansour, S.; Glasmacher, U.A.; Krob, F.C.; Casillas, R.; Albinger, M. Timing of rapid cooling and erosional decay of two volcanic islands of the Canary Archipelago: Implications from low-temperature thermochronology. *Int. J. Earth Sci. Geol. Rundsch.* **2022**, *112*, 345–382. [CrossRef]
219. Miller, R. Structural and textural evolution of the Strange Lake peralkaline rare-element (NYF) granitic pegmatite, Quebec–Labrador. *Can. Mineral.* **1996**, *34*, 349–371.
220. Danilova, Y.; Shumilova, T.; Mayer, J.; Danilov, B.S. Conditions and Formation Mechanism of carbon phases in Late Quaternary geyserites and travertines of Ol'khon Area and Ol'khon Island (Baikal Rift Zone). *Petrology* **2016**, *24*, 41–54. [CrossRef]
221. Dunn, P.J. Rare minerals of the Kombat Mine. *Mineral. Rec.* **1991**, *22*, 421–425.
222. Dill, H.G.; Melcher, F.; Botz, R. Meso-to epithermal W-bearing Sb vein-type deposits in calcareous rocks in western Thailand: With special reference to their metallogenetic position in SE Asia. *Ore Geol. Rev.* **2008**, *34*, 242–262. [CrossRef]
223. Russo, M.; Campostrini, I.; Demartin, F. Fumarolic minerals after the 1944 Vesuvius eruption. In *The Future of the Italian Geosciences–The Italian Geosciences of the Future. 87° Congresso della Società Geologica Italiana e 90° Con-gresso della Società Italiana di Mineralogia e Petrologia, Milan, Italy, 10–12 September 2014*; Cesare, B., Erba, E., Carmina, B., Fascio, L., Petti, F.M., Zuccari, A., Eds.; Abstract Book. Rendiconti Online della Società Geologica Italiana, 31, Supplemento n.1.; Mineralogical Society: Milan, Italy, 2014.
224. Arfè, G.; Boni, M.; Mondillo, N.; Aiello, R.; Balassone, G.; Arseneau, V.; Soyk, D. Supergene alteration in the Capricornio Au-Ag epithermal vein system, Antofagasta Region, Chile. *Can. Mineral.* **2016**, *54*, 681–706. [CrossRef]
225. Van den Berg, W.; Calvo, M.; Rewitzer, C. Secondary minerals from old smelter slags from the Puerto de Mazarrón area, Mazarrón, Murcia, Spain. *Miner. Up* **2020**, *5*, 8–32.
226. British Broadcasting Corporation. The BBC and the Amazing Tellurium Find in the Atlantic. *Forbes*. 2017. Available online: https://www.forbes.com/sites/timworstall/2017/04/12/the-bbc-and-the-amazing-tellurium-find-in-the-atlantic/ (accessed on 2 September 2023).

227. Joussein, E.; Petit, S.; Churchman, J.; Theng, B.; Righi, D.; Delvaux, B. Halloysite clay minerals—A review. *Clay Miner.* **2005**, *40*, 383–426. [CrossRef]
228. Fernandez-Caliani, J.C.; Crespo, E.; Rodas, M.; Barrenechea, J.F.; Luque, F.J. Formation of nontronite from oxidative dissolution of pyrite disseminated in Precambrian felsic metavolcanics of the Southern Iberian Massif (Spain). *Clays Clay Miner.* **2004**, *52*, 106–114. [CrossRef]
229. Ioannou, S.E.; Spooner, E.T.C. Miocene Epithermal Au-Ag Vein Mineralization, Dixie Claims, Midas District, North-Central Nevada; Characteristics and Controls. *Explor. Min. Geol.* **2000**, *9*, 233–252. [CrossRef]
230. Chukanov, N.V.; Aksenov, S.M.; Rastsvetaeva, R.K.; Van, K.V.; Belakovskiy, D.I.; Pekov, I.V.; Gurzhiy, V.V.; Schüller, W.; Ternes, B. Mendigite, $Mn_2Mn_2MnCa(Si_3O_9)_2$, a new mineral species from the Eifel volcanic region, Germany. *Zap. RMO* **2015**, *144*, 4860. [CrossRef]
231. Johnson, C.C.; Breward, N.; Ander, E.L.; Ault, L. G-BASE: Baseline geochemical mapping of Great Britain and Northern Ireland. *Geochem. Explor. Environ. Anal. Geol. Soc. Lond.* **2005**, *5*, 347–357. [CrossRef]
232. Klügel, A.; Hansteen, T.H.; van den Bogaard, P.; Strauss, H.; Hauff, F. Holocene fluid venting at an extinct Cretaceous seamount, Canary Archipelago. *Geology* **2011**, *39*, 855–858. [CrossRef]
233. Van den Bogaard, P. The origin of the Canary Island Seamount Province-New ages of old seamounts. *Sci. Rep.* **2013**, *2107*, 17. [CrossRef]
234. Balaram, V.; Sawant, S.S. Indicator minerals, pathfinder elements, and portable analytical instruments in mineral exploration Studies. *Minerals* **2022**, *12*, 394. [CrossRef]
235. Crocombe, R.A. Portable Spectroscopy. *Appl. Spectrosc.* **2018**, *72*, 1701–1751. [CrossRef] [PubMed]
236. Kaski, S.; Häkkänen, H.; Korppi-Tommola, J. Sulfide mineral identification using laser-induced plasma spectroscopy. *Miner. Eng.* **2003**, *16*, 1239–1243. [CrossRef]